

WADC TECHNICAL REPORT 52-335

TITANIUM PHASE DIAGRAMS

*Harold D. Kessler
William Rostoker
Robert J. Van Thyne*

*Armour Research Foundation
Illinois Institute of Technology*

November 1953

*Materials Laboratory
Contract No. AF 33(038)-8708
RDO No. 615-11*

**Wright Air Development Center
Air Research and Development Command
United States Air Force
Wright-Patterson Air Force Base, Ohio**

McGregor & Werner, Inc., Dayton, Ohio
300 - April, 1954

FOREWORD

This report was prepared by the Armour Research Foundation of Illinois Institute of Technology, under USAF Contract No. AF 33(038)-8708. The contract was initiated under Research and Development Order No. 615-11, "Titanium Metal and Alloys", and was administered under the direction of the Materials Laboratory, Directorate of Research, Wright Air Development Center, with Lt. William R. Freeman acting as project engineer.

ABSTRACT

Using high purity arc melted alloys and micrographic analysis of annealed samples as the principle method of investigation, titanium-rich, partial phase diagrams were determined for the following systems:

Ti-Cr-Fe: The titanium-rich portion of the diagram was studied in detail to 70 weight % titanium. The isotherm at 800°C was determined for the section bounded by Ti, TiFe₂, and TiCr₂. The solubility of chromium and iron in alpha titanium is less than 1% total alloy content. There is a continuous space of ternary beta solid solution between the Ti-Cr and Ti-Fe systems. A ternary eutectoid, $\beta \rightleftharpoons \alpha + \text{TiCr}_2 + \text{TiFe}$, occurs at approximately 8% Cr-13% Fe and about 540°C. The beta phase of alloys lying on the low titanium side of a tie line between 7% chromium and 4% iron is retained upon water quenching from the beta space. Hardness data are presented, illustrating the marked effect of heat treatment.

Ti-Al-O and Ti-Al-N: Titanium-rich corners of the systems from 0 to 10% aluminum and 0 to 1% oxygen or nitrogen were investigated. As aluminum, oxygen and nitrogen are alpha-stabilizers, the ternary alpha spaces extend to temperatures well above the transformation temperature of titanium (885°C). Nitrogen is more effective than oxygen in raising the $\beta/\alpha + \beta$ space boundary of the Ti-Al system. Upon water quenching the alloys, the beta phase transforms to alpha prime. Oxygen and nitrogen additions increase the hardness of the Ti-Al alloys.

Ti-Al-C: The phase diagram was determined using alloys containing 0 to 10% aluminum and 0 to 1% carbon. A study of several as-cast carbon master alloys permitted an outline of the Ti-C diagram to be constructed. A high melting compound, TiC, appears to exist over a range of compositions. A eutectic occurs at about 30% carbon between TiC and carbon.

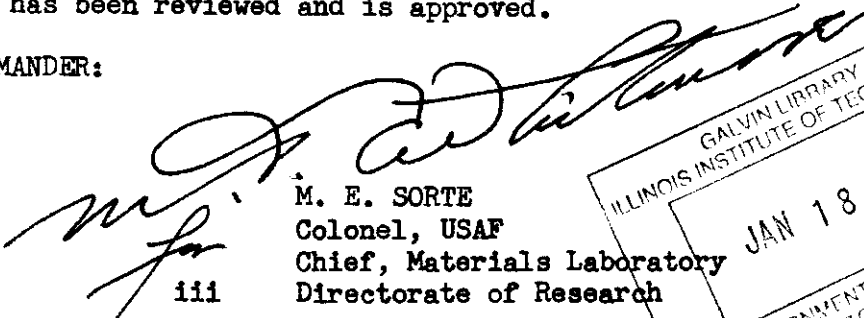
Aluminum raises the temperature of the peritectoid reaction of the Ti-C system, $\beta \rightleftharpoons \alpha + \text{TiC}$ (920°C). The maximum solubility of carbon in alpha titanium is increased by aluminum additions from about 0.5% in the binary Ti-C system to 1% at 10% aluminum. Aluminum and carbon increase the hardness of the alpha solid solution.

Ternary Oxide Phases: A family of ternary oxide phases isomorphous with Fe₃W C was discovered in which titanium was associated with one of the elements of the first transition series. The phase relationships between these ternary phases and binary phases were investigated for the Ti-Cr-O, Ti-Fe-O and Ti-Ni-O systems. An isothermal section for the Ti-Mo-O system was constructed.

PUBLICATION REVIEW

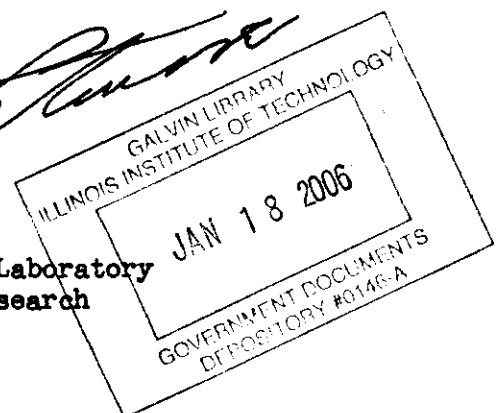
This report has been reviewed and is approved.

FOR THE COMMANDER:


M. E. SORTE
Colonel, USAF
Chief, Materials Laboratory
Directorate of Research

WADC-TR-52-335

iii



Contrails

TABLE OF CONTENTS

	Page
I. INTRODUCTION	1
II. EXPERIMENTAL PROCEDURE	1
A. Materials	1
III. RESULTS AND DISCUSSION	2
A. The Ti-Cr-Fe System	2
1. Introduction	2
2. Experimental Procedure	3
a. Melting Practice.	3
b. Annealing Treatments.	3
c. Solidus Determinations.	4
3. Results and Discussion	4
a. The Phase Diagram	4
b. Isothermal Sections	4
c. Vertical Sections	14
d. Melting Range Determinations.	14
e. Alloys Rich in Chromium and Iron.	14
f. Microstructures	26
g. Hardness.	30
B. The Ti-Al-O and Ti-Al-N Systems	35
1. Experimental Procedure	35
a. Alloy Preparation	35
b. Annealing Treatments.	35
2. Discussion of Results.	36
a. The Phase Diagrams.	36
b. Hardness.	36
C. The Ti-Al-C System.	42
1. Experimental Procedure	42
a. Alloy Preparation	42
b. Annealing Treatments.	42
2. Discussion of Results.	42
a. The Ti-C Diagram.	42
b. The Ti-Al-C Diagram	45
c. Hardness.	54
D. The Ti-O System	58
E. Studies on a Family of Ternary Phases in Titanium-Base Systems.	58
1. Identification of Ti_2X and Ti_xX_yO Type Phases Isomorphous with Ti_2Fe_3O	60
2. System Ti-Fe-O - Isothermal Section at 1000°C.	60
a. Miscibility Range of the Ternary (T) Phase.	63
b. The (α + T) Phase Field	63
c. The (TiO + T) Phase Field	63
d. The (α + TiO + T) Phase Field	63
e. The (TiO + T + $TiFe_2$) Phase Fields.	63
f. The ($TiFe_2$ + T + $TiFe$) Phase Field.	68
g. The (T + $TiFe$) and (β + $TiFe$ + T) Phase Fields.	68
h. The (β + T) and (α + β + T) Phase Fields.	68
i. The (α + β) Phase Field	68

Contrails

TABLE OF CONTENTS (Continued)

	Page
3. System Ti-Cr-O - Isothermal Section at 1000°C.	68
a. Miscibility Range of the Ternary (T) Phase.	72
b. The (α + TiCr ₂) Phase Field	72
c. The (α + T) and (TiO + T) Phase Fields.	72
d. The (α + β) and (α + β + TiCr ₂) Phase Fields.	72
e. Other Phase Fields.	72
4. Isothermal Section at 900°C - System Ti-Ni-O	75
a. Miscibility Field of the Ti ₂ Ni Phase.	75
b. The (α + Ti ₂ Ni) Phase Field	75
c. The (TiO + Ti ₂ Ni) and (α + TiO + Ti ₂ Ni) Phase Fields.	75
d. The (TiO + Ti ₂ Ni + TiNi ₃) Phase Field	75
e. The (Ti ₂ Ni + TiNi ₃) and (TiNi + Ti ₂ Ni + TiNi ₃) Phase Fields.	75
f. The (Ti ₂ Ni + TiNi) Phase Field.	79
5. Isothermal Section at 1000°C - System Ti-Mo-O.	79
IV. SUMMARY.	79
A. The Ti-Cr-Fe System	79
B. The Ti-Al-(O and N) Systems	82
C. The Ti-Al-C System.	82
D. The Ternary Oxide Phases.	83
BIBLIOGRAPHY.	84

Contrails

LIST OF TABLES

	Page
I - Annealing Conditions for Ti-Cr-Fe Alloys.	4
II - Additional Alloys Prepared to Position the Ternary Eutectoid Point	16
III - X-ray Diffraction Data for Alloys Lying on the Section $TiCr_2-TiFe_2$	22
IV - X-ray Diffraction Identification of Phases Present in Ti-Cr-Fe Alloys Annealed at 800°C	25
V - X-ray Diffraction Identification of Phases Present in Certain Ti-Cr-Fe Alloys	28
VI - Vickers Hardness of Ti-Cr Alloys Annealed at 1000°C and Rapidly Quenched.	34
VII - Annealing Conditions for Ti-Al-(O and N) Alloys	35
VIII - Annealing Times for Ti-Al-C Alloys.	43
IX - X-ray Diffraction Data for a Ti-10% Al-1% C Alloy	56
X - Crystal Structures Recognized at the Ti_2X , Ti_4X_2O and Ti_3X_3O Compositions	61
XI - Lattice Parameters of the Fe_3W_3C Type Structures.	62
XII - Summary of Observations on Alloys in the Ti-Fe-O System Annealed at 1000°C.	64
XIII - Summary of Observations on Alloys in the Ti-Cr-O System Annealed at 1000°C.	70
XIV - Summary of Observations on Alloys in the Ti-Ni-O System Annealed at 900°C	76

Contrails

LIST OF FIGURES

	Page
1 - Partial Isothermal Section at 900°C of the Ti-Cr-Fe System. . .	5
2 - Partial Isothermal Section at 800°C of the Ti-Cr-Fe System. . .	6
3 - Partial Isothermal Section at 750°C of the Ti-Cr-Fe System. . .	7
4 - Partial Isothermal Section at 700°C of the Ti-Cr-Fe System. . .	8
5 - Partial Isothermal Section at 650°C of the Ti-Cr-Fe System. . .	9
6 - Partial Isothermal Section at 600°C of the Ti-Cr-Fe System. . .	10
7 - Partial Isothermal Section at 550°C of the Ti-Cr-Fe System. . .	11
8 - Isotherms of the Lower Surfaces of the Beta Phase Space in the Ti-Cr-Fe System	15
9 - Vertical Sections of the Ti-Cr-Fe System at Constant Chromium Contents	17
10 - Vertical Sections of the Ti-Cr-Fe System at Constant Chromium and Titanium Contents	18
11 - Isotherms of the Solidus Surface of the Ti-Cr-Fe System . . .	19
12 - Partial Isothermal Section at 800°C of the Ti-Cr-Fe System. . .	21
13 - Lattice Parameters of the Hexagonal Ti(Fe,Cr) ₂ Phase.	23
14 - Vertical Section of the Ti-Cr-Fe System Through TiFe ₂ and TiCr ₂	24
15 - Hypothetical Partial Isothermal Section at Some Temperature Below 800°C of the Ti-Cr-Fe System.	27
16 - Hypothetical Partial Isothermal Section of the Ti-Cr-Fe System at Some Temperature Between 675° and 540°C	29
17 - Microstructure of a 0.5% Cr-0.5% Fe alloy, water quenched after annealing at 650°C for 432 hours	31
18 - Microstructure of a 12% Cr-2% Fe alloy, annealed at 650°C for 432 hours and water quenched	31
19 - Microstructure of a 47% Cr-20% Fe alloy, water quenched after annealing at 800°C for 144 hours	31
20 - Microstructure of a 22% Cr-22% Fe alloy, annealed at 800°C for 144 hours and water quenched	32

Contrails

LIST OF FIGURES (Continued)

	Page
21 - The same microstructure as Figure 20, now stain etched.	32
22 - Microstructure of a 50% Cr alloy, water quenched after 24 hours at 1000°C.	32
23 - Microstructure of a 40% Fe alloy, annealed the same as Figure 22	32
24 - Vickers Hardness of Ti-Cr-Fe Alloys (Fe, Cr Ratio = 1:1).	33
25 - Vertical Sections at Constant Oxygen Content of the Partial Ti-Al-O System.	37
26 - Vertical Sections at Constant Nitrogen Content of the Partial Ti-Al-N System.	38
27 - Microstructure of a 2% Al-0.25% N alloy, water quenched after annealing at 1000°C for 24 hours	39
28 - Microstructure of a 6% Al-0.25% N alloy, treated the same as the sample of Figure 27	39
29 - Microstructure of a 10% Al-0.25% N alloy, treated the same as the specimen of Figure 27	39
30 - Average Vickers Hardness of Ti-Al-O Alloys Annealed in the Alpha Phase Space at Temperatures Between 900° and 1100°C	40
31 - Average Vickers Hardness of Ti-Al-N Alloys Annealed in the Alpha Phase Space at Temperatures Between 900° and 1100°C	41
32 - Probable Type of Phase Diagram for the Partial System Ti-C	44
33 - Microstructure of a 13% C alloy, arc melted and chill cast	46
34 - Microstructure of a 30% C alloy, arc melted and chill cast	46
35 - The Partial Ti-C Phase Diagram	47
36 - Vertical Section at 2% aluminum content of the partial Ti-Al-C System	48
37 - Vertical Section at 4% aluminum content of the partial Ti-Al-C System	49
38 - Vertical Section at 6% aluminum content of the partial Ti-Al-C System	50
39 - Vertical Section at 8% aluminum content of the partial Ti-Al-C System	51

Contrails

LIST OF FIGURES (Continued)

	Page
40 - Vertical Section at 10% Aluminum Content of the Partial Ti-Al-C System	52
41 - Microstructure of a 10% Al-1% C alloy, water quenched after annealing at 1150°C for 16 hours	53
42 - Microstructure of a 0.6% C alloy, annealed at 950°C for 48 hours and water quenched	53
43 - Microstructure of a 4% Al-0.6% C alloy, annealed at 950°C and water quenched	53
44 - Microstructure of an 8% Al-0.8% C alloy, water quenched after annealing at 900°C for 72 hours.	55
45 - Microstructure of a 10% Al-0.8% C alloy, treated the same as the sample of Figure 44	55
46 - Average Vickers Hardness of Ti-Al-C Alloys Annealed in the Alpha Phase Space at Temperatures Between 600° and 1150°C . .	57
47 - Microstructures of a 19% O alloy, quenched after 24 hours	
48 - at 1000°C.	59
49 - Microstructures of a 19% O sample initially treated as the	
50 - specimen of Figures 47 and 48, then subsequently annealed at 800°C for 168 hours	59
51 - 1000°C Isothermal for Partial Ti-Fe-O System	66
52 - Microstructure of a 15% O-30% Fe Alloy, Annealed at 1000°C and Water Quenched	67
53 - Microstructure of a 15% O-20% Fe Alloy, Annealed at 1000°C and Water Quenched	67
54 - Microstructure of a 20% O-25% Fe Alloy, Annealed at 1000°C and Water Quenched	67
55 - Microstructure of TiO-TiFe ₂ Phase, Annealed at 1000°C and Water Quenched	69
56 - Microstructure of a 8% O-42% Fe Alloy, Annealed at 1000°C and Water Quenched	69
57 - 1000°C Isothermal for Partial Ti-Cr-O System	71
58 - Microstructure of a 15% O-20% Cr Alloy, Annealed at 1000°C and Water Quenched	73

Contrails

LIST OF FIGURES (Continued)

	Page
59 - Microstructure of a 25% 0-15% Cr Alloy, Annealed at 1000°C and Water Quenched	73
60 - Microstructure of a 15% 0-35% Cr Alloy, Annealed at 1000°C and Water Quenched	73
61 - Microstructure of a 10% 0-25% Cr Alloy, Annealed at 1000°C and Water Quenched	73
62 - Microstructure of a 10% 0-55% Cr Alloy, Annealed at 1000°C and Water Quenched	74
63 - 900°C Isothermal for Partial Ti-Ni-O System	77
64 - Microstructure of a 5% 0-30% Ni Alloy, Annealed at 900°C and Water Quenched	78
65 - Microstructure of a 10% 0-20% Ni Alloy, Annealed at 900°C and Water Quenched	78
66 - Microstructure of a 25% 0-20% Ni Alloy, Annealed at 900°C and Water Quenched	78
67 - Microstructure of a 35% 0-5% Ni Alloy, Annealed at 900°C and Water Quenched	78
68 - Microstructure of a 25% 0-30% Ni Alloy, Annealed at 900°C and Water Quenched	80
69 - Microstructure of a 5% 0-50% Ni Alloy, Annealed at 900°C and Water Quenched	80
70 - Microstructure of a 5% 0-35% Ni Alloy, Annealed at 900°C and Water Quenched	80
71 - 1000°C Isothermal for Partial Ti-Mo-O System	81

Contrails

I. INTRODUCTION

This is a summary report of the third year's work on Contract No. AF 33(038)-8708 covering the period of November 8, 1951 to January 8, 1953. As Ti-Cr-Fe alloys were among the first to find commercial application, the constitution of the system was investigated during last year's work on this project. The study of the system was expanded during this year's effort and is now completed.

Work on Contract No. AF 33(038)-22806 has shown that Ti-Al alloys show much promise for use at elevated temperatures. For this reason, the effect of the interstitially soluble contaminants, oxygen, nitrogen and carbon, on the Ti-Al system was investigated and partial phase diagrams were determined for the ternary systems.

A series of ternary oxide phases was investigated and isolated. As these ternary phases may be involved in the constitution of commercial titanium alloys, single partial isothermal sections were constructed for the Ti-Fe-O, Ti-Cr-O, Ti-Ni-O, and Ti-Mo-O systems.

The principle method used to investigate the alloy systems was metallographic analysis of arc melted samples, water quenched after annealing. Solidus determinations and x-ray diffraction analysis were also employed.

II. EXPERIMENTAL PROCEDURE

Alloy ingots weighing 10 to 20 grams were melted in a nonconsumable tungsten electrode arc melting furnace using water-cooled copper hearths and a helium atmosphere. The ingots were remelted enough times to insure homogeneity. The techniques of melting, annealing, solidus determinations, metallography, and x-ray diffraction were the same as those reported for the first year's work on this project (1). Where needed, details will be given in the sections of the report where they apply.

A. Materials

The titanium used in the preparation of the alloys was iodide crystal bar (99.9+% pure) produced by the New Jersey Zinc Company and Foote Mineral Company.

Vacuum melted chromium and iron were purchased from the National Research Corporation and the impurities were:

Contrails

<u>Iron</u>		<u>Chromium</u>	
Silicon	0.0093	Carbon	0.015
Nickel	0.012	Oxygen	0.066
Phosphorus	0.0023	Nitrogen	0.0022
Sulphur	0.013		
Carbon	0.011		

The aluminum was obtained from the Aluminum Company of America in the form of sheet. The given analysis was:

Silicon	0.0006%
Iron	0.0005
Copper	0.0022
Magnesium	0.0003
Calcium	<0.0006
Sodium	<0.0005
Aluminum	99.99

High purity titanium dioxide purchased from the National Lead Company was used in the preparation of the oxygen-bearing alloys. The spectrographic analysis of this material is as follows:

SiO ₂	0.07%	Pb	0.002%
Fe ₂ O ₃	0.002	Mn	<0.00005
Al ₂ O ₃	<0.001	W	<0.01
Sb ₂ O ₃	<0.002	V	<0.002
SnO ₃	<0.001	Cr	<0.002
Mg	0.001	Ni	<0.001
Nb	<0.01	Mo	<0.002
Cu	0.0004		

Special spectroscopic graphite rod purchased from the National Carbon Company was used in the preparation of the Ti-Al-C alloys.

III. RESULTS AND DISCUSSION

A. The Ti-Cr-Fe System - by R. J. Van Thyne

1. Introduction

The investigation of the Ti-Cr-Fe system was continued from the previous year's work to clarify some uncertainties. An attempt was made to more accurately locate the ternary eutectoid point and to obtain observable ternary

Contrails

eutectoid decomposition of the beta phase. Phase relationships were studied for alloys containing over 30% total chromium and iron content and solidus determinations were made.

The results of work on this system reported last year are included so that a comprehensive summary is available. No information on the constitution of the titanium-rich corner of the Ti-Cr-Fe system was available prior to the initiation of this work. The only work previously reported on the system was that for titanium-poor alloys studied by Vogel and Wenderott (2).

As part of the previous year's work, the binary systems Ti-Cr and Ti-Fe were determined (3,4). Other investigators have also studied the systems Ti-Cr (5,6,7,8,9) and Ti-Fe (5,10,11,12). Both of the binary systems are characterized by the eutectoid decomposition of the beta phase.

Most of the work has been concentrated on the titanium-rich corner with compositions of less than 30% total chromium and iron content. The determination of isothermal sections was the experimental approach used to obtain the ternary phase diagram. Vertical sections were used to check the consistency of the isothermal sections.

While this investigation was in progress, a study of the Ti-Mo-Cr system* at Armour Research Foundation disclosed the existence of a high temperature modification of $TiCr_2$ above at least 1300°C (13). This allotrope has a hexagonal structure of the $MgZn_2$ type, isomorphous with $TiFe_2$; whereas, the low temperature modification of $TiCr_2$ (8) is cubic, of the $MgCu_2$ type. The existence of allotropy in $TiCr_2$, of course, means a more complicated set of phase relationships in this general region than if the phase were monomorphic, as was first assumed.

Additional studies were made late in the investigation in order to clarify the part that the hexagonal $TiCr_2$ phase plays in the ternary phase relationships. These will be discussed in a separate section. Because they are of greatest practical significance, the phase relationships in the titanium-rich corner will be presented first, omitting the equilibria involving the hexagonal modification of $TiCr_2$ in an effort to simplify the presentation.

2. Experimental Procedure

a. Melting Practice

The alloy charges and resultant ingots were weighed to the nearest milligram. The ingots were melted five times. As the average weight losses on melting were small, the actual compositions were judged to be very close to the nominal compositions. Many check analyses, particularly for the binary alloys, substantiated the general use of nominal compositions.

b. Annealing Treatments

Information on the annealing times used for various temperatures is given in Table I. All samples heat treated below 800°C were first annealed at 900°C

* Watertown Arsenal Contract No. DA 11-022-ORD-272.

TABLE I

ANNEALING CONDITIONS FOR Ti-Cr-Fe ALLOYS

Temperature, °C	Time, Hours	Temperature, °C	Time, Hours
1300	1/2	750	192 - 288
1200	1/2 - 15	700	192 - 288
1100	1 - 30	650	432
1050	24	600	576 - 600
1000	2 - 40	550	744
900	22 - 72	500	720
800	144 - 170		

for 2 to 8 hours and then slowly cooled to the temperature of final annealing. Coring was observed in some alloys containing over 5% total alloy content of chromium and iron; therefore, these alloys were homogenization annealed at 1050°C for 24 hours prior to the regular isothermal anneals.

c. Solidus Determinations

Metallographic analysis after isothermal annealing was used to outline the solidus surface. The annealing temperatures were selected by first determining the temperature of visible melting upon heating as described previously (1). The accuracy of these data is estimated to be $\pm 10^\circ\text{C}$.

3. Results and Discussion

a. The Phase Diagram

The constitution of the titanium corner of the Ti-Cr-Fe system is of the ternary eutectoid type. Curves of double saturation ($\beta \rightleftharpoons \alpha + \text{TiCr}_2$ and $\beta \rightleftharpoons \alpha + \text{TiFe}$) descend into the space model from the two binary eutectoid points at 15% Cr - 685°C and 16% Fe - 585°C, respectively, along with that expressing saturation of the two compounds ($\beta \rightleftharpoons \text{TiCr}_2 + \text{TiFe}$). These three space curves meet to form a ternary eutectoid point ($\beta \rightleftharpoons \alpha + \text{TiCr}_2 + \text{TiFe}$) at approximately 8% Cr-13% Fe and 540°C.

b. Isothermal Sections

Isothermal sections at temperatures between 900° and 550°C are presented in Figures 1 to 7. At 900°C, Figure 1, the beta field extends over most of the composition area shown. The transition from transformed to retained beta after water quenching these alloys from the beta state is shown as a shaded band. This appears to be a straight line joining the similar transition

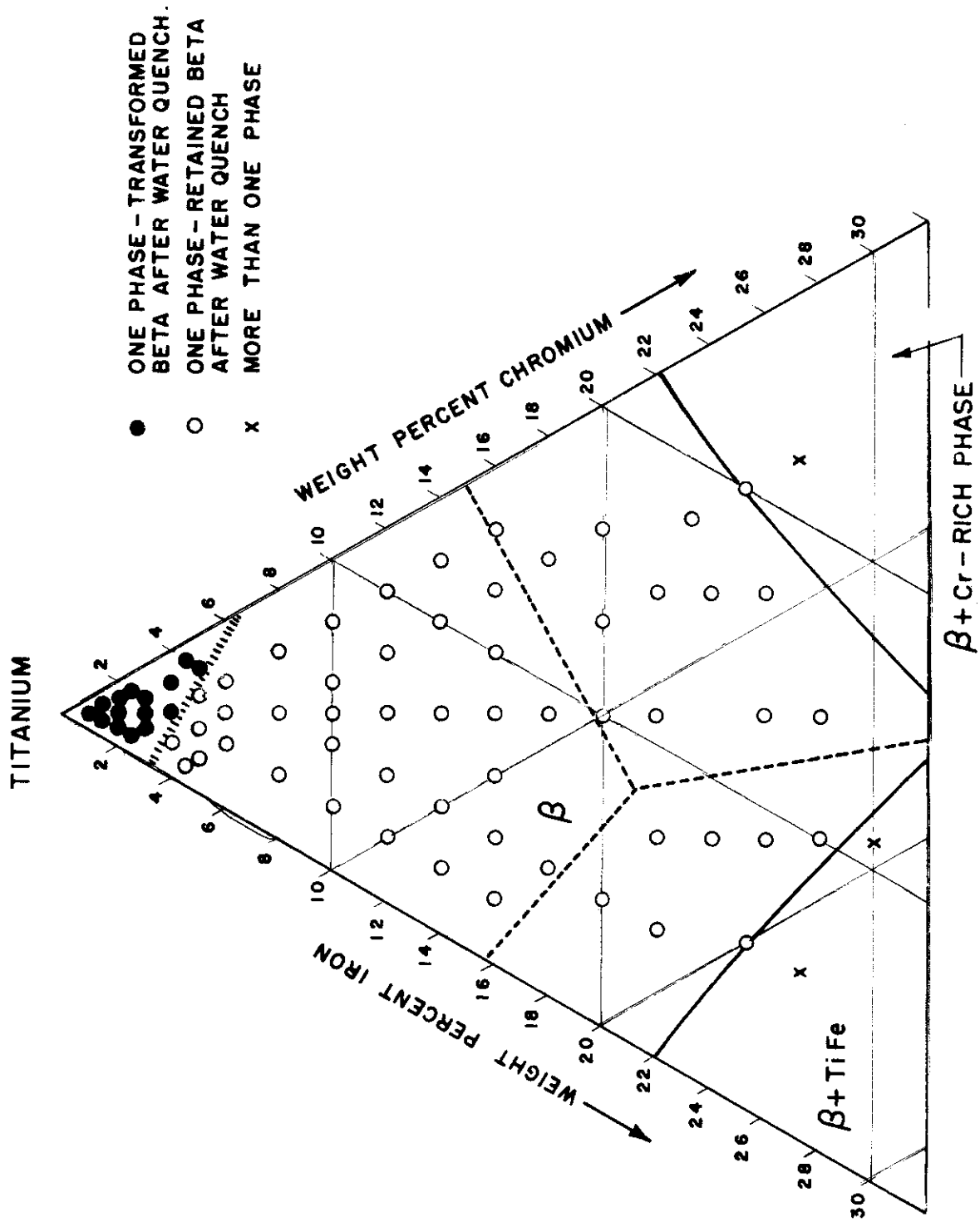


Fig. 1 - Partial Isothermal Section at 900°C of the Ti-Cr-Fe System.

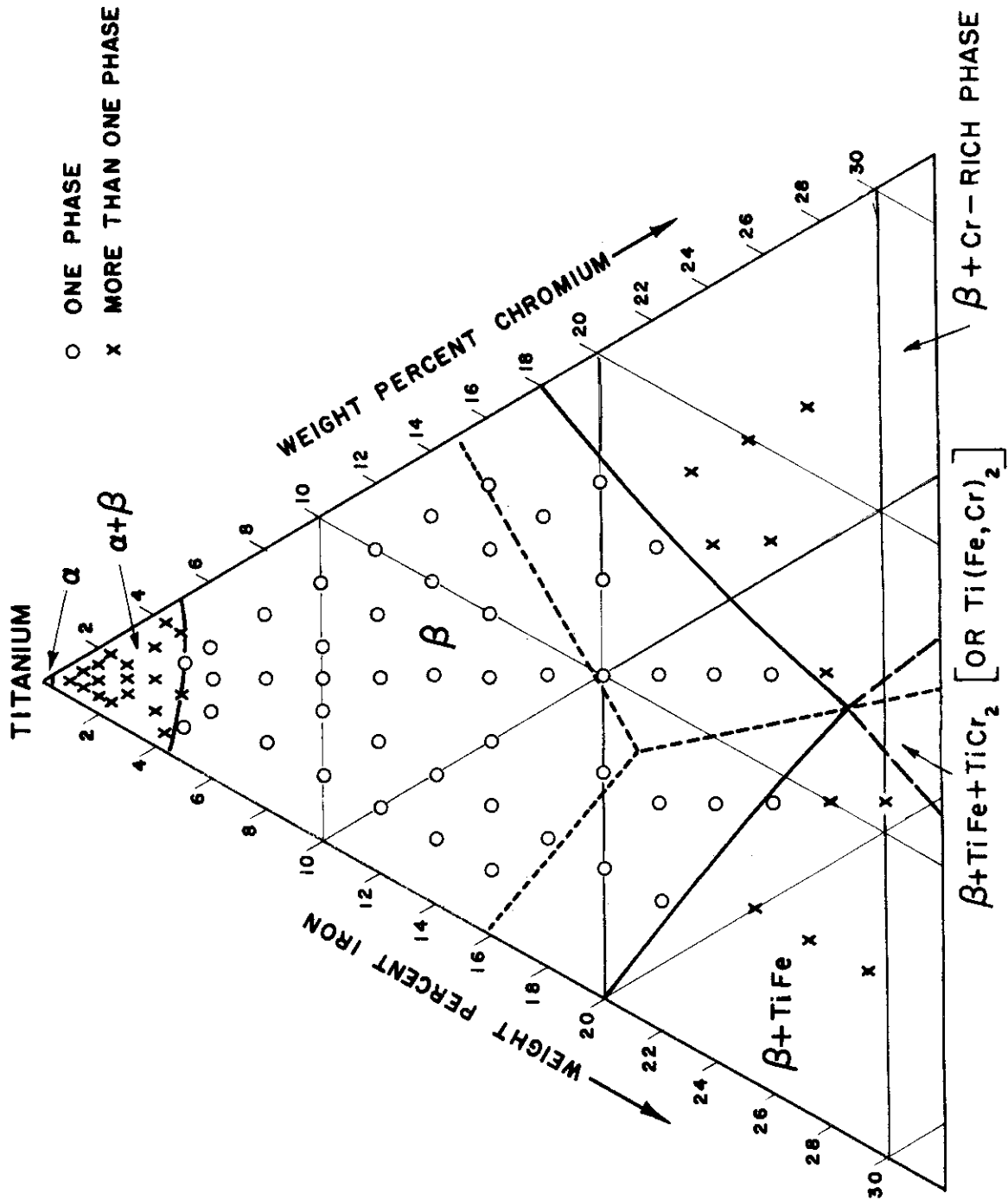


Fig. 2 - Partial Isothermal Section at 800°C of the Ti-Cr-Fe System.

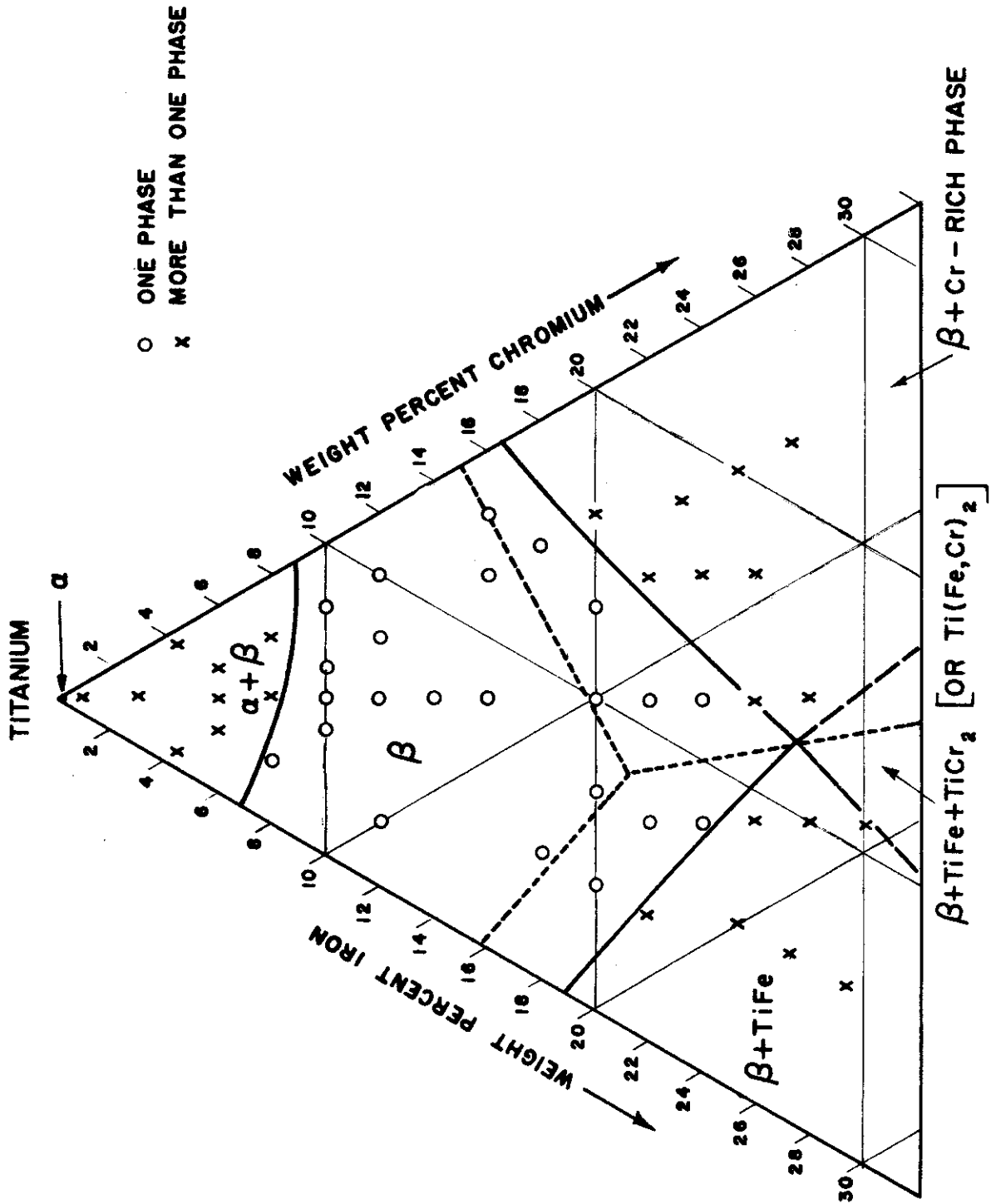


Fig. 3 - Partial Isothermal Section at 750°C of the Ti-Cr-Fe System.

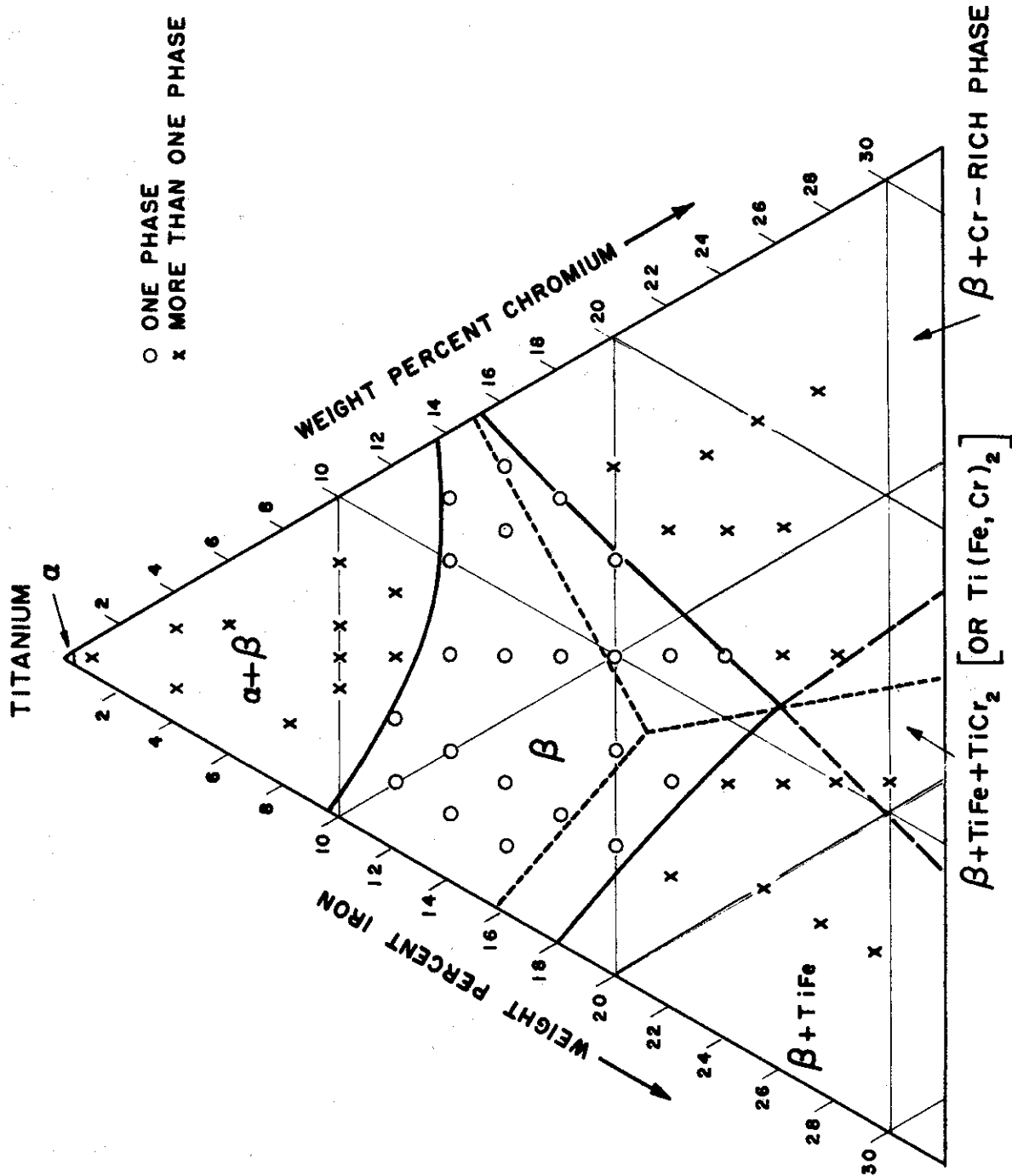


Fig. 4 - Partial Isothermal Section at 700°C of the Ti-Cr-Fe System.

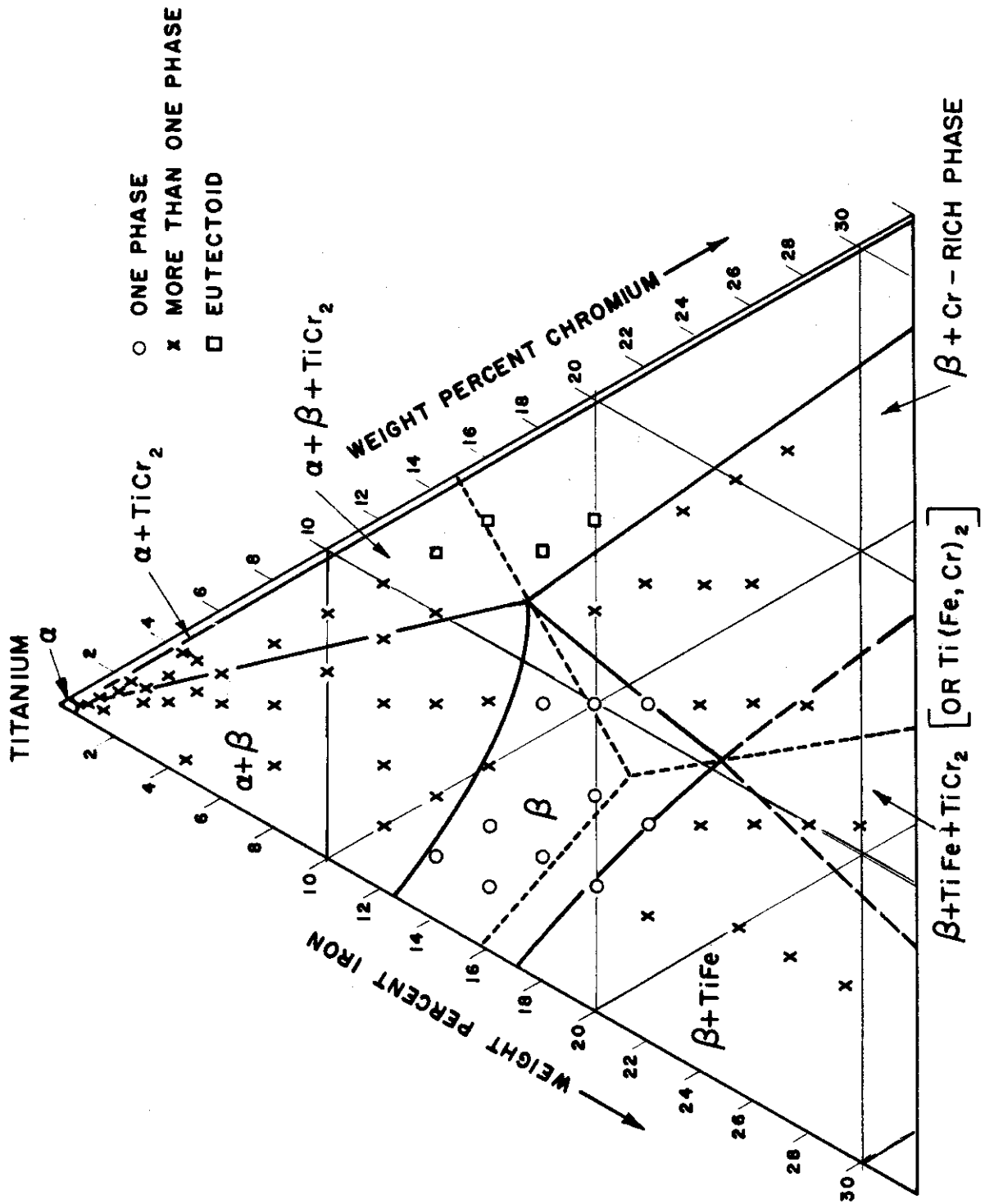


Fig. 5 - Partial Isothermal Section at 650°C of the Ti-Cr-Fe System.

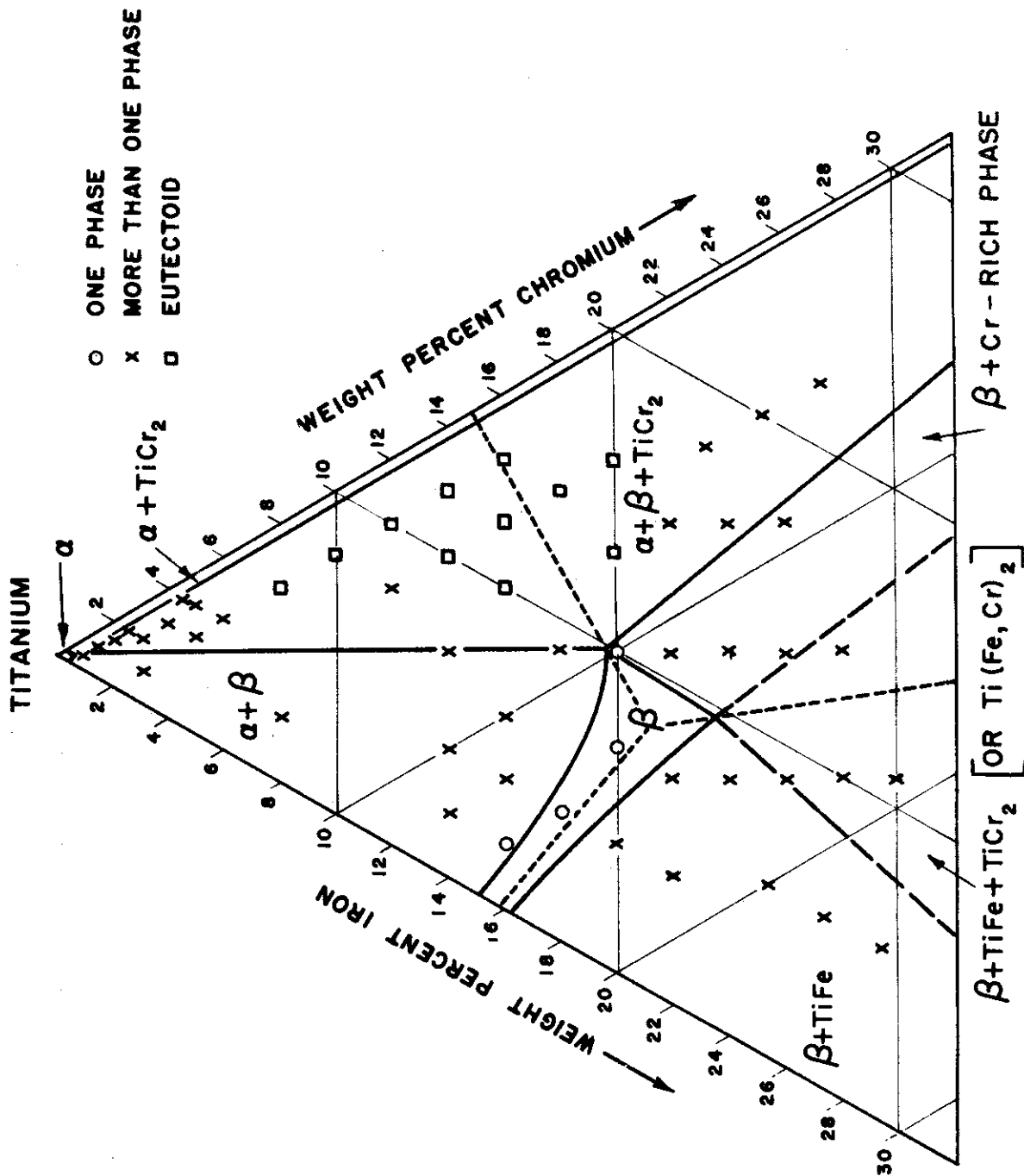


Fig. 6 - Partial Isothermal Section at 600°C of the Ti-Cr-Fe System.

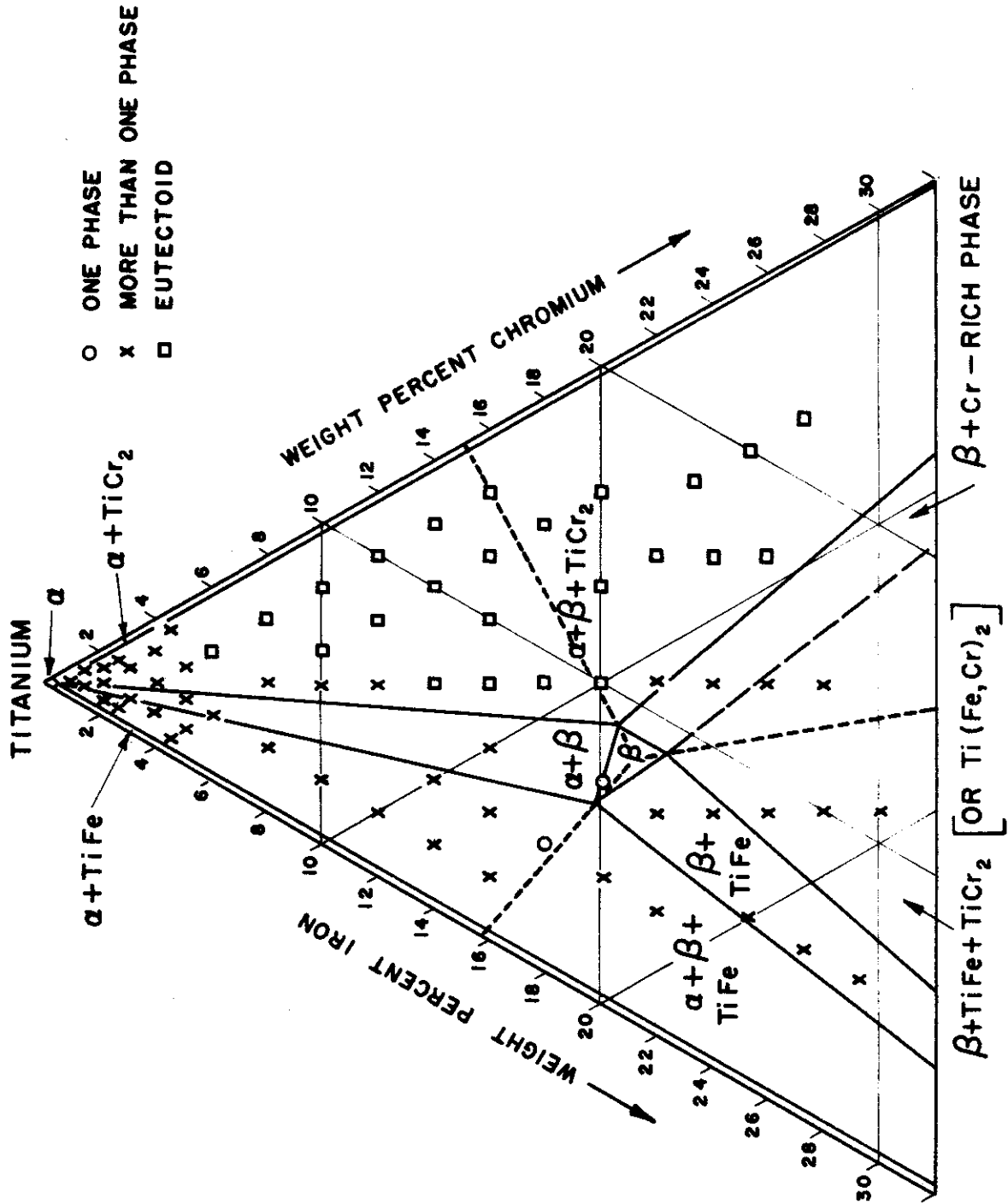


Fig. 7 - Partial Isothermal Section at 550°C of the Ti-Cr-Fe System.

Contrails

compositions in the binary systems; that is, between 6 and 7% Cr and 3 and 4% Fe. The samples of lower alloy content transformed to an acicular product, alpha prime, partially or completely during water quenching, and those of higher alloy content consisted entirely of what appears microscopically to be retained beta. The position of the three space curves of double saturation have been shown as dotted lines on all of the isotherms.

Sections through the space model at 800°, 750°, and 700°C (Figures 2 to 4) show the enlargement of the ($\alpha + \beta$) and ($\beta + \text{compound}$) fields. In general, the limits of the beta field in the isothermal sections were not determined by the data points obtained at a particular temperature alone. After the data had been obtained for all temperature levels (900°-550°C), graphical interpolation, using the isothermal and vertical sections, was done, placing emphasis on the binary intercepts. Therefore, the isotherms shown are an integration of all the data.

The exact location of the sectional phase boundaries at 650°C and below (Figures 5 to 7) was greatly impeded by the fact that the rate of diffusion at these temperatures is extremely low. As a consequence, the ternary beta phase remains in a metastable state, and only in the alloys rich in chromium was microscopic evidence found of the reaction, $\beta \rightleftharpoons \alpha + \text{TiCr}_2$.

The isothermal section for 650°C is presented in Figure 5. With the eutectoid decomposition in the Ti-Cr system occurring at 685°C, the eutectoid decomposition of the ternary beta phase, $\beta \rightleftharpoons \alpha + \text{TiCr}_2$, would take place within a certain range of compositions along the entire Ti-Cr side of the system. However, as shown in Figure 5, most of the hypoeutectoid alloys in the ($\alpha + \beta + \text{TiCr}_2$) field were actually found to be only two phase ($\alpha + \beta$), even after 18 days of annealing. The fact that the eutectoid decomposition did not occur in the hypoeutectoid alloys of low alloy content at annealing temperatures fairly close to the eutectoid temperature, was also observed in the binary systems (3,4).

Because of the reluctance of the eutectoid to develop, alloys with less than 12% Cr could not be used in positioning the boundary between the ($\alpha + \beta$) and ($\alpha + \beta + \text{TiCr}_2$) fields at 650°C. However, as alloys of compositions near the space curve of double saturation showed eutectoid decomposition and the boundaries of the adjacent beta field have to meet at the vertex of the ($\alpha + \beta + \text{TiCr}_2$) triangle, this point could be located at approximately 13% Cr-5% Fe.

The isothermal section at 600°C (Figure 6) is similar to that at 650°C, with changes only in the extent of the phase fields. Eutectoid decomposition was observed in a greater number of alloys on the chromium-rich side with falling temperature, although the beta phase in samples of low alloy content continued to be metastable. As at 650°C, the vertex point of the ($\alpha + \beta + \text{TiCr}_2$) triangle was positioned using the intersection of the sectional phase boundaries $\beta/\alpha + \beta$ and $\beta/\beta + \text{Cr-rich phase}$ in addition to the projection of the space curve of double saturation.

The section at 550°C (Figure 7) is below the binary Ti-Fe eutectoid level, 585°C; therefore, the ($\beta + \text{TiFe}$) and ($\alpha + \beta + \text{TiFe}$) fields should

Contrails

now be evident. It can be seen from the data points that no eutectoid structures were observed in ternary alloys on the iron side annealed at 550°C for 31 days although under similar annealing conditions the beta phase of the binary Ti-Fe system started to decompose eutectoidally (3,4). In the iron-rich ternary alloys, the eutectoid decomposition $\beta \rightleftharpoons \alpha + \text{TiFe}$ will start below the eutectoid temperature of the Ti-Fe system. It is not surprising, therefore, that at these low temperatures, equilibrium is approached only at a very low rate and that a definite indication of eutectoid was not observed.

The two curves of double saturation extending from the binary eutectoid points were positioned by the identification of either alpha or compound constituents in the microstructures of alloys lying on either side of the line. For example, at 550°C (Figure 7), the microstructures of the 2% Cr-14% Fe and the 4% Cr-16% Fe samples consist of ($\alpha + \beta$) and ($\beta + \text{TiFe}$), respectively. The 4% Cr-14% Fe alloy is single phase, beta, although the alloy is located in the ($\alpha + \beta + \text{TiFe}$) phase field. The apparent anomaly is explained on the basis that the composition lies very close to the space curve of double saturation. Thus, no proeutectoid constituents would be expected in the microstructure, and the indicated beta is metastable.

At 650° and 600°C, the beta field is extensive enough that data points are available to accurately locate the limits of the beta field and hence the other phase fields. However, at 550°C, the beta field is very small and the data points on the isotherm alone did not permit the accurate placement of phase boundaries. A number of vertical sections were drawn, some of which will be presented later. From the extrapolation of data from higher temperatures, it was apparent that the beta field was very restricted at 550°C and that the ternary eutectoid temperature occurs at approximately 540°C. Therefore, the beta field has been constructed as very small with the limits located at points on the space curves of double saturation. The lines expressing double saturation intersect at the ternary eutectoid point; approximately 8% Cr-13% Fe.

Although the data are not presented, alloys were annealed at 500°C for 30 days. In general, the microstructures were very fine and conclusive evidence of the binary Ti-Fe or ternary eutectoid decomposition was not observed in the ternary alloys. Several other techniques were tried to obtain the ternary eutectoid decomposition. A powder sample and a specimen that had been cold pressed were prepared. As slight amounts of contamination are known to greatly accelerate the reaction, an 8% Cr-13% Fe alloy was prepared using sponge titanium. The above samples were annealed at 525°C for 12 days but no definite evidence was found of the ternary eutectoid decomposition either metallographically or by x-ray diffraction. The extremely fine products observed in some of the microstructures may have been the ternary eutectoid, but definite identification was impossible.

The solubility of chromium and iron in alpha titanium is less than 1% total alloy content. The curve of maximum solubility has been arbitrarily drawn at equal iron and chromium contents. Only a very narrow duplex phase space exists between alpha and TiCr_2 , because of the restricted solubility of chromium and iron in alpha titanium. At equilibrium, the eutectoid reaction

would be complete in this region, and beta is consumed. No attempt was made to locate the extent of the ($\alpha + \text{TiCr}_2$) or ($\alpha + \text{TiFe}$) fields at high alloy contents because they apparently are very restricted.

Figure 8, which is a composite of isotherms of the lower surfaces of the beta phase space, illustrates the good correlation obtained on combining the results. Although not shown on the diagrams, additional alloys were prepared and annealed to more accurately locate the ternary eutectoid point. The compositions are shown in Table II. However, because of the very small size and small amounts of phases present in these microstructures, the placement of the ternary eutectoid point had to be accomplished using only the alloys investigated previously.

c. Vertical Sections

Vertical sections at constant chromium and titanium contents are illustrated in Figures 9 and 10. The data used in preparing these curves were taken from the isothermal sections presented earlier. Excellent correlation of data was obtained when plotting these sections and others that are not shown.

d. Melting Range Determinations

The results of the solidus determinations are presented in Figure 11; the data points shown were determined by metallographic examination of samples that were isothermally annealed and water quenched. The isotherms were drawn using previously determined solidus temperatures for the binary systems (3,4). Incipient melting data were obtained for a number of alloys by visible sign of melting on heating and, in general, substantiated the isotherms illustrated. Annealing at 1100°C showed that only the binary Ti-Fe alloys were melted; therefore, chromium additions raise the temperature of the binary Ti-Fe eutectic (1080°C).

e. Alloys Rich in Chromium and Iron

With the discovery of the hexagonal modification of TiCr_2 , it became evident that at high temperatures a continuous series of solid solutions may exist between TiCr_2 and TiFe_2 , which are isomorphous. At lower temperatures the cubic modification of TiCr_2 is stable. If a continuous single phase field exists between TiCr_2 and TiFe_2 at high temperatures, it must continuously retreat away from TiCr_2 with falling temperature. This by itself would not necessarily affect the titanium-rich portion of the diagram that had been investigated. However, if the hexagonal phase extends into the ternary system and enters into equilibrium with the beta phase, the isothermal sections would then necessarily contain additional two and three phase regions.

To decide if the phase relationships mentioned above do exist, an x-ray pattern was obtained for a 22% Cr-22% Fe alloy annealed at 800°C. This sample was found to contain beta, TiFe and the hexagonal modification of TiCr_2 . Therefore, the hexagonal modification does enter into equilibrium with beta. For this reason, the phase relationships concerning $\text{Ti}(\text{Fe},\text{Cr})_2$

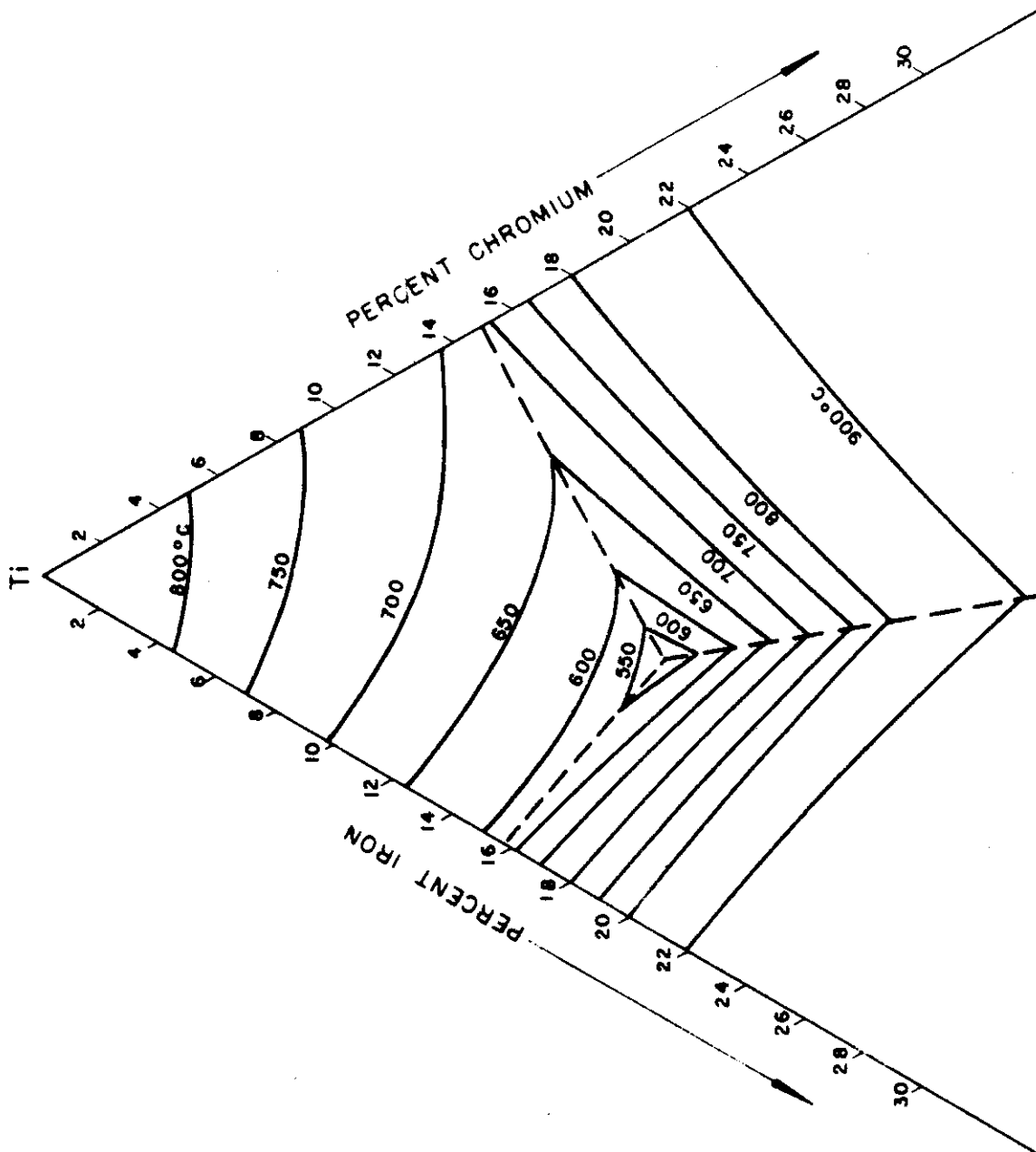


Fig. 8 - Isotherms of the Lower Surfaces of the Beta Phase Space in the Ti-Cr-Fe System

TABLE II

ADDITIONAL ALLOYS PREPARED TO POSITION THE TERNARY EUTECTOID POINT

Compositions
(Weight Per Cent)

<u>Ti</u>	<u>Cr</u>	<u>Fe</u>
83	2	15
82	2	16
82	5	13
81	5	14
80	5	15
79	5	16
79	8	13
81	9	10
79	11	10

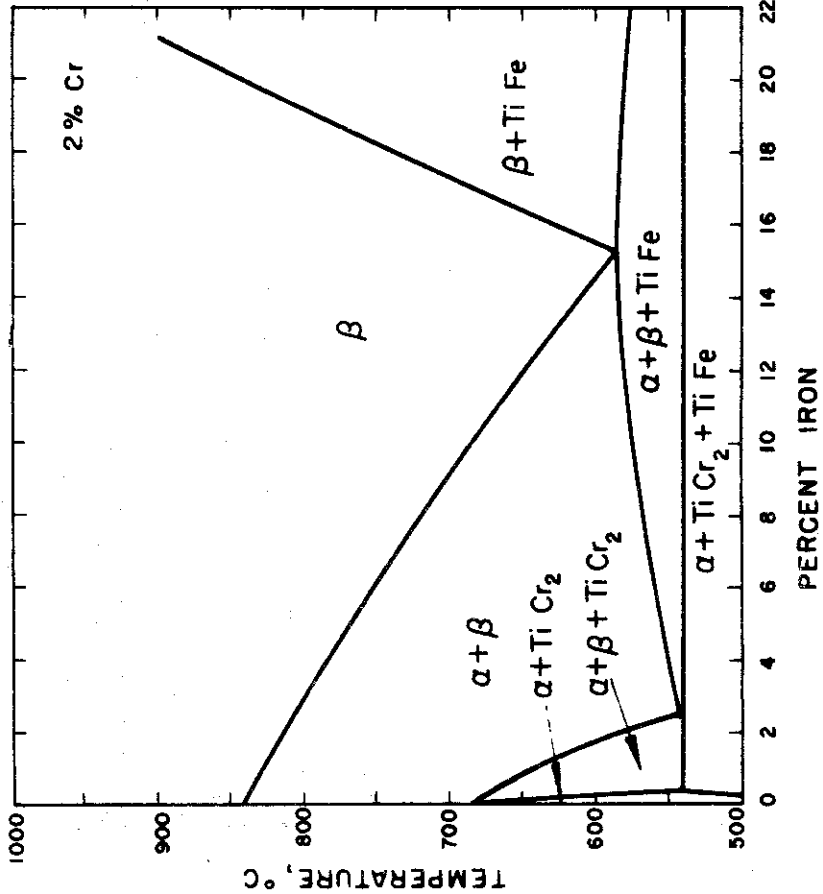
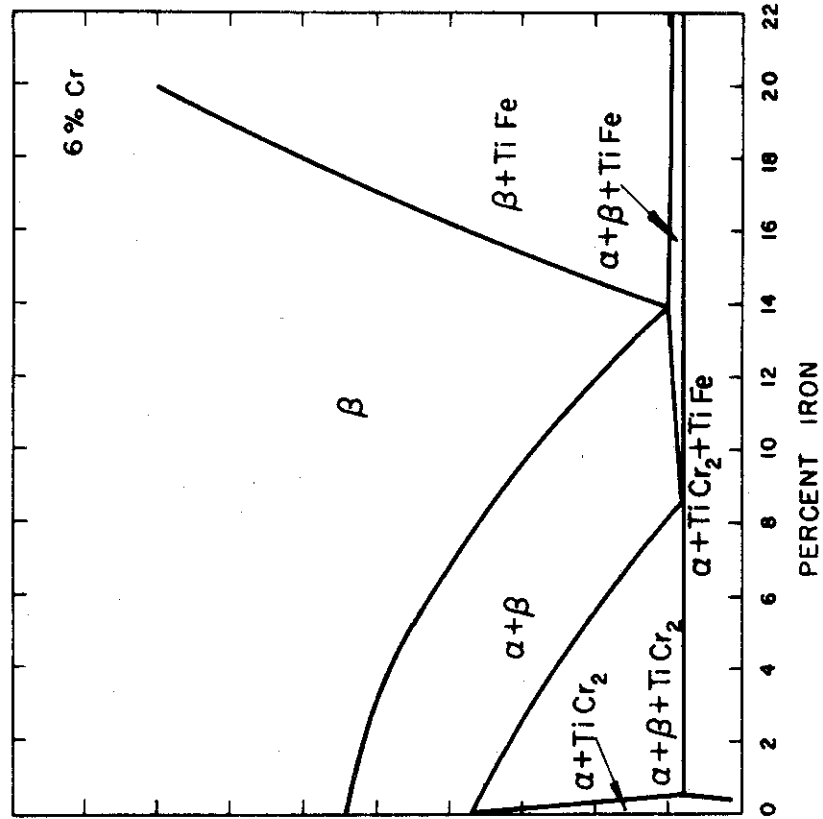


Fig. 9 - Vertical Sections of the Ti-Cr-Fe System at Constant Chromium Contents

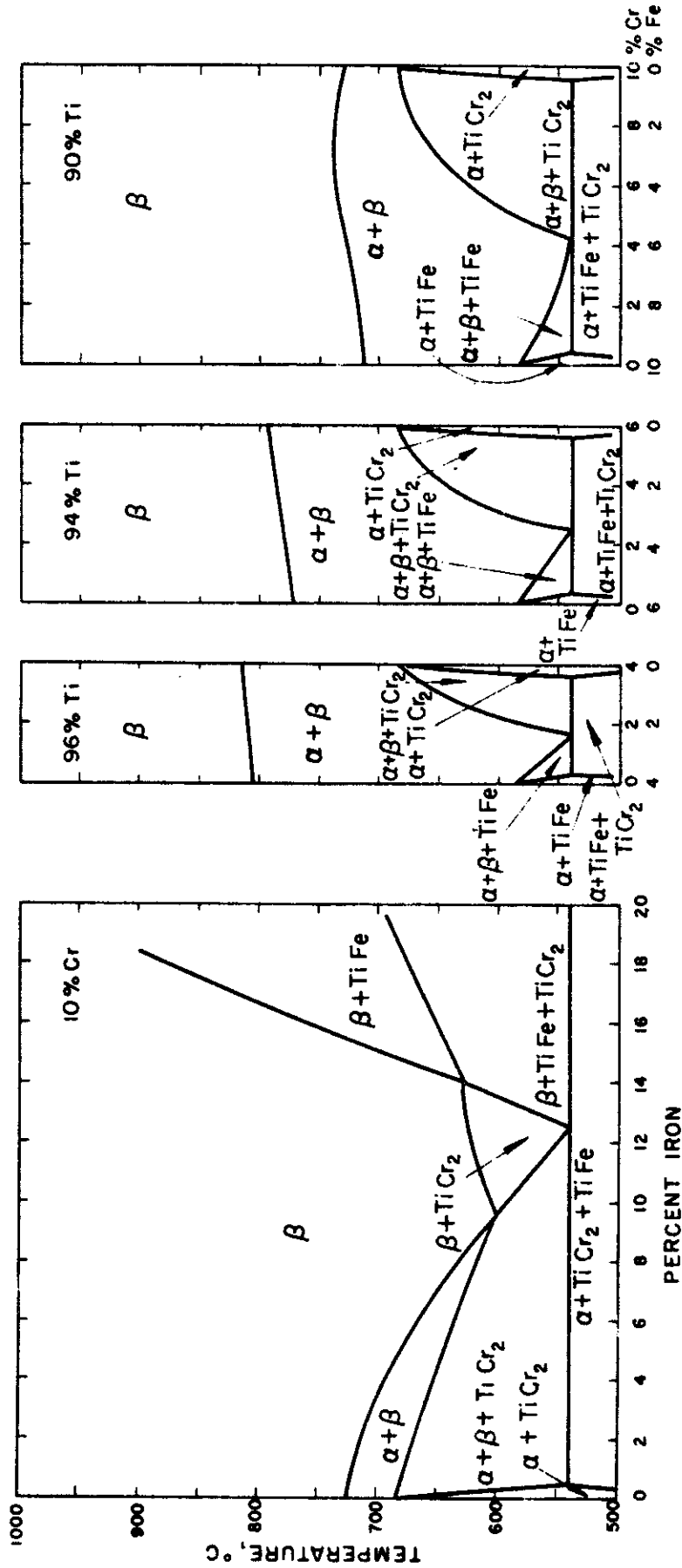


Fig. 10 - Vertical Sections of the Ti-Cr-Fe System at Constant Chromium and Titanium Contents

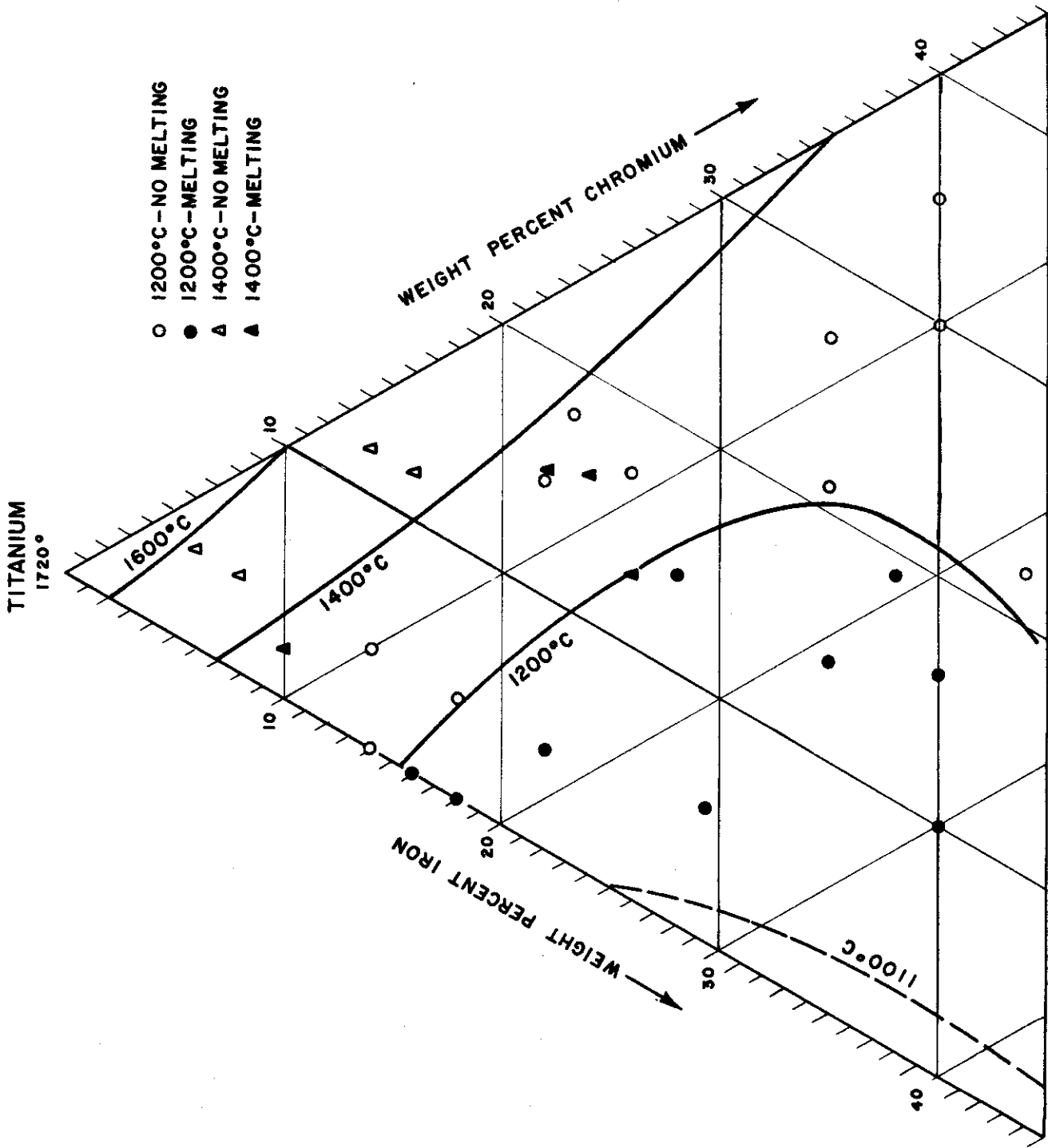


Fig. 11 - Isotherms of the Solidus Surface of the Ti-Cr-Fe System.

Conclusions

(the designation $Ti(Fe,Cr)_2$, will be used to describe the ternary phase of hexagonal structure) were studied.

Approximately 20 samples of high alloy content, the compositions of which are shown as data points in Figure 12, were annealed at several temperature levels between 1000° and 500°C. However, the 800°C isotherm will serve to illustrate the equilibria involved. As there are no metallographic differences between $TiCr_2$ and $Ti(Fe,Cr)_2$, x-ray diffraction was the principal method used to identify the phases. Micrographic analysis was used where it was helpful, such as for the identification of samples in the ($\beta + TiFe + Ti(Fe,Cr)_2$) field.

X-ray diffraction data for the group of alloys with compositions spaced along a tie line between $TiFe_2$ (70% Fe) and $TiCr_2$ (66% Cr) were obtained. Samples were annealed at temperatures between 1300° and 500°C for 1/2 hour to 29 days. All alloys treated were found to consist of only the hexagonal phase, $Ti(Fe,Cr)_2$ above 1100°C. A summary of the lattice parameter measurements is shown in Table III. The polymorphic transformation of $TiCr_2$ was found to occur between 1000° and 1100°C.

The data shown in Table III are plotted in Figure 13; smooth curves were obtained for both lattice parameter values at elevated temperatures. This proves the existence of a continuous series of solid solutions between $TiFe_2$ and hexagonal $TiCr_2$. Parameter values for a given alloy in the one phase field at different temperature levels were in close agreement. A break occurs in the lattice parameter curves (particularly a) at the chromium-rich side with lowered temperature. This is due to the appearance of the two phase field ($TiCr_2 + Ti(Fe,Cr)_2$), and hence the composition of the hexagonal phase in equilibrium with the cubic phase remains the same. Figure 14 schematically illustrates the vertical section through the two compounds. The limits of the $Ti(Fe,Cr)_2$ space lie close to the chromium-rich side of the diagram at all temperatures.

The 800°C isotherm, given in Figure 12, is based on x-ray data (Table IV) and metallographic observations. It is evident that the phase relationships are more complex than those shown in Figure 2. They indicate that the beta phase is in equilibrium with both $TiCr_2$ and $Ti(Fe,Cr)_2$ at 800°C. However, the locations of the α , ($\alpha + \beta$) and β spaces, on which most of the effort has been concentrated, are not affected by these findings.

The corners of the phase field ($\beta + TiFe + Ti(Fe,Cr)_2$) are located at the saturated beta phase, at $TiFe$ and at approximately the composition 58% Cr-8% Fe, representing the $Ti(Fe,Cr)_2$ phase. The latter value was obtained by comparing the lattice parameters of the $Ti(Fe,Cr)_2$ phase of alloys in the three phase field (Table IV) with those in the section $TiFe_2-TiCr_2$ (Figure 13). The other three phase field ($\beta + TiCr_2 + Ti(Fe,Cr)_2$) was located as shown, because the structure of the 35% Cr-5% Fe alloy was found by x-ray diffraction to consist of the three phases.

Upon examination of the 800°C isotherm, it is recognized that additional phase relationships will occur below this temperature. As there are four phases in equilibrium with beta at 800°C, a reaction must occur to eliminate one of the phases above the temperature of the ternary eutectoid. Otherwise,

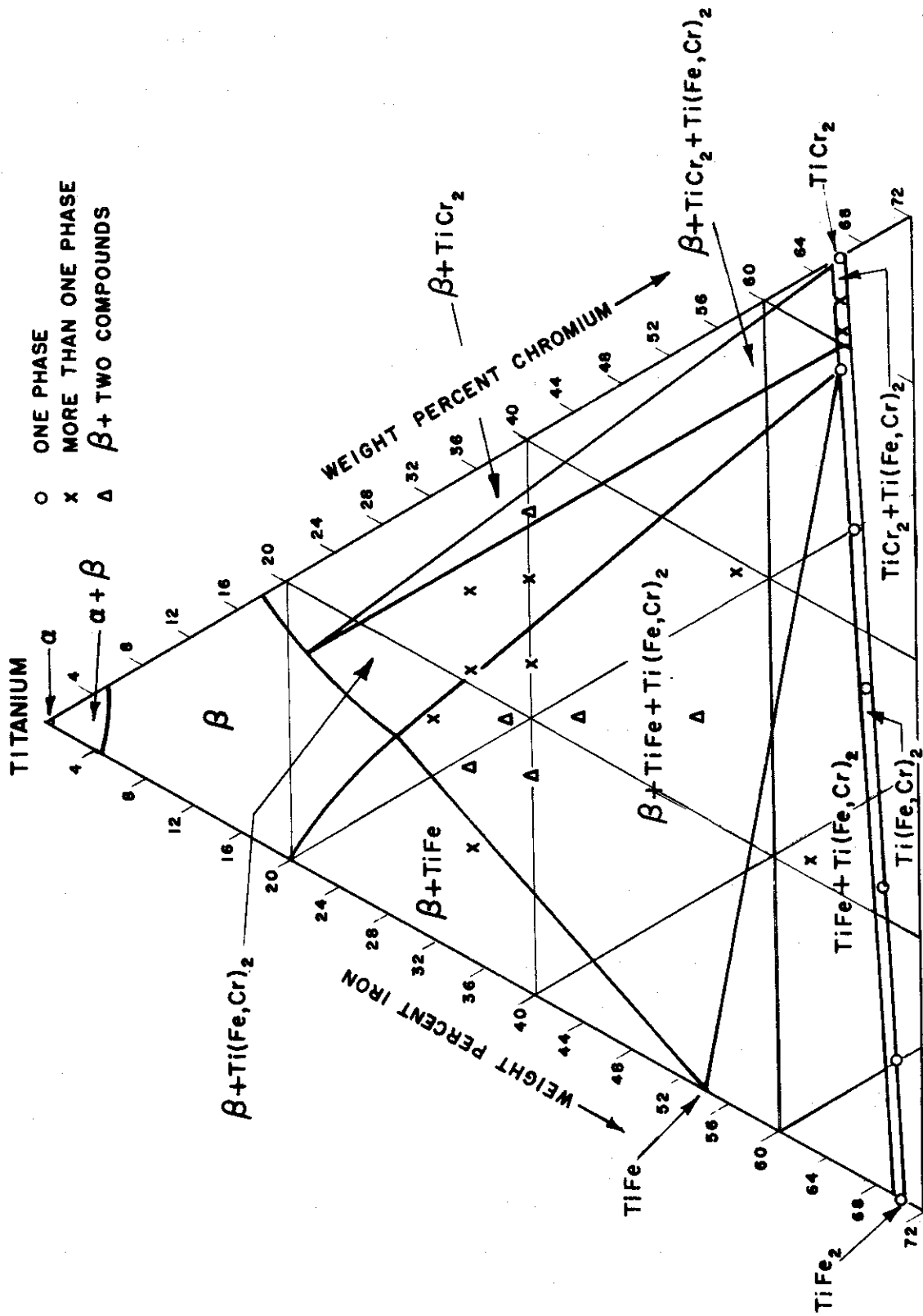


Fig. 12 - Partial Isothermal Section at 800°C of the Ti-Cr-Fe System.

TABLE III

X-RAY DIFFRACTION DATA FOR ALLOYS LYING ON THE SECTION $TiCr_2-TiFe_2$

Compositions (Wt. %)			Annealing Treatment		Phases Observed	Lattice Parameters of $Ti(Fe,Cr)_2$					
Ti	Cr	Fe	(°C)	(Hrs.)		c(kX)	a(kX)	c/a			
34	66	0	1300	1/2	$TiCr_2$ (Hex.)	7.987	4.919	1.624			
			1200	1/2	$TiCr_2$ (Hex.)						
			1200	15	$TiCr_2$ (Hex.)						
			1100	1	$TiCr_2$ (Hex.)						
			1100	30	$TiCr_2$ (Hex.)						
			1000	2	$TiCr_2$ (Hex.) + $TiCr_2$ (Cubic)						
			1000	40	$TiCr_2$ (Cubic)						
			900	22	$TiCr_2$ (Cubic)						
34	63	3	800	11/4	$Ti(Fe,Cr)_2$ + $TiCr_2$	7.976	4.899	1.628			
			700	288	$Ti(Fe,Cr)_2$				7.976	4.900	1.628
34	61	5	800	11/4	$Ti(Fe,Cr)_2$ + $TiCr_2$	7.983	4.899	1.630			
			600	576	$Ti(Fe,Cr)_2$ + $TiCr_2$				7.971	4.900	1.627
			500	696	$Ti(Fe,Cr)_2$						
34	58	8	1000	30	$Ti(Fe,Cr)_2$	7.985	4.898	1.630			
			800	170	$Ti(Fe,Cr)_2$				7.976	4.896	1.629
			700	288	$Ti(Fe,Cr)_2$				7.967	4.894	1.628
			600	576	$Ti(Fe,Cr)_2$				7.974	4.896	1.629
33	47	20	1000	30	$Ti(Fe,Cr)_2$	7.963	4.861	1.638			
			800	170	$Ti(Fe,Cr)_2$				7.968	4.862	1.639
			600	11/4	$Ti(Fe,Cr)_2$						
32	36	32	1000	30	$Ti(Fe,Cr)_2$	7.925	4.839	1.638			
			800	170	$Ti(Fe,Cr)_2$				7.928	4.838	1.639
			600	11/4	$Ti(Fe,Cr)_2$						
31	22	47	600	11/4	$Ti(Fe,Cr)_2$	7.869	4.812	1.635			
30	10	60	600	11/4	$Ti(Fe,Cr)_2$	7.806	4.780	1.633			
30	0	70	1000	30	$TiFe_2$	7.808	4.783	1.632			
			800	170	$TiFe_2$						
			600	11/4	$TiFe_2$				7.806	4.780	1.633

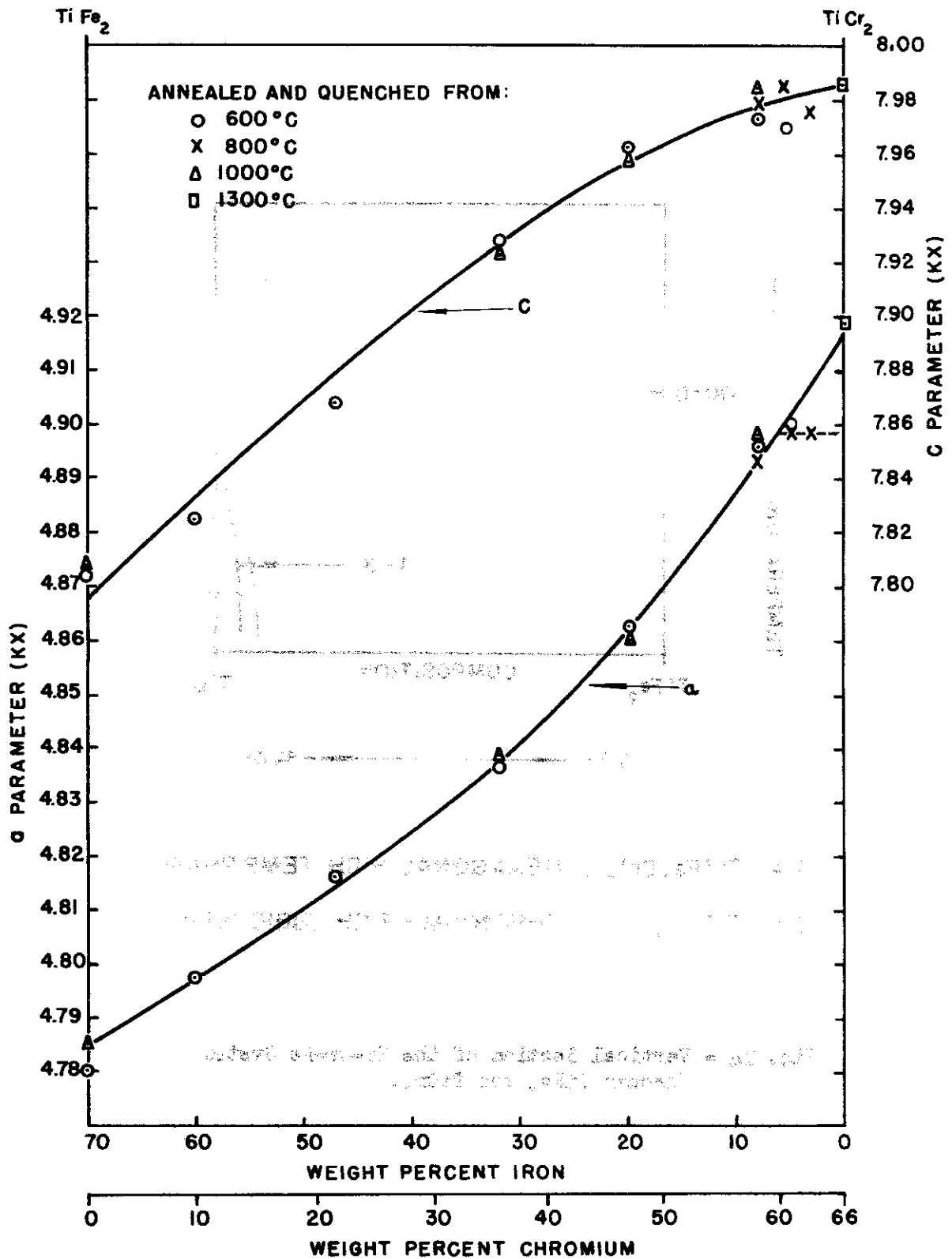
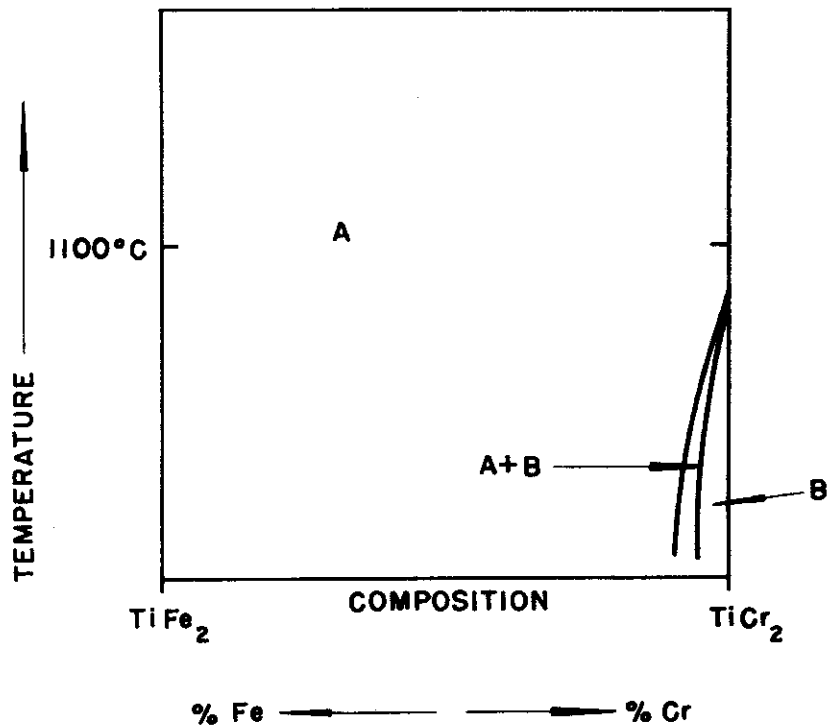


Fig. 13 - Lattice Parameters of the Hexagonal $Ti(Fe,Cr)_2$ Phase



A = $Ti(Fe, Cr)_2$; HEXAGONAL HIGH TEMP. PHASE

B = $TiCr_2$; CHROMIUM - RICH CUBIC PHASE

Fig. 114 - Vertical Section of the Ti-Cr-Fe System Through $TiFe_2$ and $TiCr_2$.

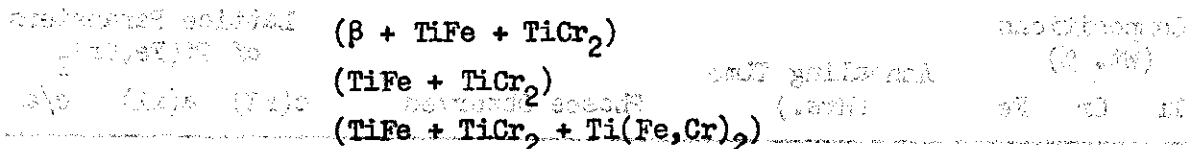
TABLE IV
X-RAY DIFFRACTION IDENTIFICATION OF PHASES PRESENT
IN Ti-Cr-Fe ALLOYS ANNEALED AT 800°C

Compositions (Wt. %)			Annealing Time (Hrs.)	Phases Observed	Lattice Parameters of Ti(Fe,Cr) ₂		
Ti	Cr	Fe			c(kX)	a(kX)	c/a
34	63	3	144	Ti(Fe,Cr) ₂ + TiCr ₂	7.976	4.899	1.628
34	61	5	144	Ti(Fe,Cr) ₂ + TiCr ₂	7.983	4.899	1.630
60	35	5	144	β + TiCr ₂ + Ti(Fe,Cr) ₂			
34	58	8	170	Ti(Fe,Cr) ₂	7.976	4.896	1.629
60	30	10	144	β + Ti(Fe,Cr) ₂			
60	24	16	144	β + Ti(Fe,Cr) ₂			
68	16	16	144	β + Ti(Fe,Cr) ₂			
43	39	18	144	Ti(Fe,Cr) ₂	7.999	4.893	1.635
33	47	20	170	Ti(Fe,Cr) ₂			
65	14	21	144	β + TiFe			
56	22	22	144	β + TiFe + Ti(Fe,Cr) ₂	7.988	4.905	1.630
32	36	32	170	Ti(Fe,Cr) ₂			
37	21	42	144	TiFe + Ti(Fe,Cr) ₂	7.904	4.849	1.631
30	0	70	170	TiFe ₂			

Contrails

five phases would be in equilibrium at the ternary eutectoid temperature and this is theoretically impossible in a ternary system.

If a four phase reaction, $\beta + \text{Ti}(\text{Fe},\text{Cr})_2 \rightleftharpoons \text{TiFe} + \text{TiCr}_2$, takes place at a temperature slightly below 800°C, an isothermal section similar to that shown in Figure 15 would result. Such a reaction will involve all alloys located within the area consisting of the following phase fields shown in Figure 15:



In alloys lying on the low titanium side of a tie line extending between TiFe and TiCr₂, beta will be consumed under equilibrium conditions and the other three phases remain. In compositions on the high titanium side of the tie line, Ti(Fe,Cr)₂ will be consumed and the phase space (beta + TiFe + TiCr₂) results. Comparing Figure 15 with Figure 2, it can be seen that the phase relationships are the same in the titanium-rich portion. Therefore, the isothermal sections at this unknown temperature and at lower temperatures would be correct as previously drawn.

To determine the temperature at which Ti(Fe,Cr)₂ is no longer in equilibrium with beta, alloys located at the chromium-rich side of the (beta + TiFe + Ti(Fe,Cr)₂) field (Figure 12) were annealed at various temperatures and examined by x-ray diffraction analysis. The results are shown in Table V. The cubic modification of TiCr₂ was not observed in the samples at any temperature; hence, the assumption that the above proposed four phase reaction exists may be wrong or the reaction may be too sluggish to proceed even though long annealing times were used.

If the previously proposed four phase reaction does not occur, an alternate reaction, $\beta + \text{TiCr}_2 \rightleftharpoons \alpha + \text{Ti}(\text{Fe},\text{Cr})_2$, could proceed at a temperature between the binary Ti-Cr eutectoid temperature (675°C) and the ternary eutectoid temperature (540°C). If this reaction should occur, a section similar to that shown in Figure 16 would result. Below the temperature of this reaction, the "binary" eutectoid decomposition on the chromium side would be $\beta \rightleftharpoons \alpha + \text{Ti}(\text{Fe},\text{Cr})_2$ and the ternary eutectoid would consist of (alpha + TiFe + Ti(Fe,Cr)₂).

Had a ternary eutectoid reaction taken place, identification of the phases present could have yielded the information as to whether either TiCr₂ or Ti(Fe,Cr)₂ was eliminated above the ternary eutectoid temperature. As discussed previously, no observable decomposition of the beta phase was obtained. For simplicity, it was assumed that the eutectoid decomposition of the ternary beta involved the phases alpha, TiFe and TiCr₂.

f. Microstructures

Only a limited number of photomicrographs are presented as, in general, the microstructures observed were similar to those of the binary alloys (3,4). The low solubility of chromium and iron in alpha titanium is indicated by the

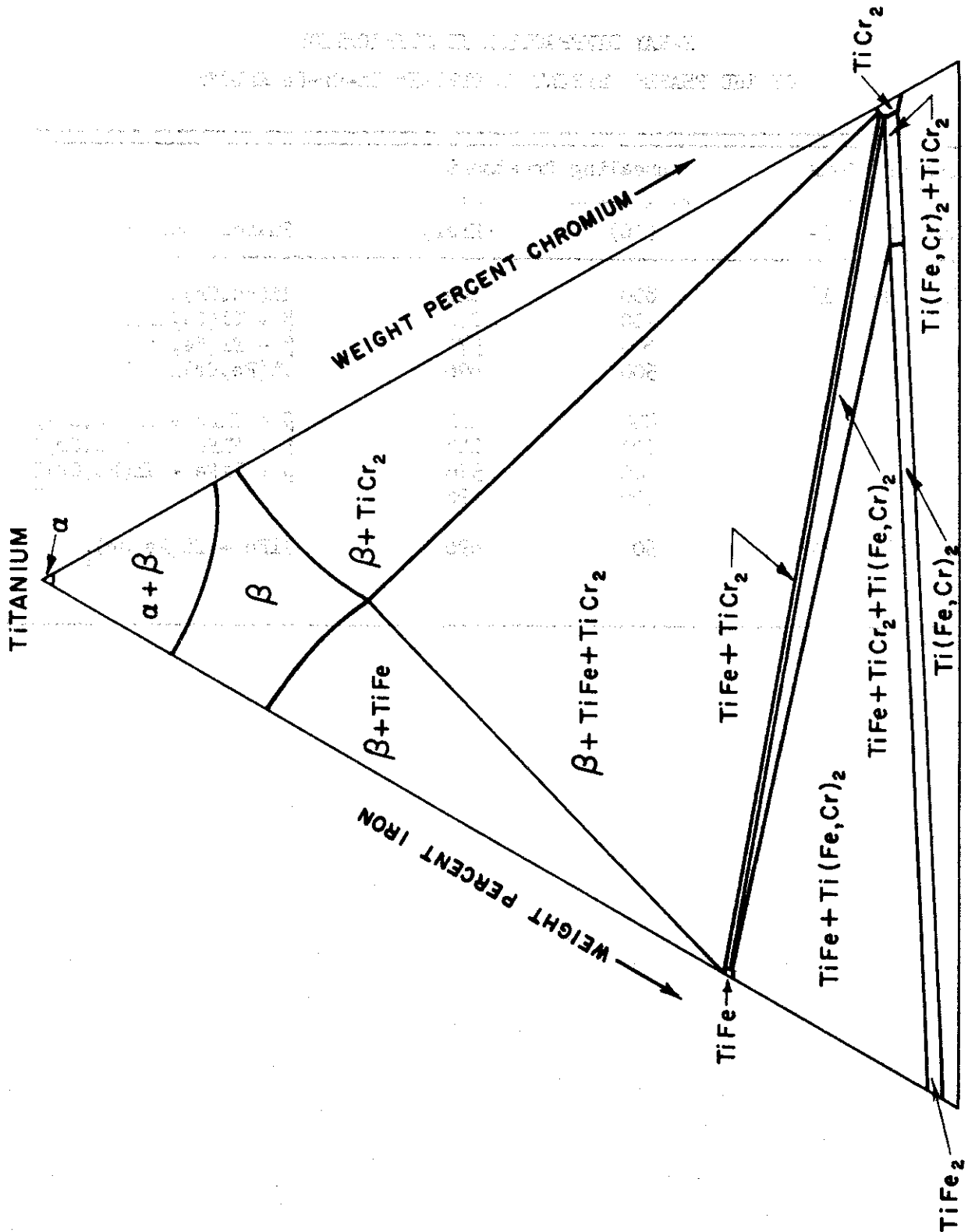


Fig. 15 - Hypothetical Partial Isothermal Section at Some Temperature Below 800°C of the Ti-Cr-Fe System.

Contrails

TABLE V
X-RAY DIFFRACTION IDENTIFICATION
OF THE PHASES PRESENT IN CERTAIN Ti-Cr-Fe ALLOYS

Compositions (Wt. %)			Annealing Treatment		Phases Observed
Ti	Cr	Fe	Temperature (°C)	Time (Hrs.)	
43	39	18	800	114	Ti(Fe,Cr) ₂
			700	288	β + Ti(Fe,Cr) ₂
			600	576	β + Ti(Fe,Cr) ₂
			500	696	Ti(Fe,Cr) ₂
56	22	22	800	114	β + TiFe + Ti(Fe,Cr) ₂
			700	288	β + TiFe + Ti(Fe,Cr) ₂
			600	576	β + TiFe + Ti(Fe,Cr) ₂
			500	696	
46	27	27	500	696	TiFe + Ti(Fe,Cr) ₂

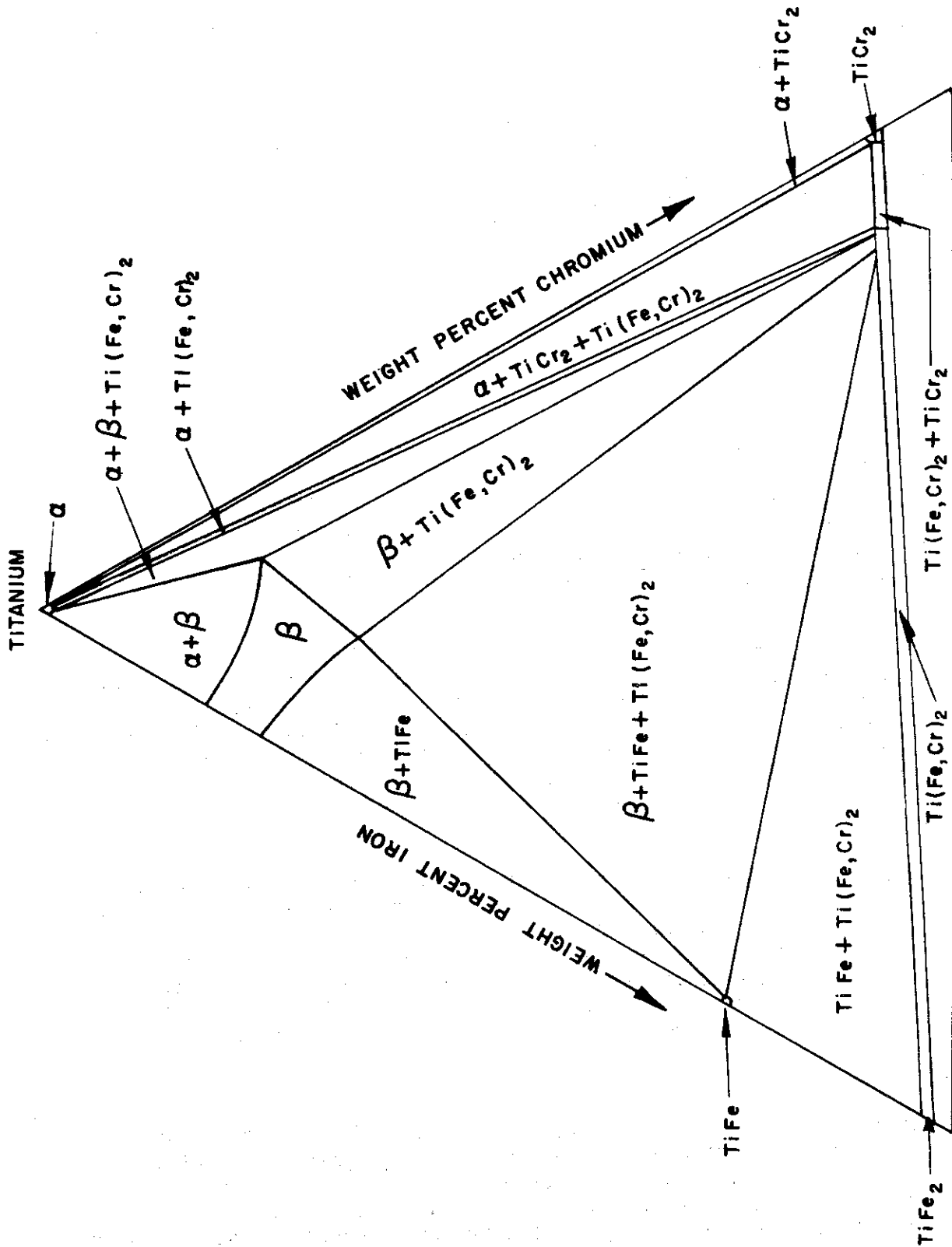


Fig. 16 - Hypothetical Partial Isothermal Section of the Ti-Cr-Fe System at Some Temperature Between 675° and 540°C.

Contrails

duplex structure of Figure 17. Figure 18 illustrates the eutectoid structures observed in the ($\alpha + \beta + \text{TiCr}_2$) space. As previously discussed in another section, there was no microstructural evidence of eutectoid in the ($\alpha + \beta + \text{TiFe}$) space. Also, no ternary eutectoid was noted at 500°C, although this temperature is below the ternary eutectoid plane. The $\text{Ti}(\text{Fe,Cr})_2$ phase is illustrated in Figure 19.

Figure 20 shows the microstructure of an alloy annealed at 800°C in the ($\beta + \text{TiFe} + \text{Ti}(\text{Fe,Cr})_2$) space. An x-ray diffraction pattern of this sample confirmed the metallographic evidence of the two intermediate phases. To differentiate between the coexisting intermediate phases, staining etchants were tested. Ten per cent aqueous solutions of the following etchants were used:

- H_2CrO_4 , swabbed and electrolytic
- KCN, swabbed
- $\text{K}_2\text{Cr}_2\text{O}_7$, swabbed
- KMnO_4 , swabbed
- $\text{K}_3\text{Fe}(\text{CN})_6 + \text{NaOH}$, swabbed and electrolytic

Of the many etchants tried, electrolytic etching with the $\text{K}_3\text{Fe}(\text{CN})_6 + \text{NaOH}$ solution was the most useful. The polished samples were etched first with a $\text{HNO}_3 + \text{HF} + \text{glycerine}$ solution (Figure 20) and were then electrolytically etched with the $\text{K}_3\text{Fe}(\text{CN})_6 + \text{NaOH}$ solution, preferentially staining $\text{Ti}(\text{Fe,Cr})_2$ (Figure 21).

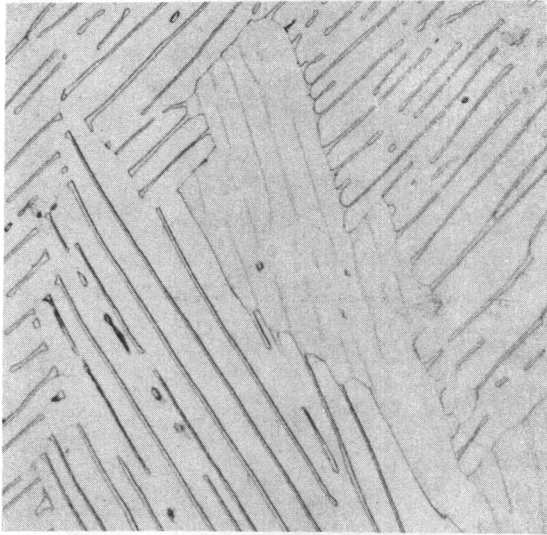
A size difference may be noted in Figure 20; $\text{Ti}(\text{Fe,Cr})_2$ is larger with the smaller TiFe crystals surrounding it. In order to prove that the differential staining in Figure 21 is due to the different phases present and not just size variations, binary alloys containing either TiCr_2 or TiFe were stained. Both alloys were polished and etched under conditions identical to those used in the preparation of Figure 21. Figures 22 and 23 conclusively show that TiCr_2 is heavily stained whereas the TiFe is unaffected by the $\text{K}_3\text{Fe}(\text{CN})_6 + \text{NaOH} + \text{H}_2\text{O}$ etchant.

As another technique of differentiating between the two compounds, heat tinting was tried. With this method a sample previously polished is placed in a preheated furnace with an air atmosphere. At 700°C, the only temperature investigated, 40 seconds appeared to be the best time. Shorter times resulted in little tinting, whereas longer times produced deeper tints that masked the true structure. By heat tinting it was possible to differentiate between the two compounds, but stain etching was found to give better results.

g. Hardness

Vickers hardness data of Ti-Cr-Fe alloys annealed at and quenched from temperatures between 1000° and 650°C are presented graphically in Figure 24. The alloys used are on the vertical section through the ternary system at the Cr:Fe ratio of 1:1. These alloys exhibit the same trends observed in the binary systems Ti-Cr and Ti-Fe (3,4). The hardness curves for samples water

Contrails

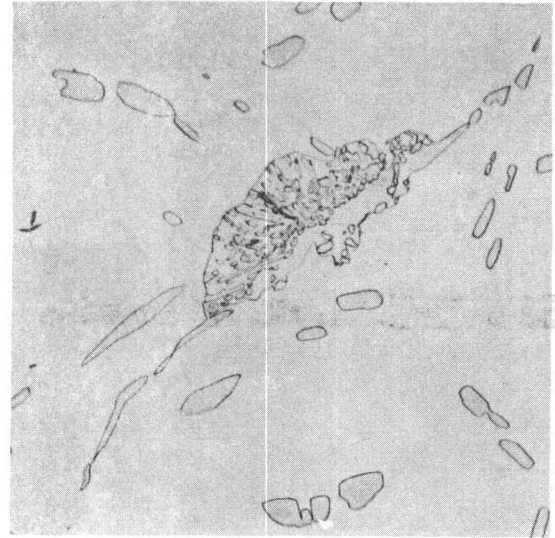


Neg. No. 3881

X 500

Fig. 17

A 0.5% Cr-0.5% Fe alloy, water quenched after annealing at 650°C for 432 hours. Alpha + retained beta (smaller amount).

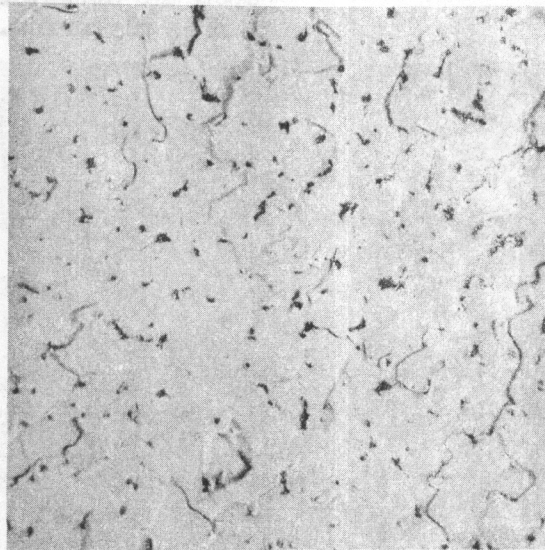


Neg. No. 3885

X 500

Fig. 18

A 12% Cr-2% Fe alloy, annealed at 650°C for 432 hours and water quenched. Eutectoid ($\alpha + \text{TiCr}_2$) and primary α in a matrix of retained β .



Neg. No. 7089

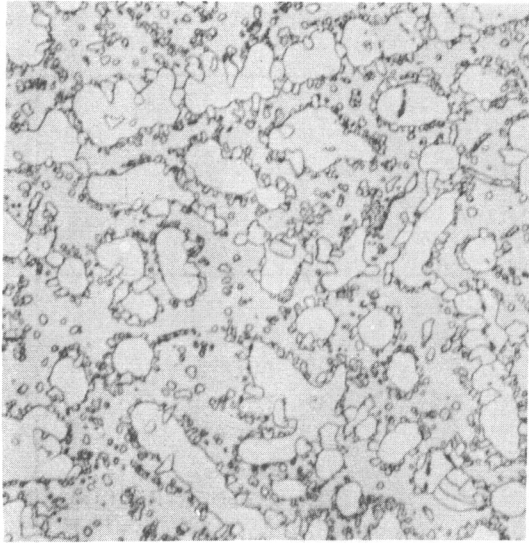
X 500

Fig. 19

A 47% Cr-20% Fe alloy, water quenched after annealing at 800°C for 144 hours. Nearly single phase, $\text{Ti}(\text{Fe},\text{Cr})_2$.

Etchant: 60 glycerine, 20 HNO_3 , 20 HF

Contrails

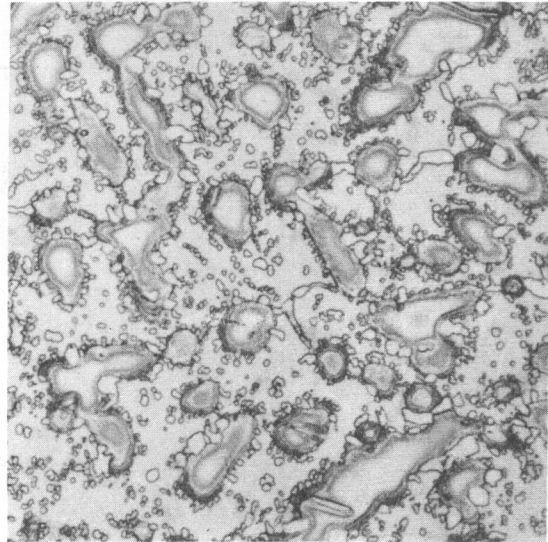


Neg. No. 5256

X 750

Fig. 20

A 22% Cr-22% Fe alloy, annealed at 800°C for 144 hours and water quenched. $Ti(Fe,Cr)_2$ (larger crystals) and $TiFe$ in a matrix of β . Etchant: $HNO_3 + HF +$ glycerine.

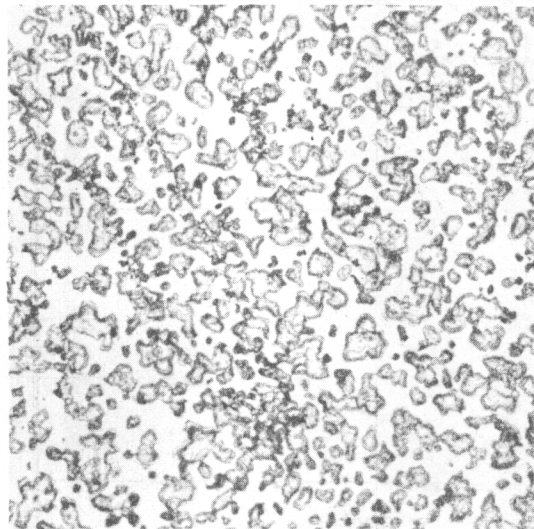


Neg. No. 5257

X 750

Fig. 21

The same microstructure as Fig. 20. $Ti(Fe,Cr)_2$ is now stained although $TiFe$ is not. Etchant: electrolytic $K_3Fe(CN)_6 + NaOH + H_2O$ superimposed upon the structure etched with $HNO_3 + HF +$ glycerine.

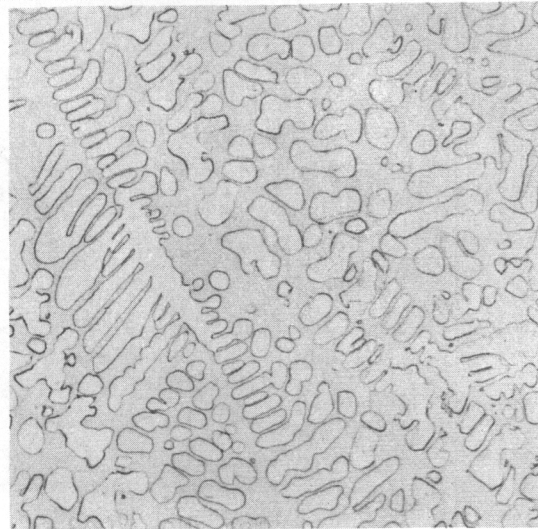


Neg. No. 5270

Fig. 22

X 750

A 50% Cr alloy, water quenched after 24 hours at 1000°C. Beta and unstained $TiFe$. Etchant: Same as Fig. 21.



Neg. No. 5269

Fig. 23

X 750

A 40% Fe alloy, annealed the same as Fig. 22. Beta and unstained $TiFe$. Etchant: Same as Fig. 21.

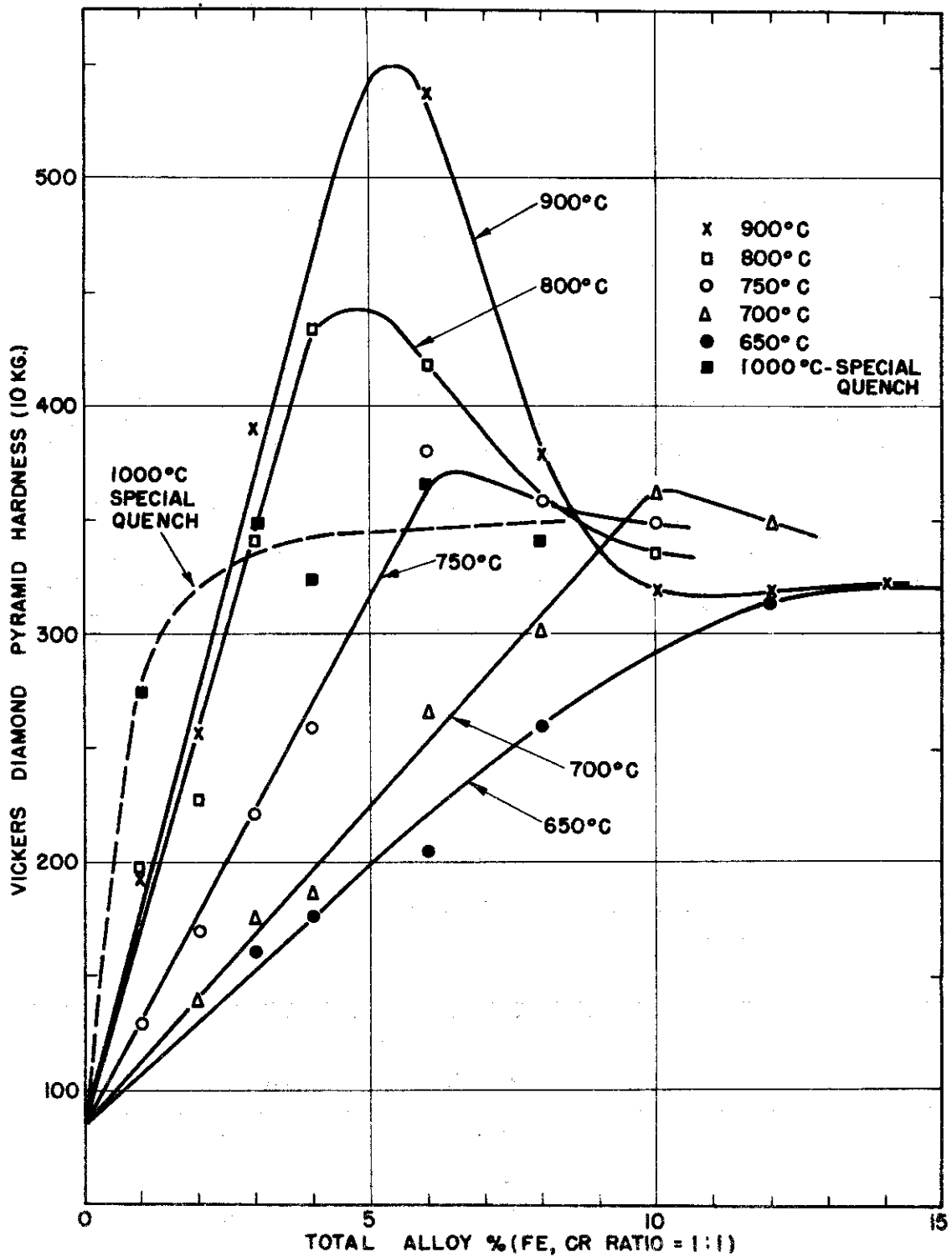


Fig. 2h - Vickers Hardness of Ti-Cr-Fe Alloys (Fe, Cr Ratio = 1:1).

Contrails

quenched from above 800°C reach a peak at about 5% total alloy content, which corresponds to the composition at which beta is retained upon water quenching. In the binary alloys, hardness peaks at 7% Cr and 4% Fe were obtained on quenching from the beta field.

Annealing the ternary alloys at 650° or 700°C resulted in a linear increase in hardness with total alloy content up to 10%. Such alloys have ($\alpha + \beta$) structures, and are much softer than the product, beta prime, obtained by quenching from above the transformation temperature. It can be seen from Figure 24 that the hardness of alloys in the lower composition range, i.e., those in the commercial alloy region, may be very greatly changed by heat treatment. The hardness of the 5% alloy annealed at 650°C is 200 DPH, but quenching the same alloy from 900°C resulted in a hardness of over 500 DPH.

With very rapid quenching from the beta field, the high hardness peak is eliminated. Samples were annealed at 1000°C for 15 minutes and rapidly quenched into an iced 10% NaOH solution. The specimen size was approximately 1/8 in. by 1/8 in. by 1/16 in. Similar results have been obtained with binary Ti-Cr alloys (14). Temperatures as low as 100°C have been found by Parris, et al., to result in age hardening of metastable beta in the Ti-Mn and Ti-Cr systems (15). Similar results have been obtained at the Armour Research Foundation with binary Ti-Cr alloys. The hardness of alloys annealed at 1000°C for 30 minutes and rapidly quenched into an iced 10% NaOH solution, before and after mounting in bakelite (150°C), are presented in Table VI. As a very drastic quench is needed to eliminate the hardness peak, probably commercial applications involving larger sections will not make use of this heat treatment.

TABLE VI
VICKERS HARDNESS OF Ti-Cr ALLOYS
ANNEALED AT 1000°C AND RAPIDLY QUENCHED

Wt. % Cr	Hardness	
	As Quenched	After Mounting
2	292	276
3	266	285
5	266	299
7	227	417
9	256	405
11	304	

B. The Ti-Al-O and Ti-Al-N Systems - by R. J. Van Thyne

1. Experimental Procedure

a. Alloy Preparation

Oxygen and nitrogen were added during ingot preparation as master alloys. An oxygen master alloy containing 25% oxygen was prepared by melting iodide titanium and pressed titanium dioxide (40% O) powder. The Ti-25% O alloy is more easily handled during weighing and charging than the pressed TiO₂ powder.

Chemical analysis indicated that titanium-nitride received from an outside source contained large amounts of impurities (2.7% calcium). Therefore, a master alloy containing approximately 12% nitrogen was prepared by melting nitrated sponge titanium. As the sponge melted with difficulty, the alloy was diluted by the addition of titanium to lower the melting point. The chemical analysis of the final alloy was 6.69% nitrogen.

Both master alloys are friable and were used as -8 +16 mesh lumps resulting from crushing the ingots. Melting the 10-gram Ti-Al-O and Ti-Al-N compositions five times produced homogeneous ingots. Previous work with similar alloys showed that actual compositions follow nominal compositions closely. Weight loss data and chemical analysis proved this to be true.

b. Annealing Treatments

Information on the annealing times used for various temperatures is given in Table VII.

TABLE VII
ANNEALING CONDITIONS FOR Ti-Al-(O and N) ALLOYS

Temperature, °C	Time, Hours	Temperature, °C	Time, Hours
1250	6	1000	36
1200	8	950	48
1100	18	900	72
1050	24		

2. Discussion of Results

a. The Phase Diagrams

Figures 25 and 26 illustrate partial vertical sections through the Ti-Al-O and Ti-Al-N space models, respectively. The phase diagrams were constructed placing emphasis on the binary intercepts of the previously determined Ti-Al (16) and Ti-O (17) systems. As can be seen, both oxygen and nitrogen raise the $\beta/\alpha + \beta$ space boundary and widen the $(\alpha + \beta)$ field of the Ti-Al system. Nitrogen raises the $\beta/\alpha + \beta$ boundary appreciably more than oxygen. No attempt was made to locate the $\beta/\alpha + \beta$ boundary for alloys containing 1% nitrogen.

Microstructures of Ti-Al-N alloys containing 0.25% nitrogen are presented in Figures 27 to 29. They depict the β , $(\alpha + \beta)$ and α fields, respectively. The beta phase is not retained upon water quenching the Ti-Al-O or Ti-Al-N alloys but transforms to a serrated or acicular alpha prime structure. The addition of the interstitially soluble elements appears to refine the transformation structure.

b. Hardness

Vickers hardness data obtained for Ti-Al-O and Ti-Al-N alloys, annealed in the alpha field, are presented graphically in Figures 30 and 31, respectively. Considerable difficulty was encountered in getting reproducible values. Large differences in average values were produced by successively grinding out the old impressions and making new ones. For example, a series of values obtained by the latter method on a Ti-8% Al-1% O sample annealed at 900°C were 394, 435, 470 and 496 DPH. The reasons behind these hardness variations are not known but upon averaging the values for several temperature levels, correlatable data were obtained as illustrated in Figures 30 and 31.

The results show that for a given aluminum level, the hardness generally increases with increasing oxygen and nitrogen content; nitrogen has the greater hardening effect. Although not conclusive, previously determined data of the Ti-Al system indicated a peak hardness at about 11% aluminum for alloys annealed in the alpha field (4,16). The average hardness data of Ti-Al alloys annealed at 700° and 800°C are reproduced in the figures for comparison.

A hardness peak is apparent for all the curves in Figures 30 and 31. The composition of maximum hardness moves to lower aluminum contents with increasing amounts of the interstitial elements. One per cent nitrogen has the greatest effect; the maximum hardness of over 500 Vickers occurs at about 3 to 4% aluminum. A minimum in the curve for 1% nitrogen has been shown as a dashed line because only a few data points are available at these compositions and only this one curve exhibits the minimum. The curve may very likely be correct as it is expected that with increasing aluminum content the hardness curve for ternary alloys has a minimum similar to that obtained for the Ti-Al alloys. Data for the latter alloys indicates a minimum hardness at 16% aluminum. As the alpha field of the Ti-Al system extends to 25% aluminum at the temperature involved, and no phase changes are known to occur at lower temperatures, the reason for the indicated hardness minimum in the binary or ternary alloys is not known.

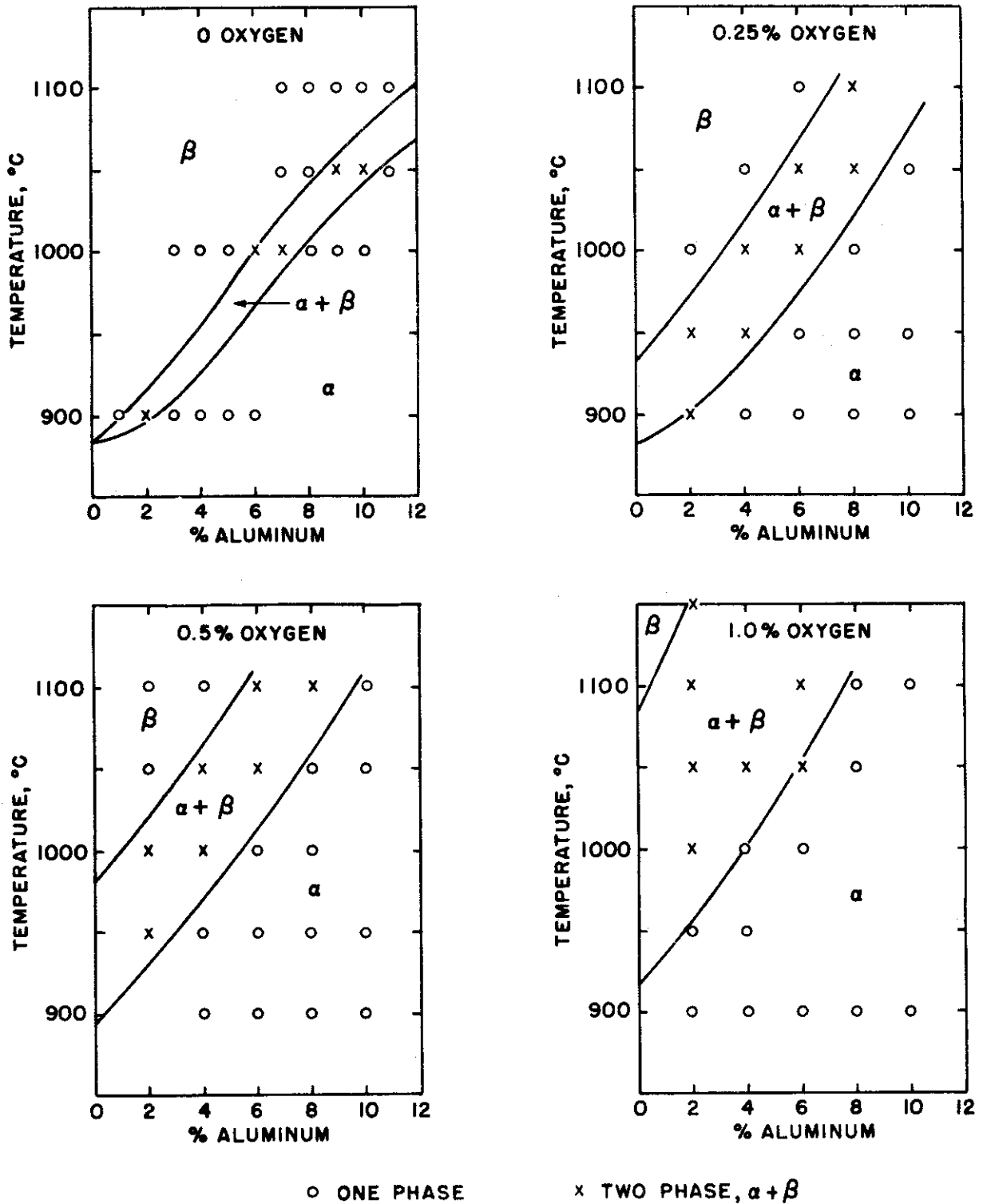


Fig. 25 - Vertical Sections at Constant Oxygen Content of the Partial Al-Al₂O₃ System

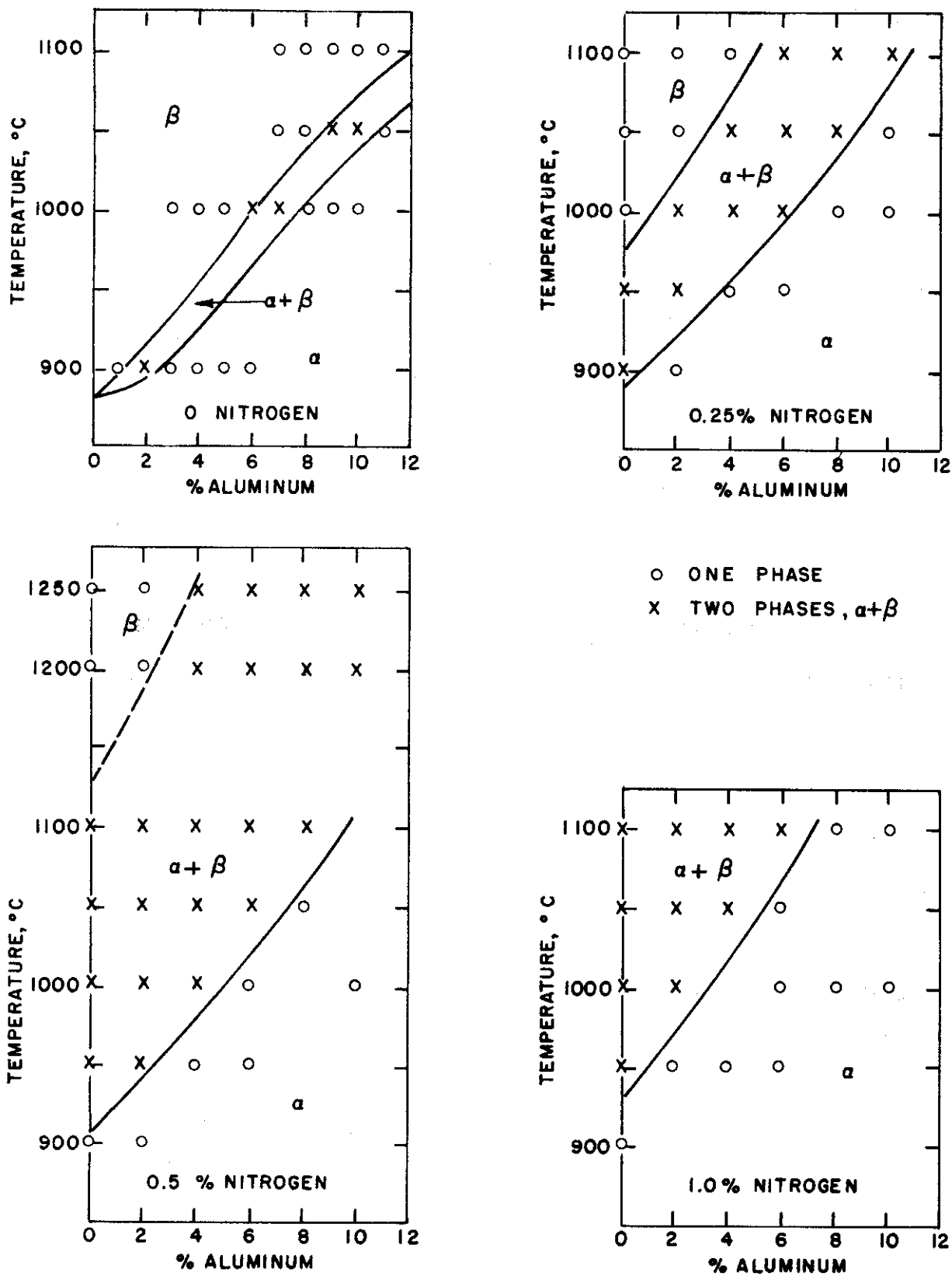


Fig. 26 - Vertical Sections at Constant Nitrogen Content of the Partial Ti-Al-N System

Contrails

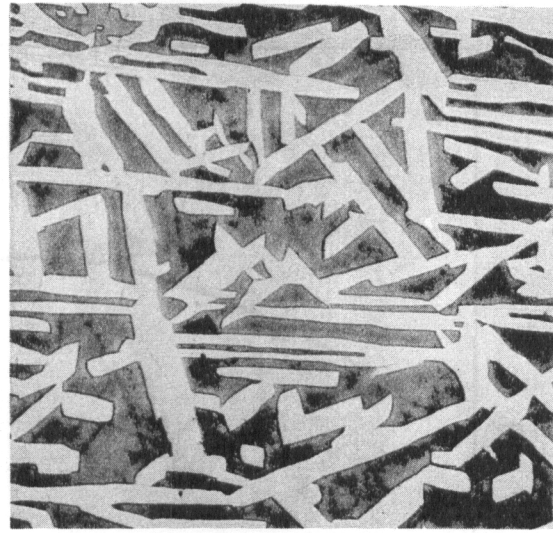


Neg. No. 7310

X 200

Fig. 27

A 2% Al-0.25% N alloy, water quenched after annealing at 1000°C for 24 hours. Transformed β .

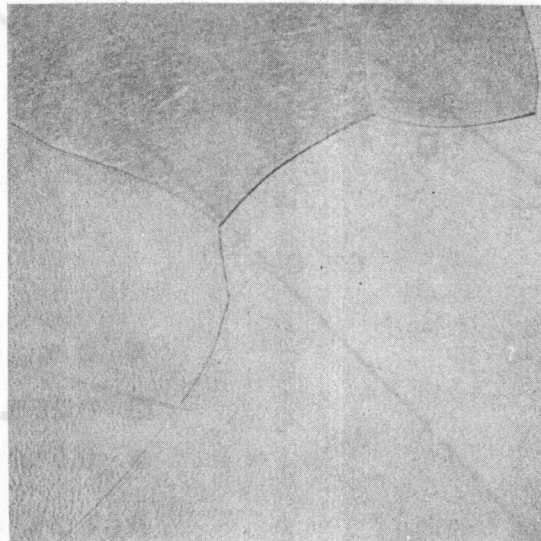


Neg. No. 7311

X 200

Fig. 28

A 6% Al-0.25% N alloy, treated the same as the sample of Fig. 27. ($\alpha + \beta$).



Neg. No. 7312

X 200

Fig. 29

A 10% Al-0.25% N alloy, treated the same as the specimen of Fig. 27. Large grained isothermal α .

Etchant: 60 glycerine, 20 HNO₃, 20 HF

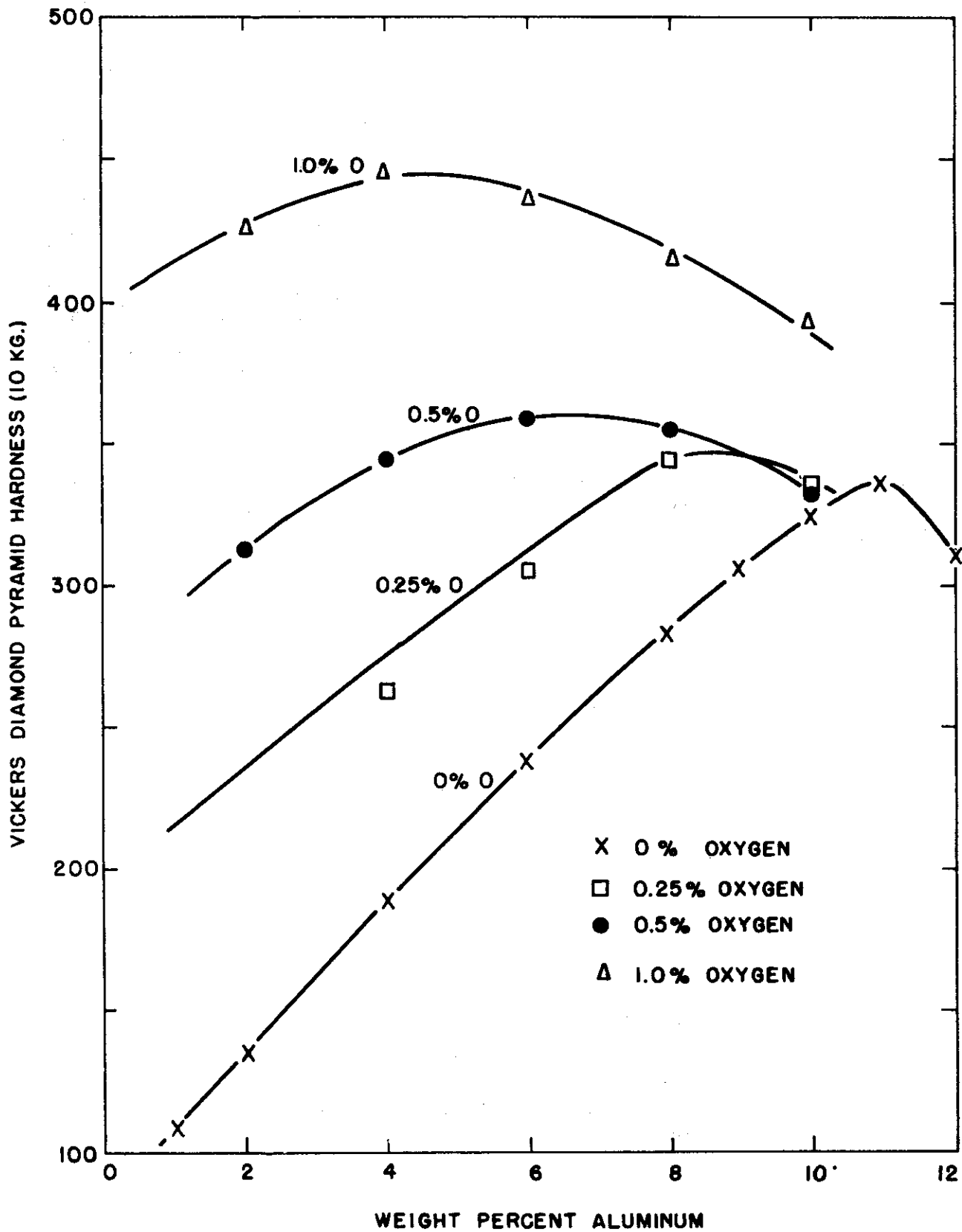


Fig. 30 - Average Vickers Hardness of Ti-Al-O Alloys Annealed in the Alpha Phase Space at Temperatures Between 900° and 1100°C.

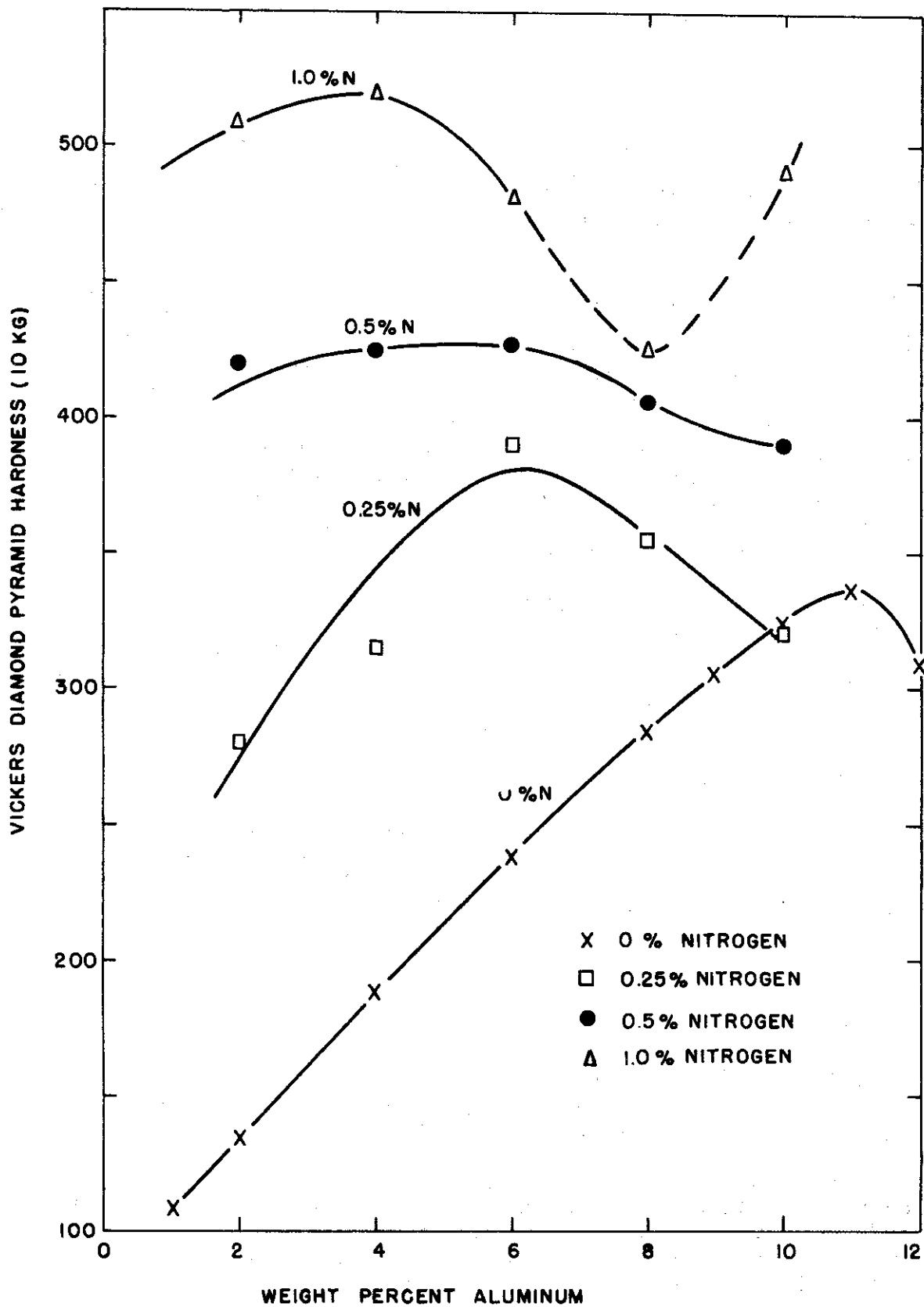


Fig. 31 - Average Vickers Hardness of Ti-Al-N Alloys Annealed in the Alpha Phase Space at Temperatures Between 900° and 1100°C

C. The Ti-Al-C System - by R. J. Van Thyne

1. Experimental Procedure

a. Alloy Preparation

The preparation of homogeneous carbon-bearing alloys caused considerable difficulty. Alloys containing less than 1% carbon were prepared using spectrographic graphite rod, 1/8 in. diameter by 1/8 in. long. However, the graphite did not dissolve even with long melting times and many remelts. The 1/8 in. pieces of graphite were used rather than powder because the low density powder is troublesome in arc melting.

Efforts were then turned to producing a good master alloy. When a tungsten-tipped electrode was used, tungsten contamination would result from the high current and long melting times required; therefore, a carbon tip was employed. The amount of carbon pick-up from the tip during melting was rather erratic. Homogeneous ingots containing a few per cent carbon were difficult to melt and were not frangible. A 13% alloy had a very high melting point; consequently, this composition was discarded. As a 30% master alloy was melted more easily than those of lower composition and was friable, this composition was used. Often the master alloy consisted of an inner core of compound surrounded by a case of apparently lower melting alloy. This difficulty was circumvented by crushing the ingot to powder and remelting.

Ti-Al-C ingots weighing 10 grams were prepared using pieces of the 30% alloy (chemical analysis: 30.0% C) approximately 1/8 in. in size and melting five times. It was found necessary to keep the ingots molten for longer times than are usually employed. A tungsten-tipped electrode was employed as the melting currents and times were not excessive. Chemical analyses indicated that carbon contents were very close to the nominal compositions.

b. Annealing Treatments

Samples were annealed at temperatures between 1150° and 600°C. The specimens that were heat treated at 750° and 600°C were first annealed at 950°C for 48 hours and then furnace cooled to the temperature of final annealing. Table VIII gives information on the annealing times used for various temperatures.

2. Discussion of Results

a. The Ti-C Diagram

Data obtained from as-cast microstructures of the various master alloys containing up to 30% carbon permitted an outline of the Ti-C system to be constructed. The probable diagram is presented in Figure 32.

Extremely high melting alloys in the compound region indicated an open maximum for TiC. Figure 33 illustrates the duplex (β + TiC) microstructure of a 13% carbon alloy. A nominal 15% carbon master alloy, previously made for an alloy development program, was entirely TiC. Therefore, the lower limit of the TiC phase field is near 15% carbon. The compound appears to

TABLE VIII
ANNEALING TIMES FOR Ti-AL-C ALLOYS

Temperature, °C	Time, Hours	Temperature, °C	Time, Hours
1150	16	900	72
1050	30	850	118
1000	40	750	240
950	48	600	576

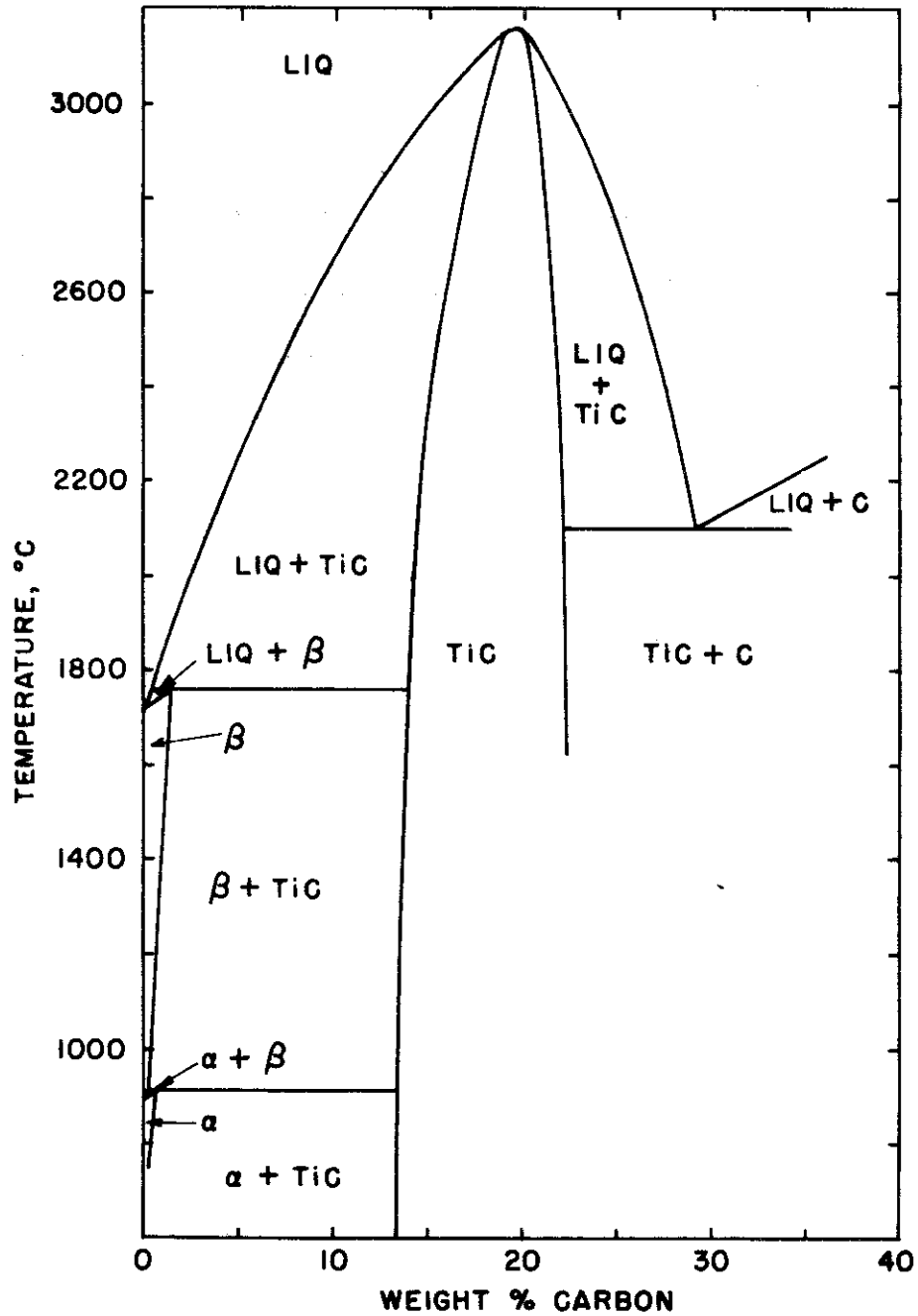


Fig. 32 - Probable Type of Phase Diagram for the Partial System Ti-C.

exist over a range of compositions; the lower limit of TiC lies close to 15% carbon and the stoichiometric composition is 20%.

The eutectic shown in Figure 32 was based on the structural appearance of a 30% alloy, Figure 34. This sample also seemed to melt at a lower temperature than the 15% carbon alloy. Collaborative x-ray diffraction studies of this eutectic alloy indicated only TiC; therefore, the other phase is apparently graphite. The fact that black material can be rubbed off the alloys of high carbon content corroborates the presence of graphite.

At the time that the tentative Ti-C diagram was constructed, the only available literature (18) covered alloys containing up to 1% carbon. As this work indicated a peritectoid reaction between beta and TiC at low carbon contents and low solubility of carbon in alpha and beta, these features were incorporated into the phase diagram. Recent work (19) indicates that the type of diagram shown in Figure 32 is correct.

As part of the Ti-Al-C investigation, the Ti-C diagram to 1% carbon was studied and the results are presented in Figure 35. A more detailed study of the binary system indicates that the peritectoid reaction occurs at $920^{\circ}\text{C} \pm 3^{\circ}\text{C}$ (19). Agreement is very close between the two diagrams.

b. The Ti-Al-C Diagram

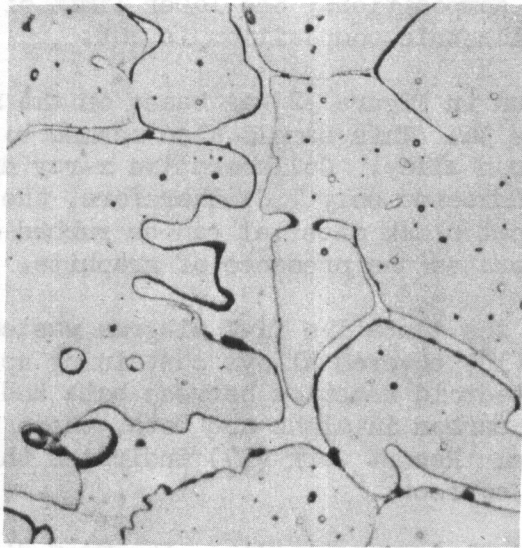
The Ti-Al-C diagram is presented by a series of vertical sections through the space model at constant aluminum contents. Although isotherms were constructed for each of the eight annealing temperatures, no isothermal sections are given as the equilibria involved are best illustrated by the vertical sections. The phase boundaries were not drawn based on data of any one vertical cut alone. Graphical interpolation, using all of the vertical and isothermal sections, was used to obtain the phase boundaries.

Emphasis was placed on the binary intercepts of the Ti-Al system and the phase boundaries of the drawings agree with the Ti-Al diagram determined during last year's work (4,16). Principle features of the Ti-Al diagram include extensive solubility of aluminum in both alpha and beta and a peritectoid reaction, β (29% Al) + TiAl (35% Al) \rightleftharpoons α (31% Al) at 1240°C . The phase relationships were drawn assuming that there is little solubility of aluminum in TiC.

An outstanding feature of the vertical sections presented in Figures 35 to 40 is the increase in the extent of the alpha field to higher temperatures and higher carbon compositions with greater aluminum contents. Whereas the maximum solubility of carbon in alpha is near 0.5% in the binary system, it is increased to over 1% with 10% aluminum in the alloy as shown in the photomicrograph of Figure 41.

It can be seen in the succeeding diagrams (Figures 36 to 40) that in the ternary system the peritectoid reaction, $\beta + \text{TiC} \rightleftharpoons \alpha$, occurs over a range of temperatures and moves to higher temperatures with greater aluminum contents. The effect of aluminum on increasing the solubility of carbon in alpha and raising the temperature of the peritectoid reaction is illustrated by Figures 42 and 43. Both alloys were annealed at 950°C ; they were located in the ($\beta + \text{TiC}$) and α spaces, respectively. Boundaries of the ($\alpha + \beta + \text{TiC}$) space

Contrails



Neg. No. 5255

X 250

Fig. 33

A 13% C alloy, arc melted and chill cast.
TiC plus transformed β at the grain
boundaries. Etchant: $\text{HNO}_3 + \text{HF} +$
glycerine.



Neg. No. 5254

X 250

Fig. 34

A 30% C alloy, arc melted and chill cast.
Eutectic structure. Unetched.

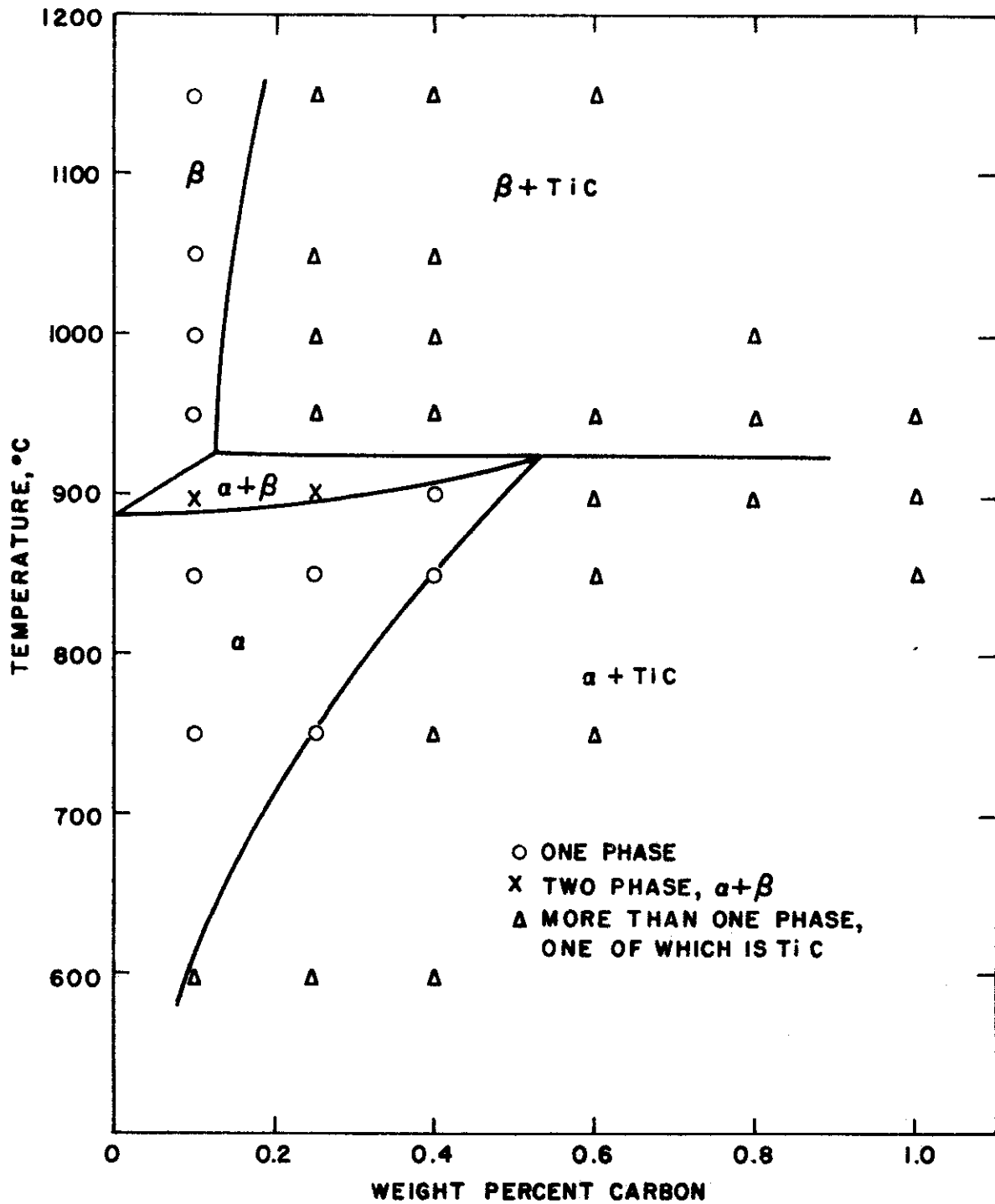


Fig. 35 - The Partial Ti-C Phase Diagram

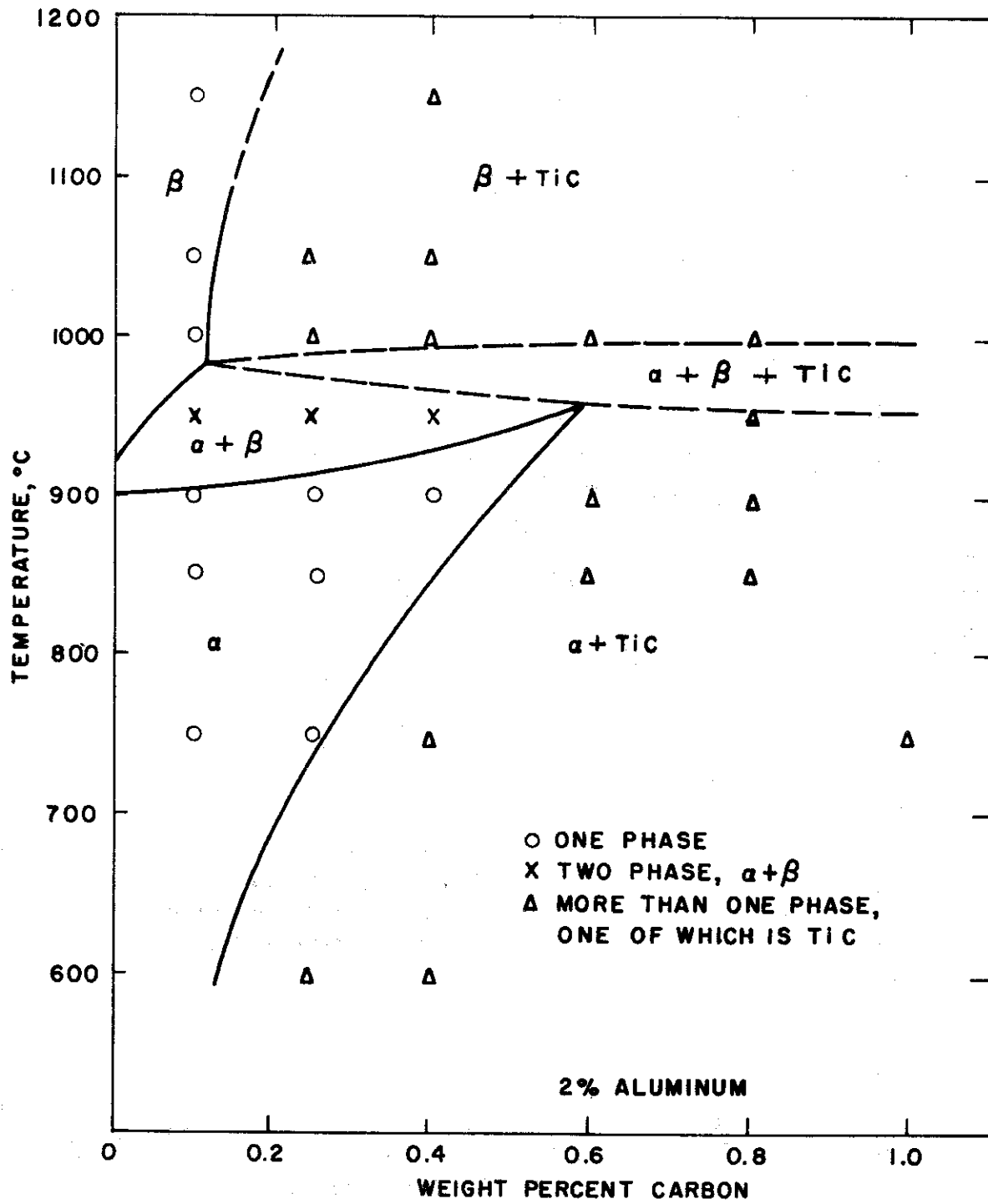


Fig. 36 - Vertical Section at 2% Aluminum Content of the Partial Ti-Al-C System

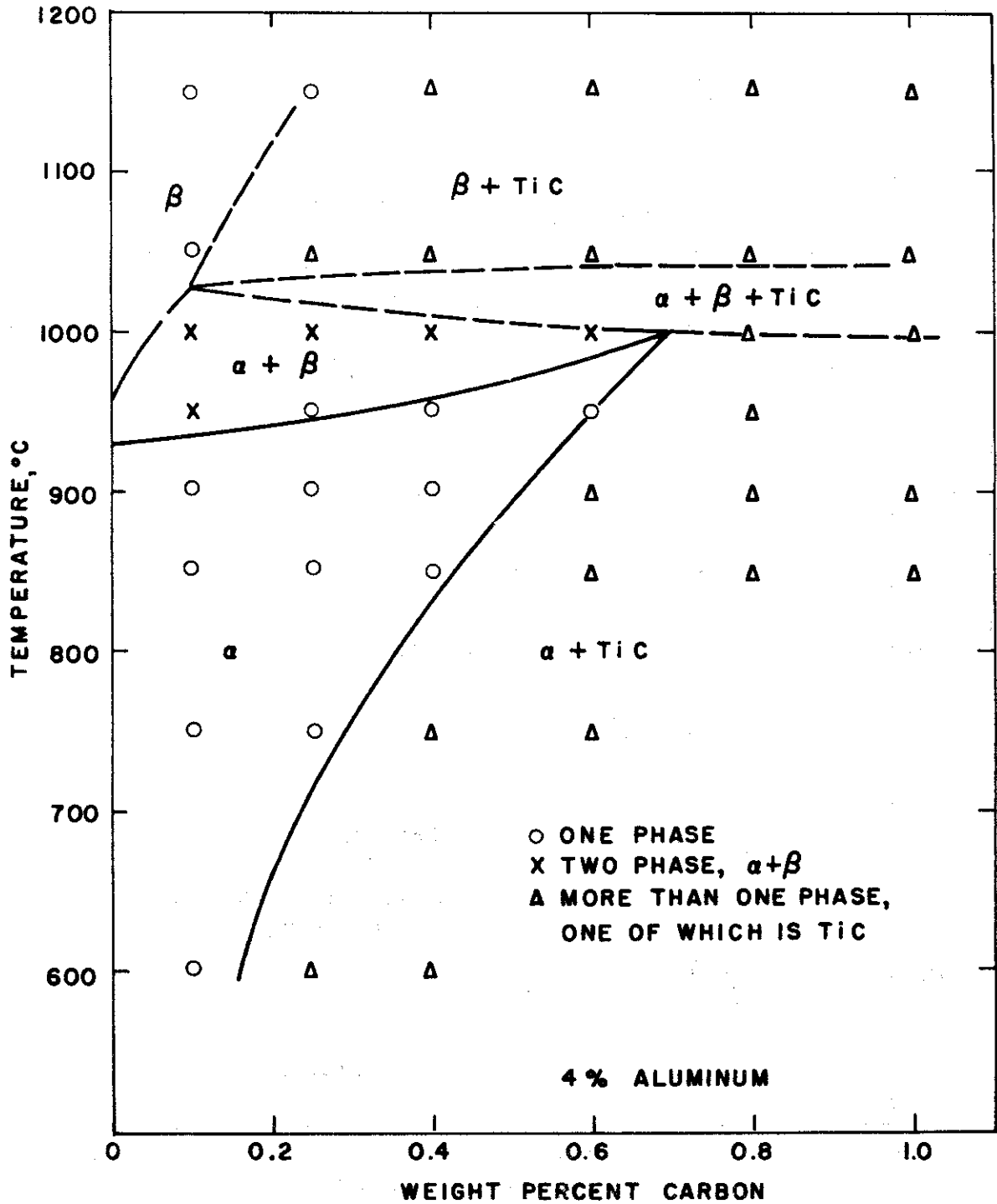


Fig. 37 - Vertical Section at 4% Aluminum Content of the Partial Ti-Al-C System

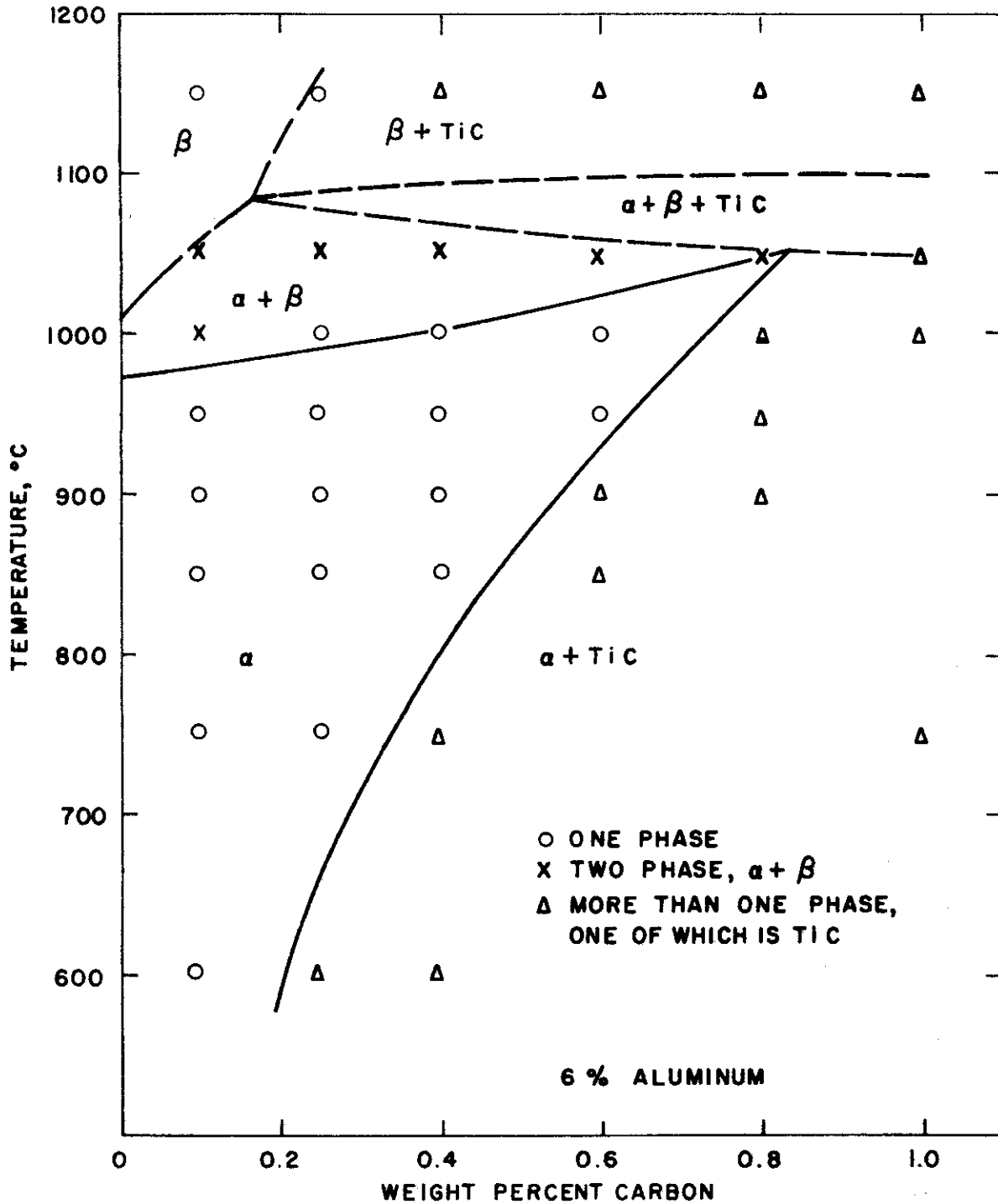


Fig. 38 - Vertical Section at 6% Aluminum Content of the Partial Ti-Al-C System

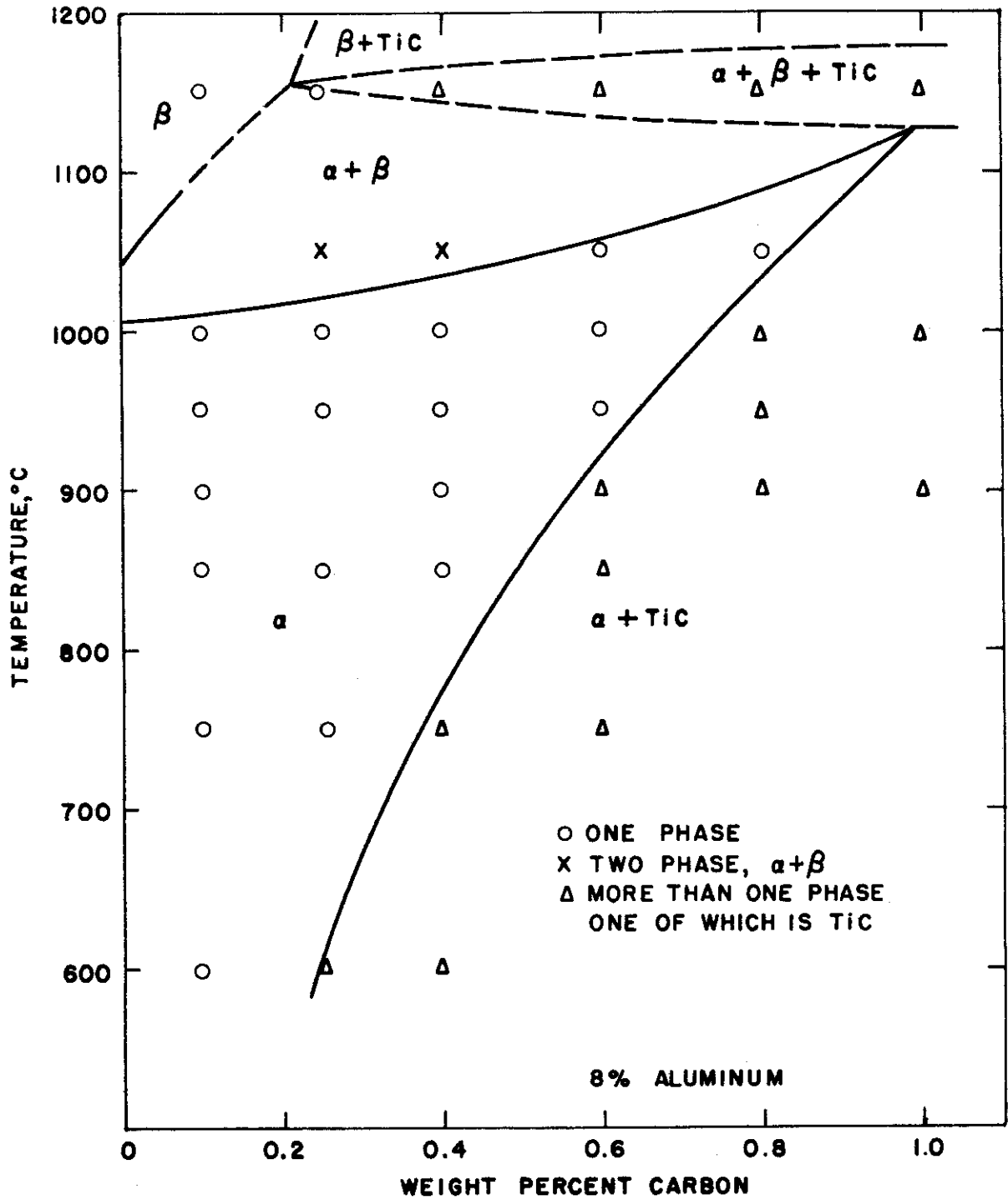


Fig. 39 - Vertical Section at 8% Aluminum Content of the Partial Ti-Al-C System

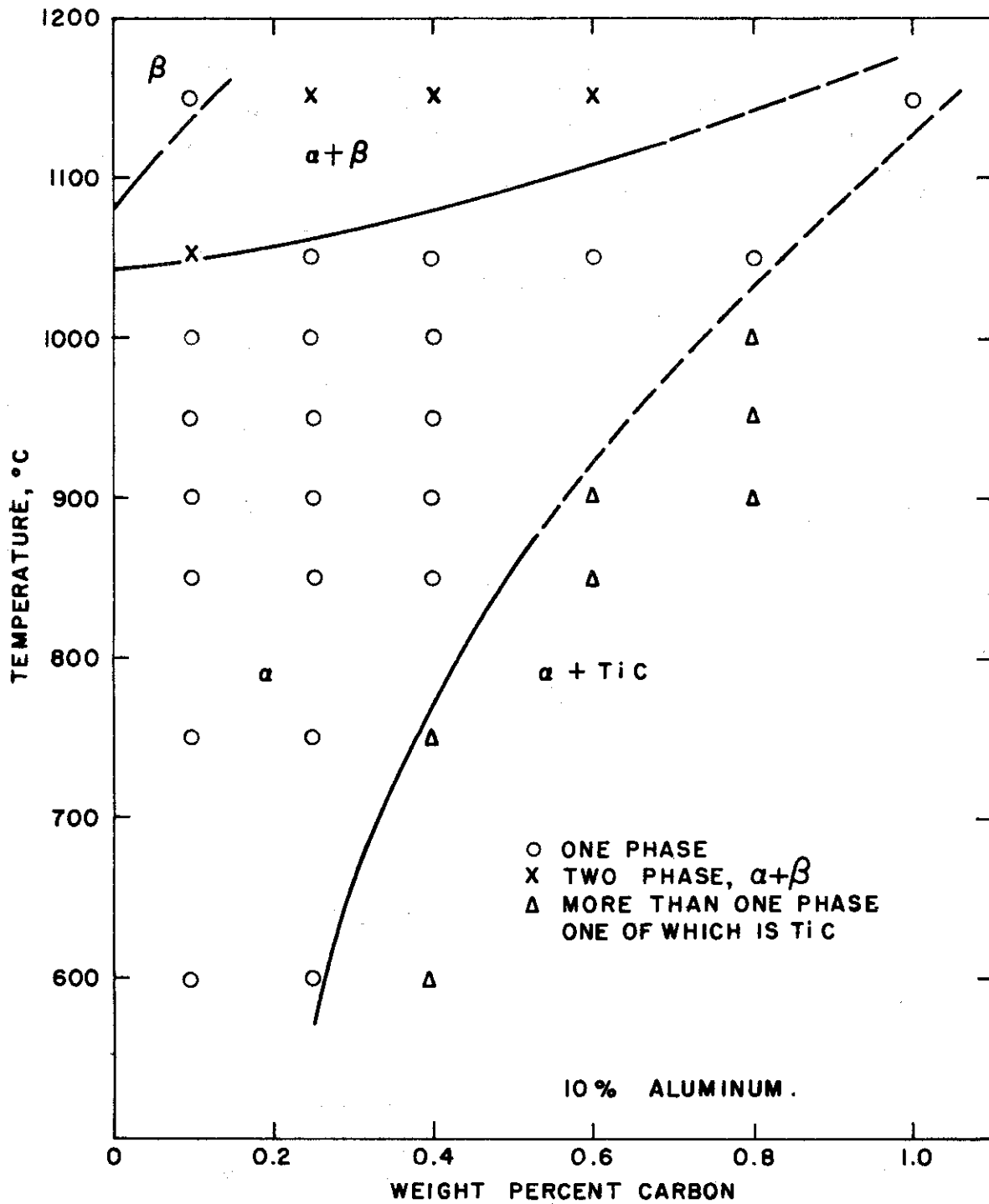
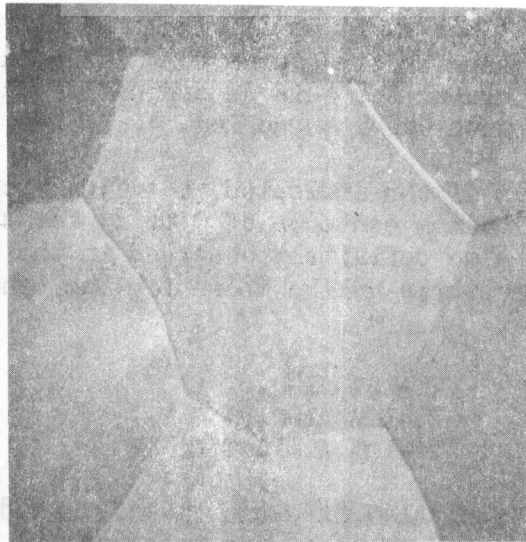


Fig. 40 - Vertical Section at 10% Aluminum Content of the Partial Ti-Al-C System

Contrails



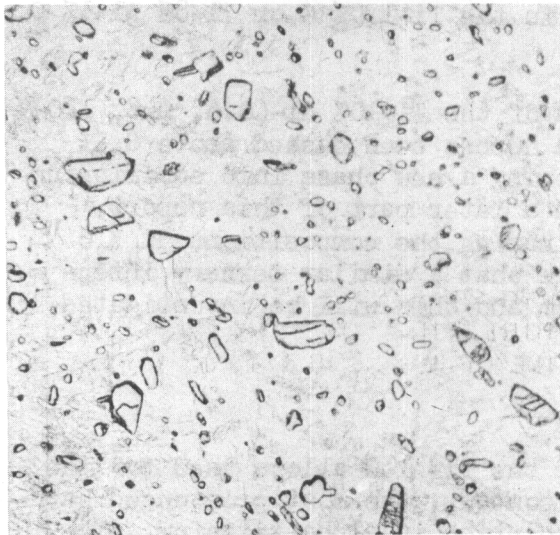
Neg. No. 7307

X 200

Polarized light

Fig. 41

A 10% Al-1.0% C alloy, water quenched
after annealing at 1150°C for 16 hours.
Equiaxed α .



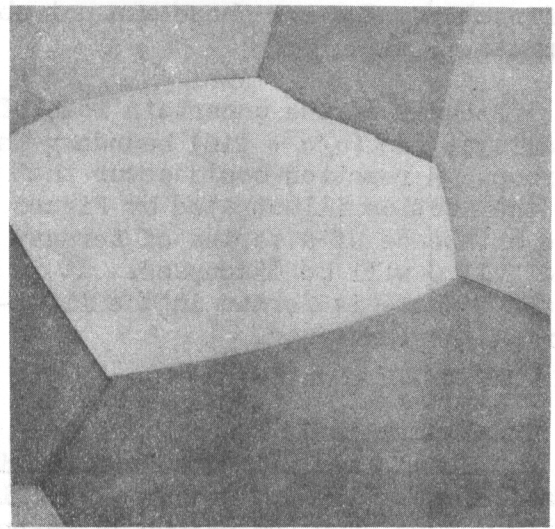
Neg. No. 6627

X 200

Fig. 42

A 0.6% C alloy, annealed at 950°C for
48 hours and water quenched. TiC in
a matrix of transformed beta.

Etchant: 60 glycerine, 20 HNO₃, 20 HF



Neg. No. 6628

X 200

Polarized light

Fig. 43

A 4% Al-0.6% C alloy, annealed at
950°C and water quenched. Large
equiaxed grains of alpha.

Contrails

have been shown as dashed lines as it is difficult to differentiate between alpha and alpha prime in the microstructures containing large amounts of TiC. X-ray diffraction was not useful for this determination as the beta phase transforms to alpha prime upon water quenching.

Certain identification of the indicated ($\alpha + \text{TiC}$) microstructures could be made for alloys with aluminum contents of 0 to 8% for all carbon compositions (0 to 1%). TiC was also definitely observed in the Ti-10% Al-0.4% C sample. However, microstructures unlike those for the other alloys were observed for the following:

Ti-10% Al-0.6% C
Ti-10% Al-0.8% C
Ti-10% Al-1.0% C

Photomicrographs of Ti-8% Al-0.8% C and Ti-10% Al-0.8% C alloys, annealed at 900°C for 72 hours and water quenched are presented in Figures 44 and 45, respectively. The former consists of ($\alpha + \text{TiC}$) and the latter is apparently alpha plus a different phase and probably TiC. An x-ray diffraction pattern was obtained for a Ti-10% Al-1.0% C alloy annealed at 750°C for 10 days and was identified as alpha plus a new phase. The lines of the new phase (Table IX) could not be indexed as TiC, TiAl, or TiAl₃ but were indexed as belonging to a cubic structure. As seen in Table IX, close correlation was obtained between the experimental and calculated lattice parameter values; therefore, the phase apparently has a cubic structure with $a = 11.20 \text{ kX}$. Using x-ray diffraction, the new phase was not observed in the Ti-1.0% C or Ti-8% Al-1% C samples.

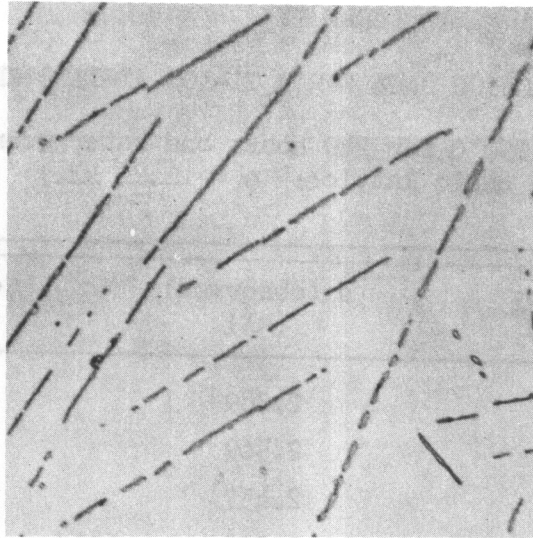
Because of the uncertain identification of the Ti-10% Al-(0.6, 0.8, 1.0)% C alloys, the ($\alpha/\alpha + \text{TiC}$) boundary in Figure 40 has been dashed above 0.5% carbon. A reaction could occur that would bring a new phase into equilibrium in the section illustrated by Figure 40. In a later part of this report, the existence of a series of ternary phases having the compositions $\text{Ti}_4\text{X}_2\text{O}$ and $\text{Ti}_3\text{X}_3\text{O}$ will be discussed. It is possible that a similar ternary intermediate phase is formed in the Ti-Al-C system and this will be investigated during the next year.

c. Hardness

Vickers hardness data were obtained for the Ti-Al-C alloys used for the phase diagram study. At any given aluminum content, the most pronounced hardening occurs when the carbon is taken into solution in alpha titanium. Increasing amounts of carbon beyond the solubility limit result in a relatively small increase in hardness.

Figure 46 illustrates the effect of increasing aluminum and carbon content on the hardness of alpha alloys. The data represent average hardness values obtained for one or more heat treatments in the alpha field. The curve for 8% aluminum lies above that for 10%; however, this is within experimental accuracy. Above 0.6% carbon, the data indicate a hardness peak or plateau; however, the curves have been shown as dashed lines as only a few data points are available at these higher alloy contents.

Contrails

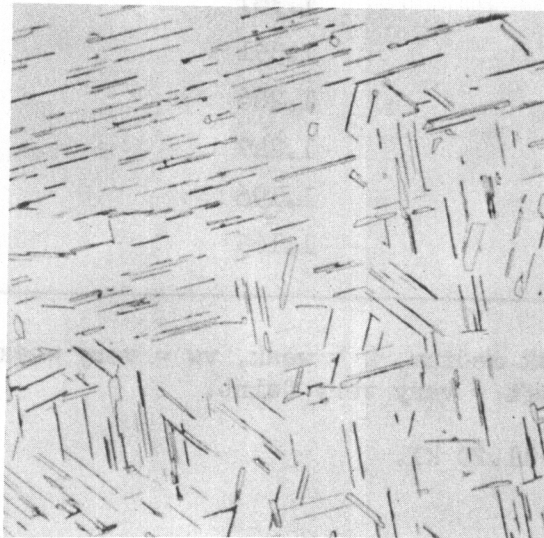


Neg. No. 7367

X 750

Fig. 44

An 8% Al-0.8% C alloy, water quenched after annealing at 900°C for 72 hours. (α + TiC)



Neg. No. 7366

X 750

Fig. 45

A 10% Al-0.8% C alloy, treated the same as the sample of Fig. 44. Alpha + unidentifiable phase and probably TiC.

Etchant: 60 glycerine, 20 HNO₃, 20 HF

Contrails

TABLE IX

X-RAY DIFFRACTION DATA FOR A Ti-10% Al-1% C ALLOY

(Annealed at 750°C for 240 hours and water quenched.
Indexed on a cubic lattice: $a = 11.20$ kX.)

hkl	Intensity Observed*	d (observed) (kX)	d (calculated)** (kX)
400	ft	2.789	2.800
331	ft	2.569	2.569
421	wm	2.457	2.444
332	ft	2.394	2.388
511	vvft	2.147	2.155
520	ft	2.075	2.080
531	ft	1.892	1.893
610	vft	1.845	1.841
444	ft	1.614	1.616
800	vvft	1.399	1.400
733	vw	1.367	1.368
821	ft	1.351	1.348
662	vvft	1.286	1.285
840	vvft	1.249	1.252
664	vvft	1.196	1.194
852	ft	1.165	1.161

* m = medium, wm = weak medium, w = weak, vw = very weak, ft = faint, vft = very faint, vvft = very very faint.

** Calculated from $a = 11.20$ kX.

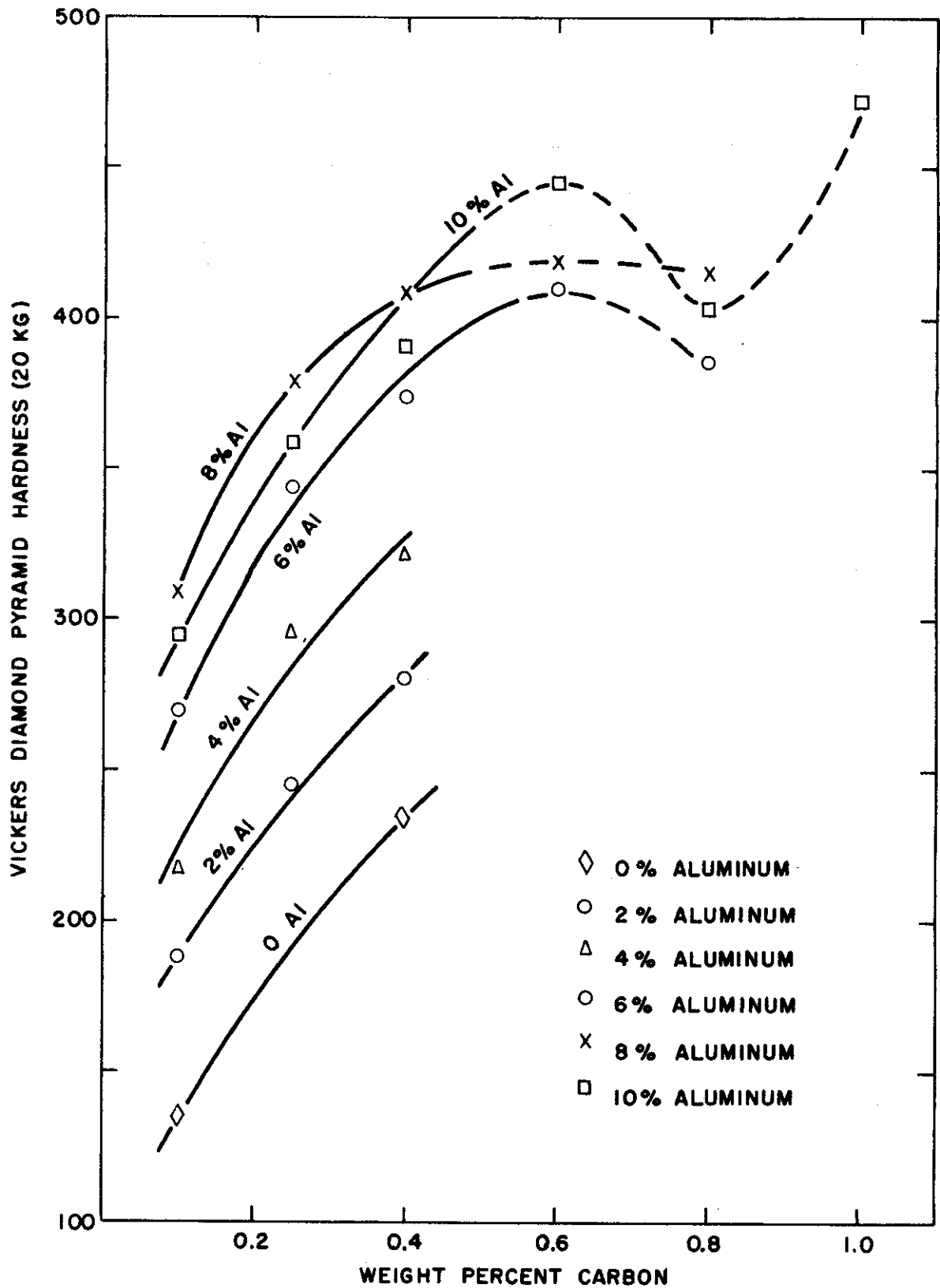


Fig. 46 - Average Vickers Hardness of Ti-Al-C Alloys Annealed in the Alpha Phase Space at Temperatures Between 600° and 1150°C.

D. The Ti-O System - by H. D. Kessler

Additional information has been obtained supporting the existence of the peritectoid reaction ($\alpha + \text{TiO} \rightleftharpoons \delta$) in the titanium-oxygen system as reported previously (4,17). A 19% oxygen sample was selected for the study as this composition lies close to the region where the delta phase is believed to exist. Upon annealing this alloy at 1000°C, alpha phase was rejected at the grain boundaries; however, the matrix remained the banded structure characteristic of the ($\alpha + \text{TiO}$) phase field (see Figures 47 and 48). Re-annealing this alloy, previously treated at 1000°C, for long times at 800°C resulted in the structure shown in Figures 49 and 50. The TiO of the banded structure has reacted with the massive alpha in the grain boundaries forming a delta rim about the alpha phase. This rim effect is characteristic of a peritectoid reaction. As noted in previous work the delta phase is also generally distributed throughout the sample, having been nucleated at various points in the banded matrix.

E. Studies on a Family of Ternary Phases in Titanium-Base Systems - by W. Rostoker

In earlier work on this project, a search for the origin of evidence for a Ti_2Fe phase led to the discovery of a ternary phase with oxygen of the general designation $\text{Ti}_1\text{Fe}_2\text{O}-\text{Ti}_3\text{Fe}_3\text{O}$ which is isomorphous with the cubic carbide $\text{Fe}_3\text{W}_3\text{C}$. It was shown that the Ti_2Fe phase does not actually exist but that the results reported (20,21) were due to oxygen contamination of the alloys examined.

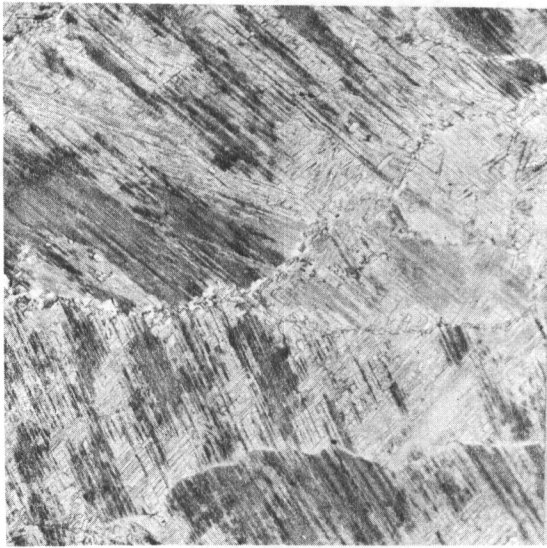
The work of the past year has been directed toward:

- (a) The discovery of other phases in titanium-metal-oxygen systems, and the verification of the existence of phases of the Ti_2X type where X is Cu, Ni, Mn, or Cr.
- (b) The study of phase relationships into which these compounds enter.

Topic (b) had a pragmatic as well as academic interest from the point of view of embrittlement phenomena in titanium alloys. Single isothermal sections for the titanium-rich corners of the Ti-Fe-O, Ti-Cr-O, Ti-Ni-O, and Ti-Mo-O systems were constructed. Each of these systems corresponds to a different range and location of the miscibility field of the oxide phase. In the latter case, no oxide phase was discovered so that its behavior may be compared to that of the other three systems where ternary phases exist.

Phase relationships were studied by both x-ray diffraction and metallographic methods. Alloys were prepared by melting in a non-consumable electrode, water-cooled copper crucible arc melting furnace. Oxygen was quantitatively introduced by the use of weighed amounts of TiO_2 or TiO. Iodide titanium and the purest available alloying metals were used. All results are discussed in terms of the nominal composition of the melts. Debye-Scherrer powder patterns were taken in a 14 cm. diameter camera using filtered $\text{CuK}\alpha$ radiations (1.541232 and 1.53739 kX). Specimens were prepared by crushing and screening of previously homogenized ingots. In general, the x-ray diffraction results were used to identify the major phases present, while the metallographic examinations were more useful in indicating the number of phases present. By the use

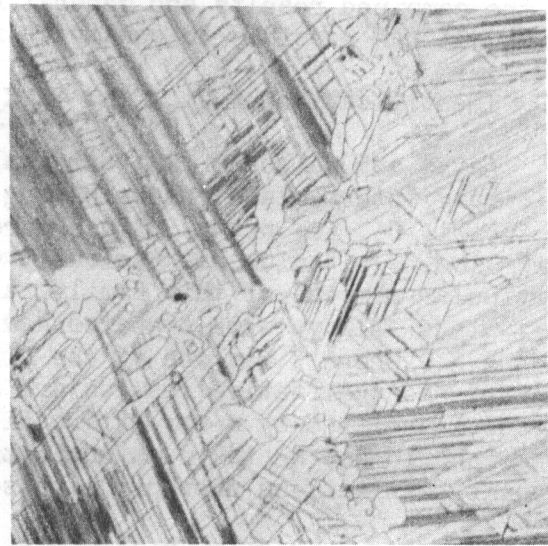
Contrails



Neg. No. 4078

X 150

Fig. 47

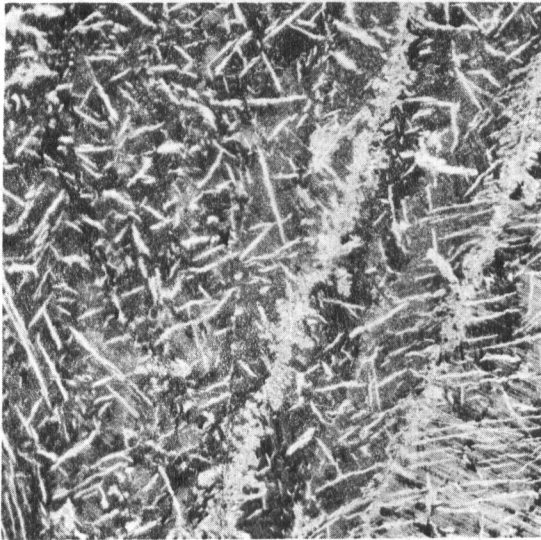


Neg. No. 4079

X 750

Fig. 48

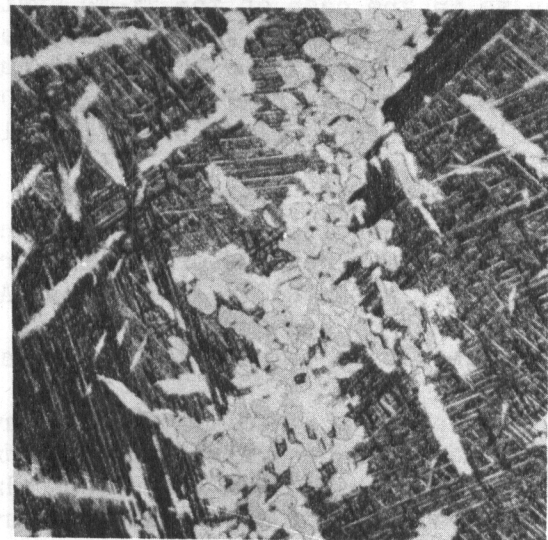
A 19% O alloy, quenched after 24 hours at 1000°C. Grain boundary alpha and the banded $\alpha + \text{TiO}$ matrix.



Neg. No. 5184

X 150

Fig. 49



Neg. No. 5183

X 750

Fig. 50

A 19% O sample initially treated as the specimen of Figs. 47 and 48, then subsequently annealed at 800°C for 168 hours. Grain boundary alpha (grey) having reacted with the TiO of the banded structure to give a delta rim (white). Also delta precipitated in the matrix.

Etchant: 60 glycerine, 20 HNO_3 , 20 HF

of the combined results and general fundamental rules governing ternary equilibrium, it was possible to construct isothermal sections in good detail.

1. Identification of Ti_2X and Ti_xX_yO Type Phases Isomorphous With Ti_3Fe_3O

Laves and Wallbaum (20) originally claimed the existence of a whole family of binary intermediate phases having the general formula Ti_2X where X could be Cu, Ni, Co, Fe, or Mn. Since more recent work on titanium binary systems using iodide titanium has variously confirmed or disputed the presence of particular members of this family, a re-examination of the whole problem seemed warranted. Alloys were prepared having the general compositions Ti_2X , Ti_4X_2O and Ti_3X_3O where X was one of the first transition metals Cu, Ni, Co, Fe, Mn, or Cr. The qualitative results are summarized in Table X. These represent phases identified by x-ray diffraction patterns. The recognition of only one phase should not be taken as indicating a single phase structure. Metallographic examinations showed the presence of other phases in many cases.

The Ti_2Cu and Ti_4Cu_2O compositions gave almost identical patterns. This is in disagreement with Karlsson (22) as regards the Ti_2Cu structure, whose presence he denies, but is in agreement with others (20,23). The Ti_2Ni and Ti_4Ni_2O compositions yielded similar results. This indicates the possibility of a miscibility field of this structure in the Ti-Cu-O and Ti-Ni-O systems. It also appears that under certain conditions the Fe_3W_3C type structure can tolerate a complete evacuation of oxygen atoms. The Ti_4Co_2O composition yielded another member of the family, but no unique phase was found at the Ti_2Co composition as in the case of the Ti-Fe system. The Ti_4Mn_2O composition has a structure isomorphous with Fe_3W_3C , but the Ti_2Mn composition gave a pattern of beta titanium. According to the recent publication of the Ti-Mn system, no unique Ti_2Mn phase exists (24). The Ti_4Cr_2O composition yielded a mixed pattern of alpha and $TiCr_2$, while the Ti_3Cr_3O alloy possessed an Fe_3W_3C type structure.

Karlsson (25) briefly described studies of oxide ternary phases which were conducted chronologically prior to the work reported here but published later. In general, the results presented agree closely, although Karlsson was apparently unconcerned with the Ti_2X problem. As one point of disagreement, Karlsson reports that no ternary phase exists at the composition Ti_3Cr_3O which is contrary to the results obtained in the present work.

In summary, a family of structures having a cubic lattice isomorphous with Fe_3W_3C has been recognized as present in the compositions defined by Ti_4X_2O and Ti_3X_3O with certain exceptions which depend on the identity of the metal X. When X is Cu or Ni, this structure occurs with or without oxygen. When X is Co, Fe, or Mn, the structure occurs with oxygen but not without. When X is Cr, the structure can be recognized only at the Ti_3Cr_3O composition. The results of lattice parameter calculations are given in Table XI.

2. System Ti-Fe-O - Isothermal Section at 1000°C

The binary systems Ti-O (17) and Ti-Fe (3) have been published. Although preliminary x-ray diffraction studies indicated the presence of a ternary phase in the composition range Ti_4Fe_2O - Ti_3Fe_3O , metallographic examination of two specimens at these compositions revealed the presence of other phases also. An isothermal section was constructed to more positively verify the existence

Contrails

TABLE X

CRYSTAL STRUCTURES RECOGNIZED AT THE Ti_2X , Ti_4X_2O and Ti_3X_3O COMPOSITIONS

Composition	Structures Identified
Ti_2Cu	Cubic (Fe_3W_3C type)
Ti_4Cu_2O	Cubic (Fe_3W_3C type)
Ti_3Cu_3O	Cubic (Fe_3W_3C type)
Ti_2Ni	Cubic (Fe_3W_3C type)
Ti_4Ni_2O	Cubic (Fe_3W_3C type)
Ti_3Ni_3O	Cubic (Fe_3W_3C type)
Ti_2Co	b.c.c. (TiX type), c.f. Duwez and Taylor (21)
Ti_4Co_2O	Cubic (Fe_3W_3C type)
Ti_3Co_3O	TiO and some unidentified phase
Ti_2Fe	b.c.c. (TiX type), c.f. Duwez and Taylor (21)
Ti_4Fe_2O	Cubic (Fe_3W_3C type)
Ti_3Fe_3O	Cubic (Fe_3W_3C type)
Ti_2Mn	Beta titanium
Ti_4Mn_2O	Cubic (Fe_3W_3C type)
Ti_3Mn_3O	Cubic (Fe_3W_3C type)
Ti_2Cr	Beta titanium and $TiCr_2$
Ti_4Cr_2O	Alpha titanium and $TiCr_2$
Ti_3Cr_3O	Cubic (Fe_3W_3C type)

TABLE XI

LATTICE PARAMETERS OF THE Fe_3W_3C TYPE STRUCTURES

Composition	a_0 in kX Units	
	Measured	Reported Elsewhere
Ti_2Cu	11.24	
Ti_4Cu_2O	11.47	11.44 (25)
Ti_3Cu_3O	11.22	11.24 (25)
Ti_2Ni	11.29	11.31 (21)
Ti_4Ni_2O	11.30	11.31 (25)
Ti_3Ni_3O	11.30	11.18 (25)
Ti_4Co_2O	11.295	11.32 (25)
Ti_3Co_3O		11.16 (25)
Ti_4Fe_2O	11.275	11.31 (25)
Ti_3Fe_3O	11.15	11.14 (25)
Ti_4Mn_2O	11.29	11.28 (25)
Ti_3Mn_3O	11.20	11.10 (25)
Ti_3Cr_3O	13.01	

Contrails

of this ternary phase, and to investigate under what conditions it might be expected to occur as an embrittling agent in commercial and experimental alloys.

Thirty-eight alloys were used to delineate phase boundaries. Anneals were conducted in evacuated Vycor bulbs at 1000°C for 24 hours. Several specimens were annealed for 7 days to develop equilibrium in sluggish alloys. Portions of the annealed ingots were examined metallographically and by x-ray diffraction.

A summary of observations is given in Table XII, and the isothermal section with data points is shown in Figure 51.

a. Miscibility Range of the Ternary (T) Phase

The ternary phase appears to tolerate only a small range of oxygen contents, approximately between 12 and 16 atomic per cent. Based on the appearance of mixed phase fields at either extremity, the limits in iron content seem to lie between 25 and 40%. This estimate is further supported by the range of lattice parameters of the ternary phase shown by the single phase alloys, and by the two phase alloys in the ($\alpha + T$), ($TiFe + T$), and ($TiO + T$) fields. Figure 52 shows a microstructure of almost pure ternary phase.

b. The ($\alpha + T$) Phase Field

Three alloys were shown to contain α and ternary phase. From the lattice parameters of the α phase determined in previous work, it was possible to show that the tie lines radiate fanwise from the ternary phase field to include a broad range of α phase compositions lying roughly between 10 and 24 atomic per cent oxygen. Figure 53 shows a two phase structure of ($\alpha + T$).

c. The ($TiO + T$) Phase Field

The lattice parameters of TiO and ternary phase in three two-phase alloys locate this phase field as bounded by 45 and 51% oxygen on the TiO side and 25 and 40% iron on the ternary phase side. Figure 54 shows a microstructure of ($TiO + T$).

d. The ($\alpha + TiO + T$) Phase Field

A three phase field must, of necessity, separate the ($\alpha + T$) and ($TiO + T$) fields. The composition of the α phase must be taken as the binary extremity of the α field at 1000°C in the $Ti-O$ system. The composition of the TiO phase must be taken as the minimum oxygen extremity in the binary system. In both cases, the assumptions are that α and TiO phases can tolerate only a very small oxygen content. The position of the ternary phase corner of the triangular field cannot be located with exactness from the available data; but it must reasonably occur at about the 25% Fe-16% O composition. One specimen was found to be in this three phase field.

e. The ($TiO + T + TiFe_2$) Phase Field

Both x-ray and metallographic evidence suggest a large ($TiO + T + TiFe_2$) three phase field. Since the 60% Fe-5% O alloy is almost single phase, it

* Note: Atomic percentages will be used exclusively in this section of the report.

TABLE XII
SUMMARY OF OBSERVATIONS
ON ALLOYS IN THE Ti-Fe-O SYSTEM ANNEALED AT 1000°C

Nominal Analyses (atomic %)			Metallographic Observations	Phase Identification by X-ray Analysis
Ti	Fe	O		
85	10	5**	Two phases	α , β
80	15	5**	Two or three phases	α , β
75	20	5**	Two phases, beta + probably T phase	β
70	25	5**	Two phases	
65	30	5*	Two phases	Ternary phase
60	35	5**	Two phases	TiFe, ternary phase
45	50	5*	Three phases	TiFe ₂ , TiFe, ternary phase
40	55	5**	Two phases	TiFe ₂ , ternary phase
35	60	5**	Nearly single phase	TiFe ₂
30	65	5**	Three phases, predominantly one	TiFe ₂
77	15	8*	Three phases	α , β , ternary phase
72	20	8*	Three phases	α , β , ternary phase
70	22	8*	Two phases	Ternary phase
60	32	8**	Primary dendrites + eutectic	TiFe, ternary phase
50	42	8**	Primary dendrites + eutectic	TiFe, ternary phase
42	50	8**	Two or three phases	TiFe, ternary phase
40	52	8*	Two phases	TiFe ₂ , ternary phase
22	70	8**	Primary dendrites + eutectic	Fe, second phase unidentified
80	10	10**	Two phases	α , ternary phase
55	35	10*	Two phases	TiFe, ternary phase
62.5	25	12.5**	Two phases	α , ternary phase
50	37.5	12.5**	Almost single phase	Ternary phase
42.5	45	12.5**	Two phases	TiFe ₂ , ternary phase
70	15	15**	Two phases	α , ternary phase
65	20	15**	Two phases	α , ternary phase
60	25	15**	Almost single phase	Ternary phase
57	28	15**	Single phase	Ternary phase

TABLE XII (Continued)

Nominal Analyses (atomic %)			Metallographic Observations	Phase Identification by X-ray Analysis
Ti	Fe	O		
55	30	15 ^{**}	Single phase	Ternary phase
42	43	15 ^{**}	Two or three phases	TiFe ₂ , ternary phase
35	50	15 ^{**}	Three phases	TiO, TiFe ₂ , possibly ternary phase
33	52	15 [*]	Three phases	TiO, TiFe ₂
48	34	18 ^{**}	Two phases, one phase pre- dominant	
55	25	20 ^{**}	Two phases	TiO, ternary phase
50	25	25 ^{**}	Two phases	TiO, ternary phase
45	30	25 ^{**}	Two phases	TiO, TiFe ₂ , ternary phase
37	38	25 ^{**}	Two phases	TiO, TiFe ₂
60	10	30 ^{**}	Three phases	Ternary phase

* Annealed for 7 days

** Annealed for 24 hours

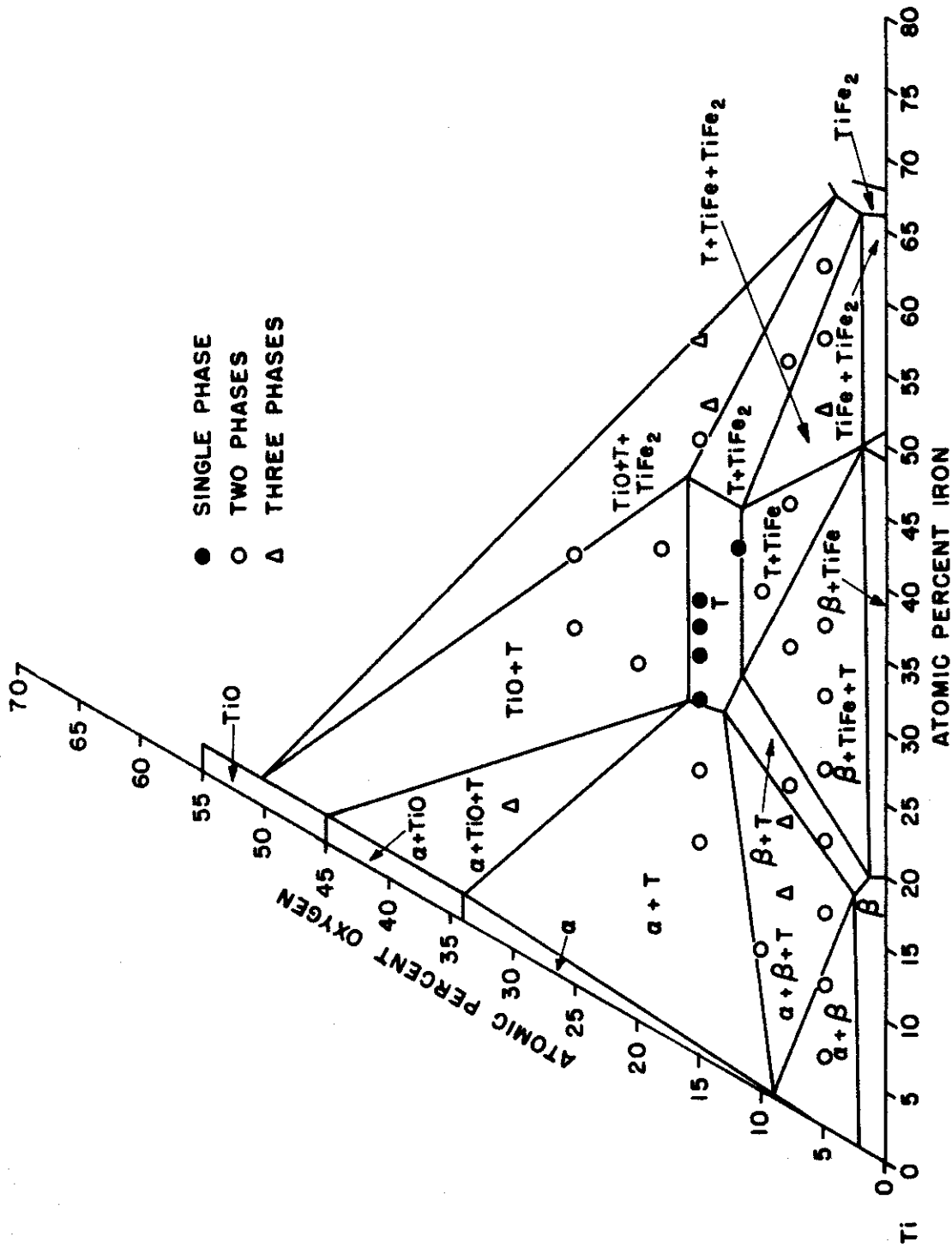
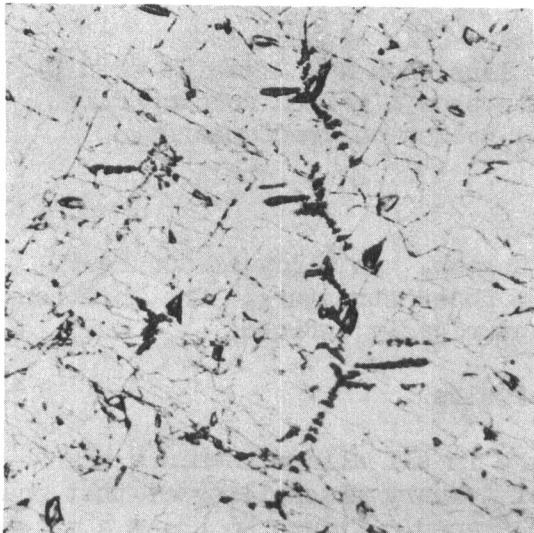


Fig. 51 - 1000°C Isothermal for Partial Ti-Fe-O System

Contrails

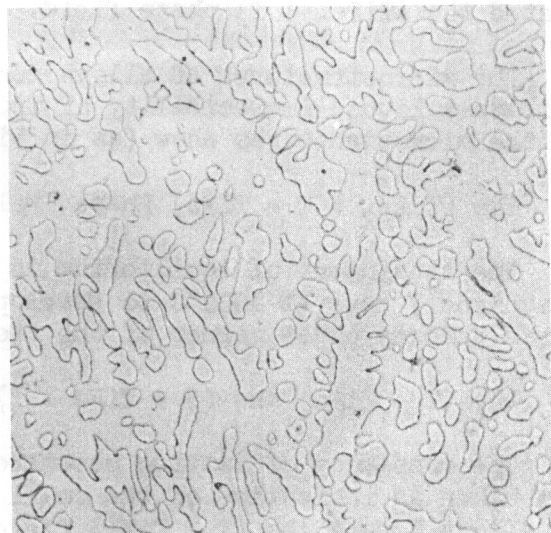


Neg. No. 5070

X 500

Fig. 52

Composition: 15% O, 30% Fe, 55% Ti.
Structure of almost pure ternary phase.
Trace dendrites of TiO.

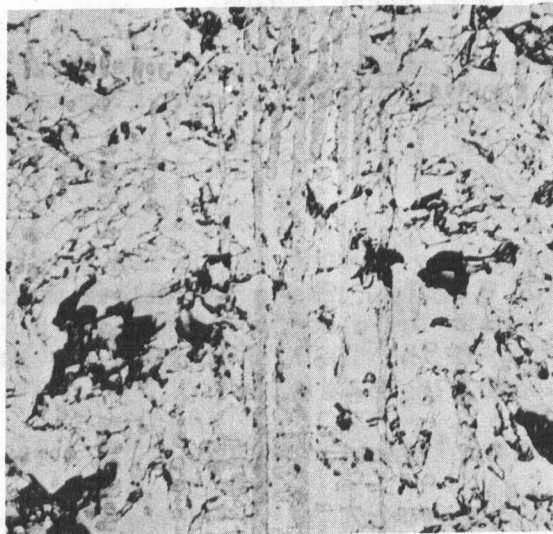


Neg. No. 5071

X 500

Fig. 53

Composition: 15% O, 20% Fe, 65% Ti.
Mixed structure of α and ternary phases.



Neg. No. 5072

X 500

Fig. 54

Composition: 20% O, 25% Fe, 55% Ti.
Mixed structure of TiO and ternary phase.

Etchant: 2% HF, 3% HNO₃ in water

Annealing Treatment: 1000°C for 24 hours, water quench

Contrails

appears that the TiFe_2 phase has some ability to dissolve oxygen. Two alloys located the $(\text{TiFe}_2 + \text{T})$ phase field.

The microstructures of alloys containing less than 45% titanium seem to indicate a liquid immiscibility of TiO . Ingots show a golden colored film and the microstructures show (as in Figure 55) golden colored spheres.

f. The $(\text{TiFe}_2 + \text{T} + \text{TiFe})$ Phase Field

The attainment of equilibrium is very sluggish. An alloy of 50% Fe-5% O required 7 days at 1000°C to develop a three phase structure. The location of the ternary phase corner of the field is not rigidly defined.

g. The $(\text{T} + \text{TiFe})$ and $(\beta + \text{TiFe} + \text{T})$ Phase Fields

The constancy of lattice parameter of TiFe in all alloys examined has been taken as indicative of the small range of ternary miscibility of that phase. Two alloys locate the $(\text{T} + \text{TiFe})$ field as fan-shaped. Figure 56 shows a microstructure of this field.

The $(\beta + \text{TiFe} + \text{T})$ phase field must exist from phase rule considerations. However, even after 7 days at 1000°C , all alloys in the expected location of the field were still two phase. The location of this field has been set between the best estimates of the bounding tie lines of the three surrounding two phase fields.

h. The $(\beta + \text{T})$ and $(\alpha + \beta + \text{T})$ Phase Fields

The $(\beta + \text{T})$ field is quite narrow. Two alloys locate its position. The three phase field $(\alpha + \beta + \text{T})$ was located largely from the bounding two phase fields.

i. The $(\alpha + \beta)$ Phase Field

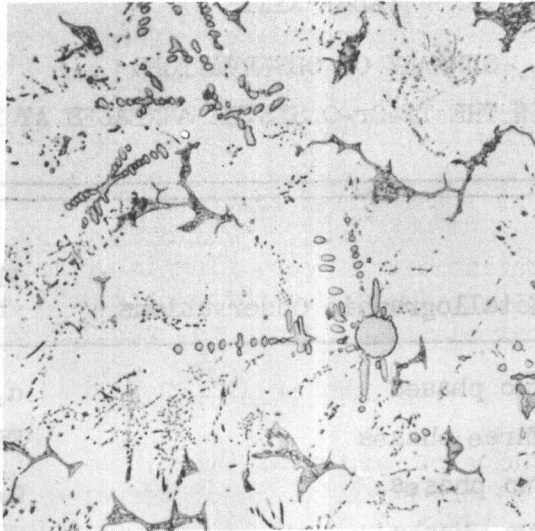
The lattice parameter of the α phase of the 10% Fe-5% O alloy was identical with that of the 10% Fe-10% O alloy. These two alloys must therefore be on boundary tie lines which serve to locate the α corner of the $(\alpha + \beta + \text{T})$ field at 9% oxygen. The other extremity of the tie line through the 10% Fe-5% O alloy located the beta composition at about 17% Fe-2% O.

3. System Ti-Cr-O - Isothermal Section at 1000°C

A ternary oxide phase was recognized in this system, but unlike the isomorphous phase in the Ti-Fe-O system, its range of miscibility appeared to be in more chromium-rich regions of the diagram. The Ti-Cr system has been published (3).

Twenty-three alloys were used to delineate phase boundaries. Anneals were conducted in evacuated Vycor bulbs at 1000°C for 24 hours. Several specimens were annealed for 7 days to more closely approach equilibrium in sluggish alloys. Both x-ray diffraction and metallographic analyses were made of each alloy. A summary of observations is given in Table XIII and the isothermal section with data points is shown in Figure 57. It is evident that the ternary oxide

Contrails

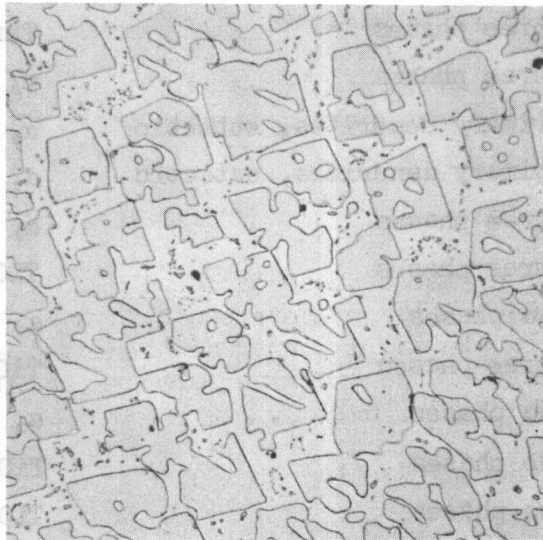


Neg. No. 5074

X 750

Fig. 55

Structure of ternary phase, $TiFe_2$ and TiO , indicating a liquid immiscibility.



Neg. No. 5073

X 500

Fig. 56

Composition: 8% O, 42% Fe, 50% Ti.
Mixed structure of $TiFe$ and ternary phase.

Etchant: 2% HF, 3% HNO_3 in water

Annealing Treatment: 1000°C for 24 hours, water quench

Contrails

TABLE XIII

SUMMARY OF OBSERVATIONS
ON ALLOYS IN THE Ti-Cr-O SYSTEM ANNEALED AT 1000°C

Nominal Analyses (atomic %)			Metallographic Observations	Phase Identification by X-ray Analysis
Ti	Cr	O		
77	20	3*	Two phases	α , β
30	67	3*	Three phases	TiCr ₂ , Cr, ternary phase
90	5	5*	Two phases	α , β
85	10	5*	Two phases	α , β
65	25	10**	Three phases	α , TiCr ₂
50	40	10**	Two phases	α , TiCr ₂
40	50	10**	Three phases	Ternary phase
35	55	10**	Three phases (TiO recognizable)	TiCr ₂ , ternary phase
39	49	12*	Three phases	Ternary phase
43	43	14**	Three phases	Ternary phase, TiO, α
75	10	15*	Three phases	α , TiCr ₂
65	20	15**	Primary dendrites, eutectic	α , TiCr ₂
57	28	15**	Primary dendrites, eutectic	α , TiCr ₂
50	35	15**	Three phases	α , TiCr ₂ , ternary phase
35	50	15**	Three phases	TiO, TiCr ₂ , ternary phase
65	15	20**	Two phases	α , TiCr ₂
35	45	20**	Three phases	TiO, ternary phase
60	15	25**	Two phases	α , ternary phase
45	30	25**	Two phases	TiO, ternary phase
40	35	25**	Two phases	TiO, ternary phase
55	15	30*	Three phases	α , TiO, ternary phase
68	2	30*	Two phases	α , ternary phase
49	2	49*	Two phases	TiO

* Annealed for 7 days

** Annealed for 24 hours

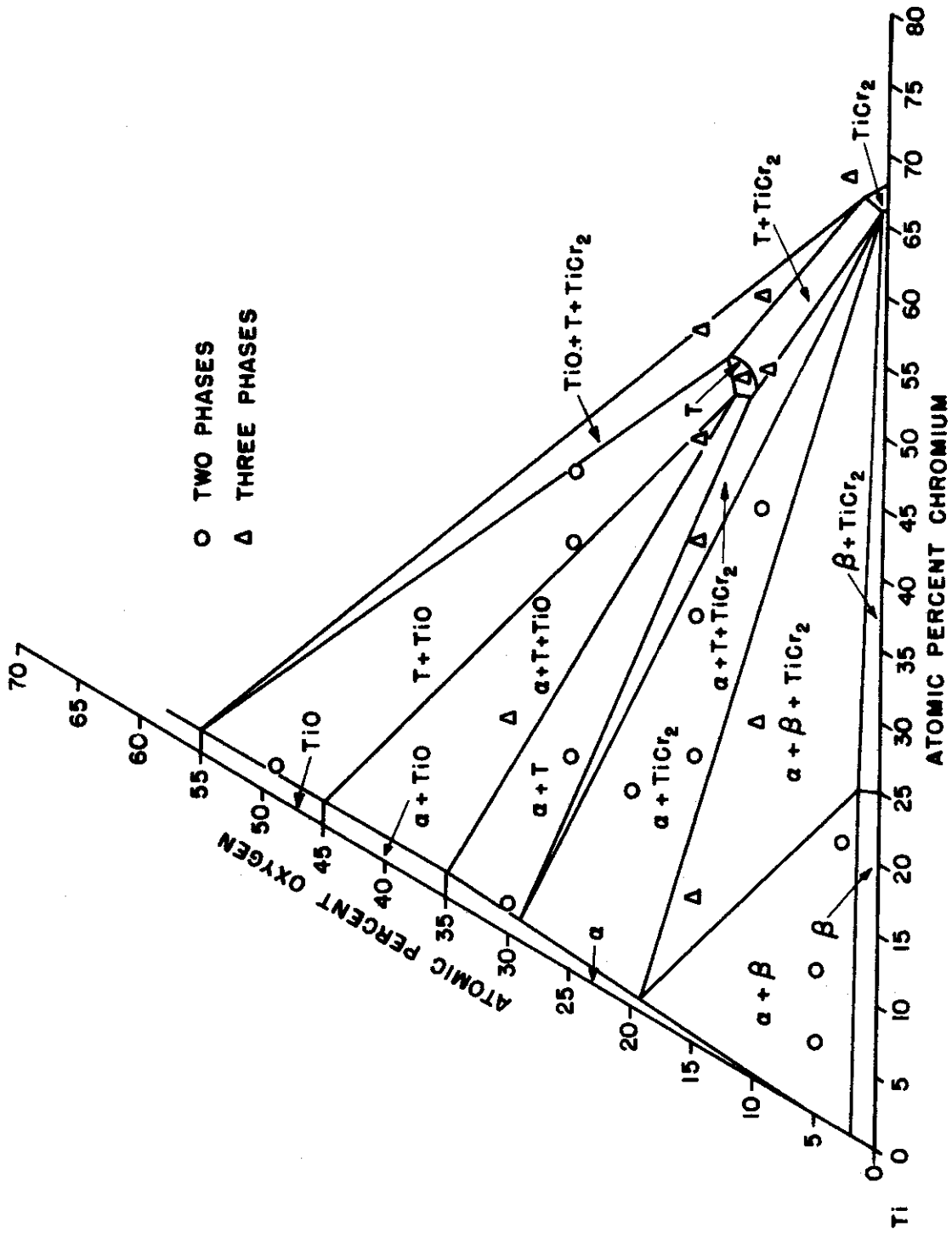


Fig. 57 - 1000°C Isothermal for Partial Ti-Cr-O System

phase is not encountered at this or lower temperatures in the commercially important range of Ti-Cr compositions. An isothermal section for this system at 1200°C has appeared recently (26). The same general form of phase equilibria was established as encountered in the present work. The presence of the ternary phase is confirmed. One point of disagreement lies in the extent of projection of the α and TiO phases into the ternary field. The section presented by Wang, et al., shows as much as 15 atomic per cent Cr solubility in each of these phases although there is little evidence to support this. It is to be noted that in the 1000°C section presented here, two alloys showed that the chromium solubility in these two phases was less than 2 atomic per cent.

a. Miscibility Range of the Ternary (T) Phase

The lines of a cubic phase isomorphous with other members of the ternary oxide group were consistently noted as the predominant diffraction pattern in high chromium content alloys. It was not found possible to develop a completely single phase structure in an alloy which from the directions of phase boundaries must be expected to be in the single phase field. The narrow region of occurrence of this phase was inferred from the directions of phase boundaries and tie lines. Its location must be considered approximate. The miscibility range does not include the ideal composition Ti_3Cr_3O .

b. The ($\alpha + TiCr_2$) Phase Field

Four alloys confirm the existence of an ($\alpha + TiCr_2$) field at this temperature. A typical microstructure is shown in Figure 58.² The presence of this field effectively excludes the possibility of the ternary phase appearing as a constituent of commercial titanium-chromium alloys.

c. The ($\alpha + T$) and (TiO + T) Phase Fields

The existence of these two phase fields was indicated by two and three alloys, respectively. Between ($\alpha + T$) and (TiO + T) a three phase field ($\alpha + TiO + T$) must necessarily exist. Two alloys confirmed the presence of this phase field. Two alloys containing 2% chromium and 30 and 49% oxygen, respectively, showed that the solubilities of chromium in α and TiO were very small. Another three phase field ($\alpha + TiCr_2 + T$) must exist between the ($\alpha + TiCr_2$) and ($\alpha + T$) fields. Two alloys were found to lie in this field. Figures 59 and 60 are pertinent to this discussion.

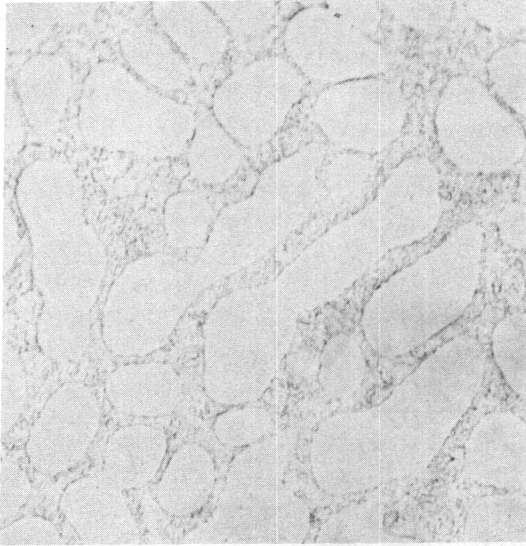
d. The ($\alpha + \beta$) and ($\alpha + \beta + TiCr_2$) Phase Fields

Two alloys exhibiting three phase structures (Figure 61) served to locate the $\alpha + TiCr_2/\alpha + \beta + TiCr_2$ boundary. The other two boundaries of the ($\alpha + \beta + TiCr_2$) field depend on the solubility of oxygen in β . The 3% O-20% Cr alloy showed this to be less than 3%. Accordingly, the ($\alpha + \beta + TiCr_2$), ($\alpha + \beta$) and ($\beta + TiCr_2$) fields were located without difficulty.

e. Other Phase Fields

Several alloys indicated the presence of a three phase field ($TiCr_2 + TiO + T$), Figure 62. A two phase field necessarily exists between $TiCr_2$ and the ternary phase T.

Contrails

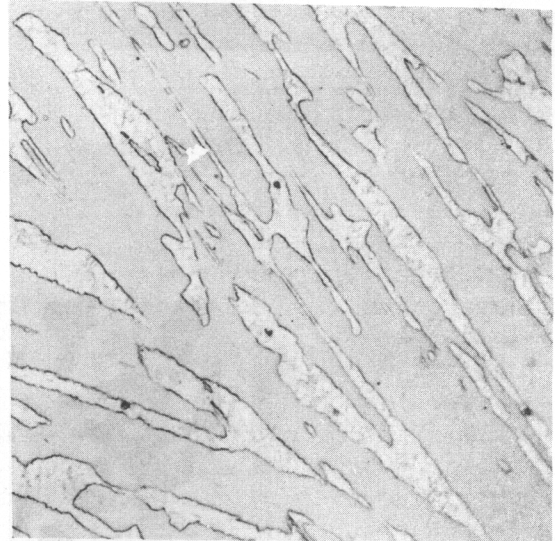


Neg. No. 5189

X 750

Fig. 58

Composition: 15% O, 20% Cr, 65% Ti.
Primary dendrites of alpha in a matrix
of alpha and $TiCr_2$.

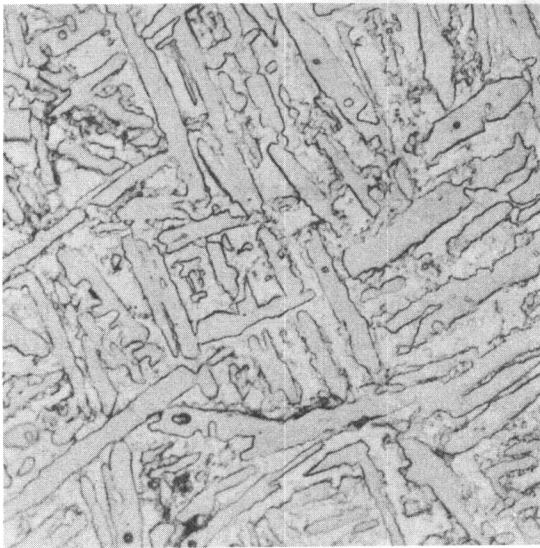


Neg. No. 5190

X 750

Fig. 59

Composition: 25% O, 15% Cr, 60% Ti.
Two phase structure of alpha and
ternary phase.



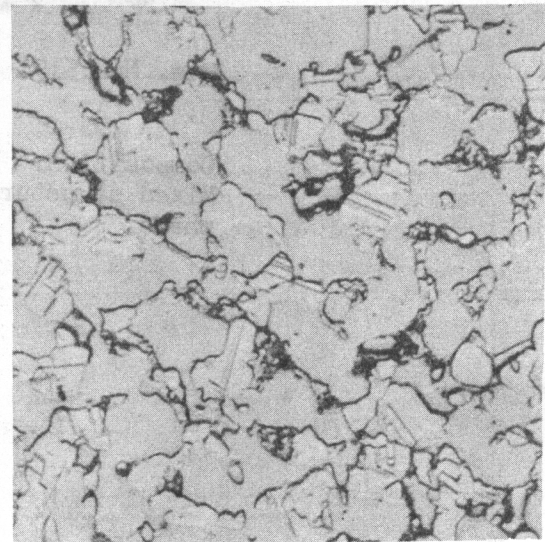
Neg. No. 5192

X 750

Fig. 60

Composition: 15% O, 35% Cr, 50% Ti.
Mixed structure of alpha, $TiCr_2$ and
ternary phase as identified by x-ray
diffraction analysis.

Annealing Treatment: 1000°C for 24 hours, water quench.
Etchant: 60 glycerine, 20 HNO_3 , 20 HF.

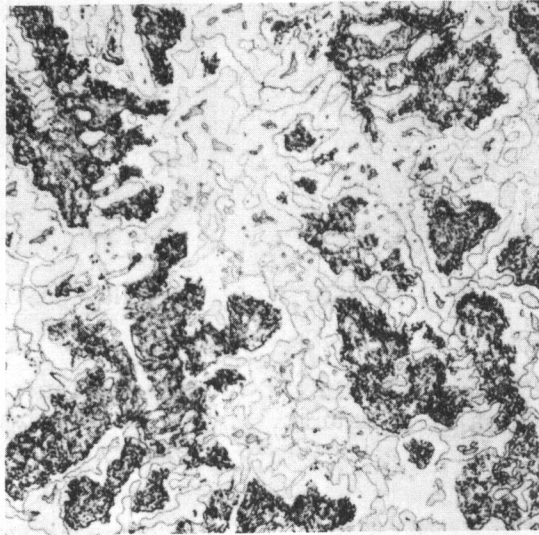


Neg. No. 5188

X 750

Fig. 61

Composition: 10% O, 25% Cr, 65% Ti.
Mixed structure of alpha, beta and
 $TiCr_2$.



Neg. No. 5191

X 750

Fig. 62

Composition: 10% O, 55% Cr, 35% Ti.
Mixed structure of TiO , $TiCr_2$ and ternary
phase.

Annealing Treatment: 1000°C for 24 hours, water quench
Etchant: 60 glycerine, 20 HNO_3 , 20 HF

4. Isothermal Section at 900°C - System Ti-Ni-O

The Ti-Ni system (27) has been published. The Ti_2Ni phase is known to have a cubic structure isomorphous with the ternary phases under study. The Ti-Ni-O system is of particular interest as a case where the ternary phase lattice can tolerate a complete evacuation of the interstitial atoms. The arbitrary compositions Ti_4Ni_2O and Ti_3Ni_3O both indicated the presence of the Ti_2Ni structure but gave no indication of the ternary miscibility field of the phase.

Twenty-seven alloys were used to delineate phase boundaries in the ternary section. Anneals were conducted in evacuated Vycor bulbs at 900°C for 48 hours. The lower temperature was necessary to avoid the presence of the liquid phase because of the low eutectic temperature (995°C) in the Ti-Ni system. Annealed alloys were subjected to both x-ray diffraction and metallographic analysis. A summary of observations is given in Table XIV and the isothermal section with data points is shown in Figure 63.

a. Miscibility Field of the Ti_2Ni Phase

Judging from three alloys which were single phase or nearly so and from the directions of phase boundaries, it is concluded that the Ti_2Ni phase has a narrow miscibility field extending into the ternary system in the direction of a constant ratio of Ti:Ni. The interpretation is that the structure is permitting the occupation of vacant interstitial sites approximately up to the saturation which the other isomorphous ternary phases permit. Figure 64 shows the structure of a 5% O-30% Ni alloy which is nearly single phase.

b. The ($\alpha + Ti_2Ni$) Phase Field

This phase field proved to be very extensive. Six alloys were identified as lying in this field. Figure 65 is a characteristic structure. Because of the extent of this field the adjoining ($\alpha + \beta + Ti_2Ni$) field was necessarily restricted.

c. The ($TiO + Ti_2Ni$) and ($\alpha + TiO + Ti_2Ni$) Phase Fields

Two alloys identified the existence of a ($TiO + Ti_2Ni$) phase field. Figure 66 shows a typical microstructure. The three phase field ($\alpha + TiO + Ti_2Ni$) was automatically defined by the $\alpha + Ti_2Ni/\alpha + TiO + Ti_2Ni$ and $TiO + Ti_2Ni/\alpha + TiO + Ti_2Ni$ boundaries. Figure 67 shows a microstructure from this field.

d. The ($TiO + Ti_2Ni + TiNi_3$) Phase Field

TiO enters into equilibrium with $TiNi_3$ rather than $TiNi$ and accordingly a very large ($TiO + Ti_2Ni + TiNi_3$) field is formed. Five alloys showed three phase structures belonging to this field. An exemplary microstructure is shown in Figure 68.

e. The ($Ti_2Ni + TiNi_3$) and ($TiNi + Ti_2Ni + TiNi_3$) Phase Fields

The occurrence of two different three phase structures at 5% O-45% Ni and 10% O-45% Ni signifies that there must be a narrow two phase field ($Ti_2Ni + TiNi_3$)

Contrails

TABLE XIV

SUMMARY OF OBSERVATIONS
ON ALLOYS IN THE TI-NI-O SYSTEM ANNEALED AT 900°C

Nominal Analyses (atomic %)			Metallographic Observations	Phase Identification by X-ray Analysis
Ti	Ni	O		
67	33	0	Single phase	Ti ₂ Ni
87.5	10	2.5	Two phases	
85	12	3	Three phases	α, Ti ₂ Ni
90	5	5	Two phases	α, β
75	20	5	Two phases	α, Ti ₂ Ni
65	30	5	Nearly single phase	Ti ₂ Ni
62	33	5	Two phases	Ti ₂ Ni
60	35	5	Two phases	Ti ₂ Ni
55	40	5	Two phases	Ti ₂ Ni
50	45	5	Three phases	TiNi, Ti ₂ Ni
45	50	5	Three phases	Ti ₂ Ni, TiNi ₃
70	20	10	Two phases	α, Ti ₂ Ni
65	25	10	Two phases	α, Ti ₂ Ni
60	30	10	Nearly single phase	Ti ₂ Ni
57	33	10	Two phases	Ti ₂ Ni
55	35	10	Two phases	Ti ₂ Ni
50	40	10	Three phases	Ti ₂ Ni, TiNi ₃
45	45	10	Three phases	Ti ₂ Ni, TiNi ₃
43	43	14	Three phases	Ti ₂ Ni, TiNi ₃
70	15	15	Two phases	α, Ti ₂ Ni
65	10	25		α, Ti ₂ Ni
60	15	25	Three phases	α, Ti ₂ Ni
55	20	25	Two phases	TiO, Ti ₂ Ni
50	25	25	Three phases	TiO, Ti ₂ Ni, TiNi ₃
45	30	25	Three phases	Ti ₂ Ni, TiO, TiNi ₃
60	5	35	Three phases	α, TiO, Ti ₂ Ni
50	5	45	Two phases	TiO, Ti ₂ Ni

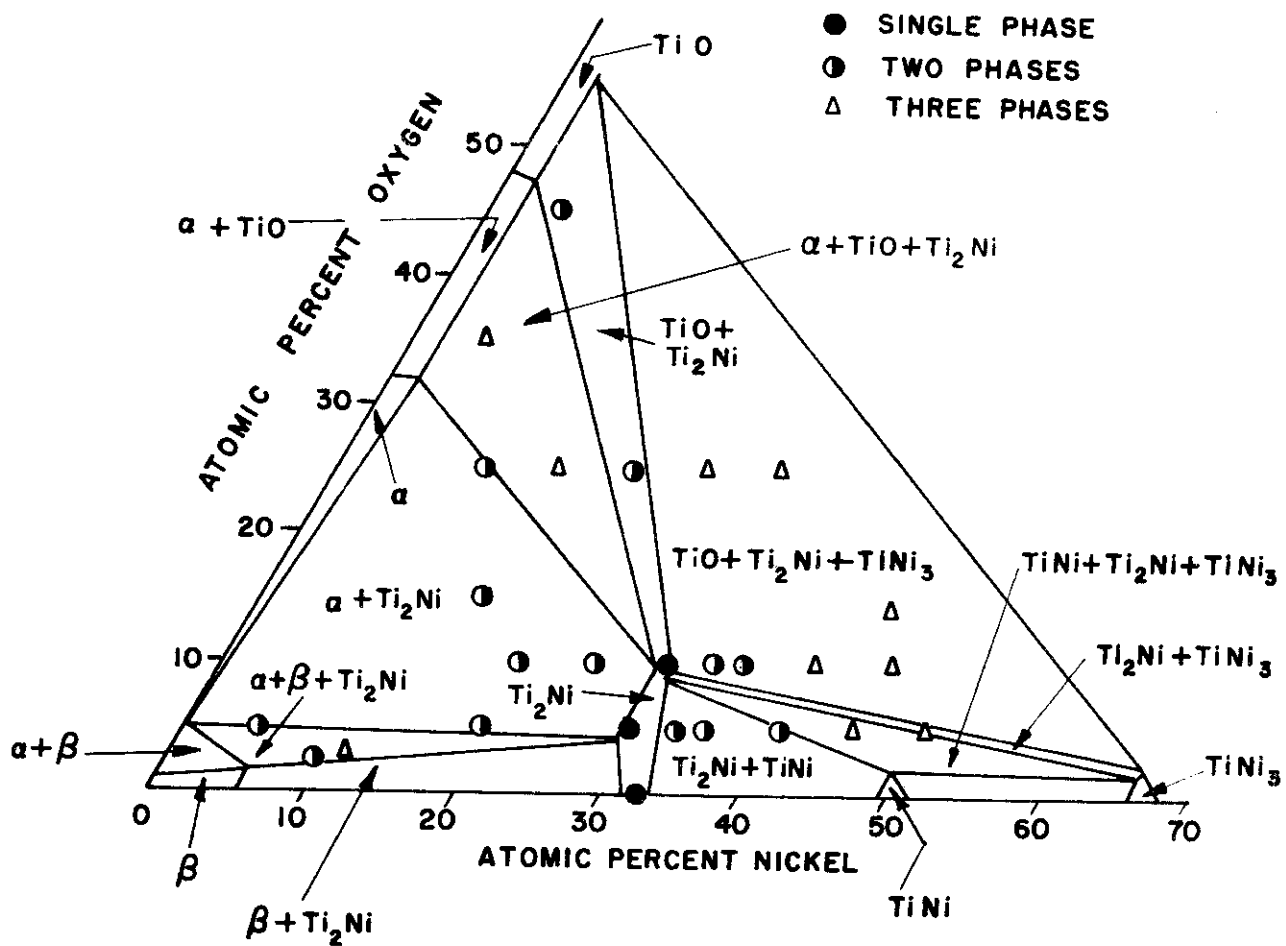
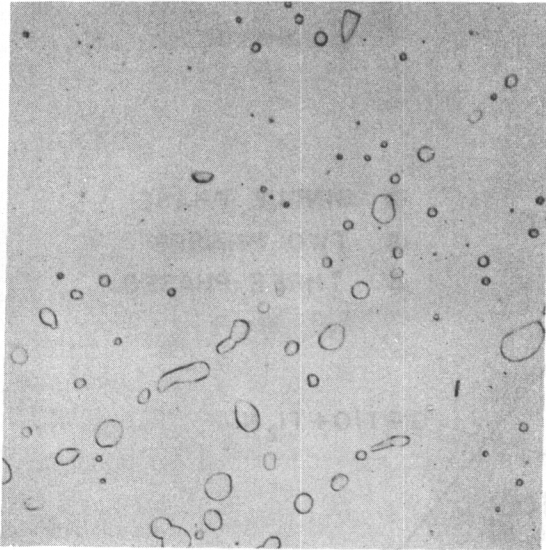


Fig. 63 - 900°C Isothermal for Partial Ti-Ni-O System

Contrails

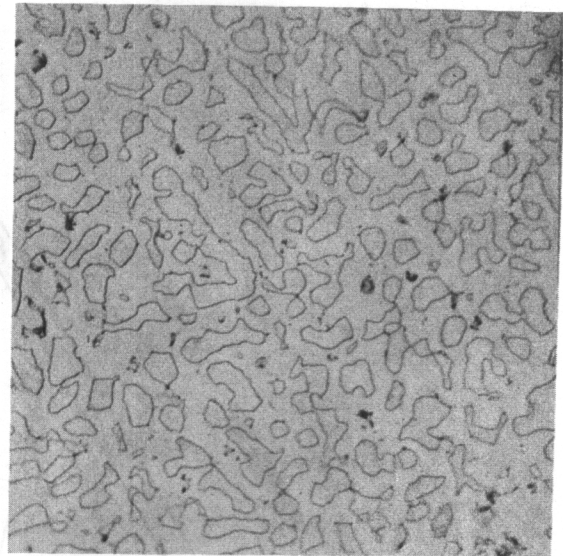


Neg. No. 7070

X 500

Fig. 64

Composition: 5% O, 30% Ni, 65% Ti.
Structure of almost pure Ti_2Ni .

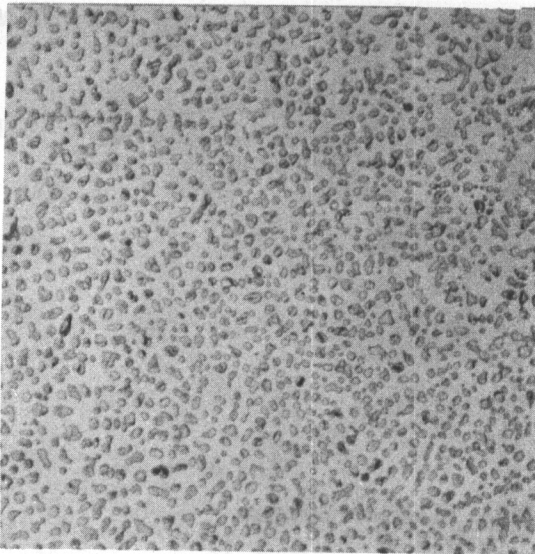


Neg. No. 7067

X 500

Fig. 65

Composition: 10% O, 20% Ni, 70% Ti.
Two phase structure of $(\alpha + Ti_2Ni)$.

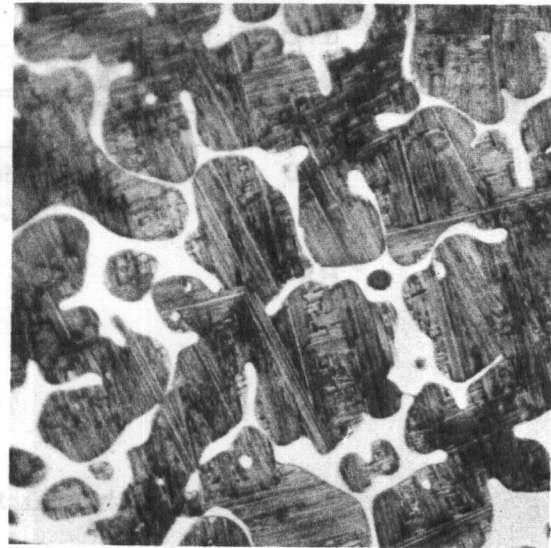


Neg. No. 7066

X 750

Fig. 66

Composition: 25% O, 20% Ni, 55% Ti.
Two phase structure of $(TiO + Ti_2Ni)$.



Neg. No. 7064

X 750

Fig. 67

Composition: 35% O, 5% Ni, 60% Ti.
Three phase structure of $(\alpha + TiO + Ti_2Ni)$.

Annealing Treatment: 900°C for 48 hours, water quench
Etchant: 60 glycerine, 20 HNO_3 , 20 HF

Contrails

between the three phase fields ($\text{TiO} + \text{Ti}_2\text{Ni} + \text{TiNi}_3$) and ($\text{TiNi} + \text{Ti}_2\text{Ni} + \text{TiNi}_3$). Two alloys were found to be in the latter three phase field (see Figure 69). There was no evidence to indicate that the TiNi phase had any appreciable miscibility range in the ternary system.

f. The ($\text{Ti}_2\text{Ni} + \text{TiNi}$) Phase Field

Three alloys located the extent of this field. In doing so, confirmation was given to the assumption of a very narrow field for ($\text{Ti}_2\text{Ni} + \text{TiNi}_3$). Figure 70 shows a structure of ($\text{Ti}_2\text{Ni} + \text{TiNi}$).

5. Isothermal Section at 1000°C - System Ti-Mo-O

Preliminary experiments indicated that no ternary oxide phase occurred in this system in the general composition field in which ternary phases were found in the Ti-Fe-O, Ti-Cr-O and Ti-Ni-O systems. The isothermal section at 1000°C for the Ti-Mo-O system serves as a basis of comparison with the other three. In particular, it was of interest to note the influence of the ternary phases in restricting the solubility of iron, chromium, and nickel in the alpha phase.

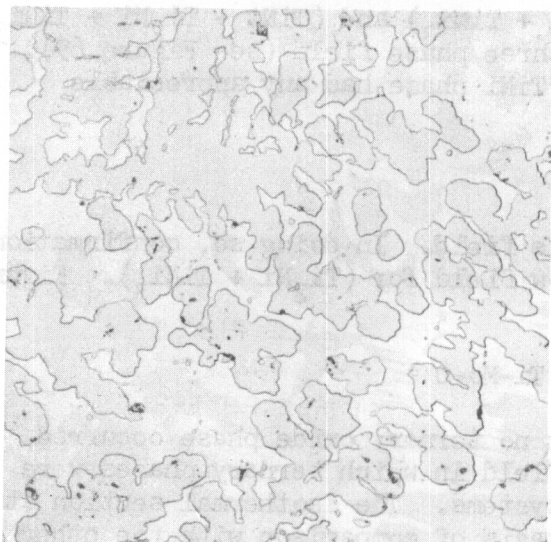
Twenty-two alloys were used to outline phase boundaries in the titanium corner of this system. Metallographic examination was used to determine the number and identity of the phases. The isothermal section with data points is shown in Figure 71. Two points are worthy of comment. The TiO phase is likely to appear only at very high molybdenum contents (>20 atomic per cent). The restricted solubility of nickel and chromium in alpha is not particularly due to the presence of the ternary phase because molybdenum follows the same trend.

IV. SUMMARY

A. The Ti-Cr-Fe System

There is a continuous space of ternary beta solid solution ranging from the Ti-Cr to the Ti-Fe system. Under equilibrium conditions, the following phase changes will occur with fall in temperature: according to the composition of the alloy, the ternary beta phase starts to decompose by primary rejection of either one of the three phases, α , TiFe or TiCr_2 . This is followed by the eutectoid decomposition into ($\alpha + \text{TiCr}_2$), ($\alpha + \text{TiFe}$), or ($\text{TiFe} + \text{TiCr}_2$), respectively, taking place within a temperature interval. The phase changes are terminated by the formation of the ternary eutectoid ($\alpha + \text{TiFe} + \text{TiCr}_2$) at about 540°C . The ternary eutectoid is located at approximately 8% Cr-15% Fe. Whereas the precipitation of α , TiFe and TiCr_2 , respectively, takes place at a high rate, the "binary" and especially the ternary eutectoid decompositions, due to the low temperature at which they occur, are extremely sluggish and can be initiated only by very long annealing times. Therefore, under ordinary conditions

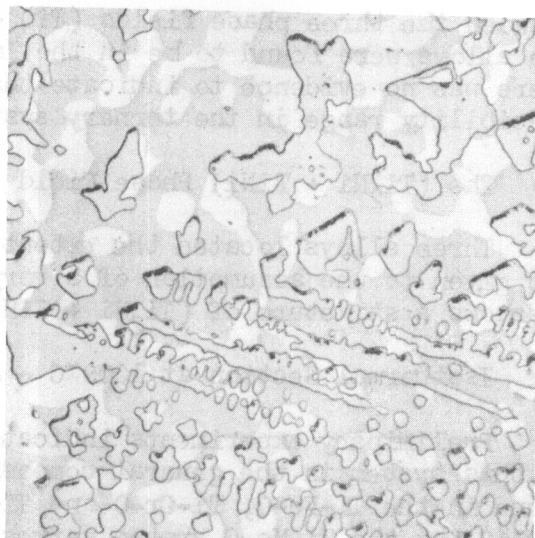
Contrails



Neg. No. 7065 X 750

Fig. 68

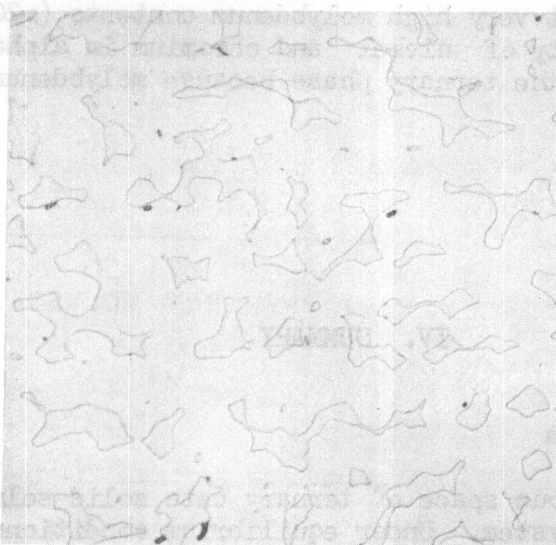
Composition: 25% O, 30% Ni, 45% Ti.
Three phase structure of $(TiO + Ti_2Ni + TiNi_3)$.



Neg. No. 7068 X 750

Fig. 69

Composition: 5% O, 50% Ni, 45% Ti.
Three phase structure of $(Ti_2Ni + TiNi + TiNi_3)$.



Neg. No. 7069 X 500

Fig. 70

Composition: 5% O, 35% Ni, 60% Ti.
Two phase structure of $(Ti_2Ni + TiNi)$.

Annealing Treatment: 900°C for 48 hours, water quench

Etchant: 60 glycerine, 20 HNO₃, 20 HF

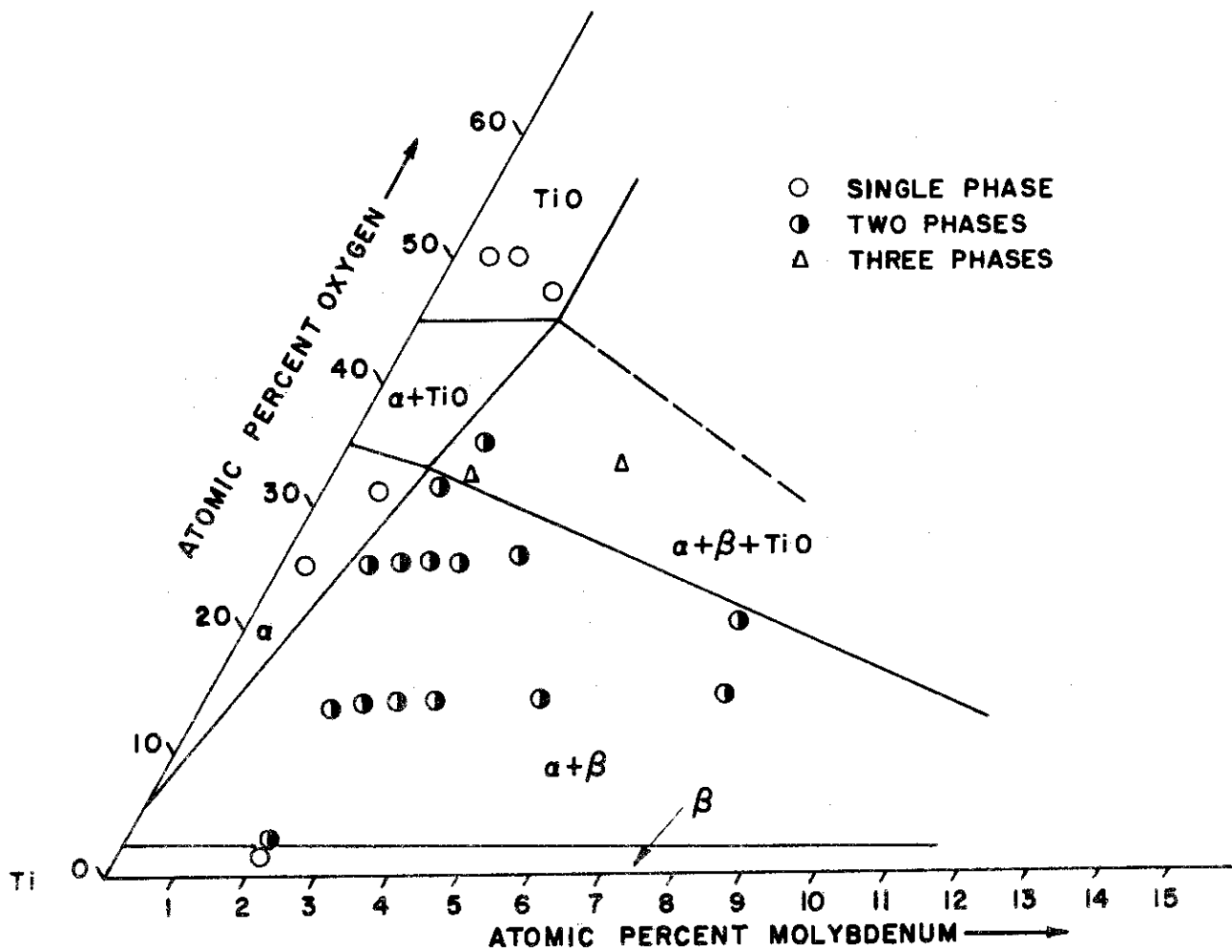


Fig. T1 - 1000°C Isothermal for Partial Ti-Mo-O System

of heat treatment, the beta phase remains metastable, similar to the conditions in the binary systems Ti-Cr and Ti-Fe.

The beta phase of alloys lying on the low titanium side of a tie line between 7% chromium and 4% iron is retained upon water quenching from the beta space. The solubility of chromium and iron in alpha titanium is less than 1% total alloy content.

A continuous series of solid solutions exists above 1100°C between $TiFe_2$ and the high temperature modification of $TiCr_2$. Solidus data are presented and show that chromium raises the binary Ti-Fe eutectic temperature (1080°C). Hardness data are presented and illustrate the pronounced effect of heat treatment.

B. The Ti-Al-(O and N) Systems

Both oxygen and nitrogen raise the β/α and β space boundary and widen the (α/β) field of the Ti-Al system although nitrogen is more effective. The beta phase transforms to alpha prime upon water quenching. Data are presented illustrating the fact that the hardness of ternary alloys is increased by the addition of oxygen or nitrogen.

C. The Ti-Al-C System

A probable Ti-C diagram to 30% carbon is presented. The essential features include: a very high melting compound, TiC , with a solubility limit near 15% carbon. A eutectic between TiC and carbon occurs at about 30% carbon.

Vertical sections of the Ti-Al-C system illustrate the increased solubility of carbon in alpha with greater aluminum contents. The solubility is increased to over 1% carbon at 10% aluminum. The peritectoid reaction of the Ti-C system occurs at successively higher temperatures in the ternary system. An unidentified phase was observed in samples of high alloy content. Data are presented illustrating the hardening effect of aluminum and carbon on alpha titanium.

D. The Ternary Oxide Phases

A family of ternary oxide phases isomorphous with $\text{Fe}_2\text{W}_2\text{C}$ was discovered. The group had the general formula $\text{Ti}_4\text{X}_2\text{O}_2\text{Ti}_3\text{X}_3\text{O}_3$ where X was copper, nickel, cobalt, iron, manganese or chromium.

The phase relationships by which these ternary phases entered into equilibrium were investigated in single isothermal sections for the systems Ti-Fe-O, Ti-Cr-O and Ti-Ni-O. By way of comparison with a system in which no ternary oxide appears, the 1000°C level of the Ti-Mo-O system was constructed.

It was demonstrated that these oxide phases are not to be expected to appear in commercial alloy compositions.

BIBLIOGRAPHY

1. D. J. McPherson, H. D. Kessler, M. Hansen, and E. L. Kamen, The Titanium-Columbium, Titanium-Molybdenum and Titanium-Silicon Phase Diagrams, Air Force Technical Report No. 6225, June, 1951.
2. R. Vogel and B. Wenderott, The Constitution Diagram Iron-Chromium-Titanium, Archiv fur das Eisenhüttenwesen, Vol. 11, 1940, p. 279.
3. R. J. Van Thyne, H. D. Kessler, and M. Hansen, The Systems Titanium-Chromium and Titanium-Iron, Trans. ASM, Vol. 44, 1952, p. 974.
4. R. J. Van Thyne, E. S. Bumps, H. D. Kessler, and M. Hansen, Phase Diagrams of the Titanium-Aluminum, Titanium-Chromium-Iron, and Titanium-Oxygen Systems, Wright Air Development Center Technical Report No. 52-16, December, 1952.
5. C. M. Craighead, O. W. Simmons, and L. W. Eastwood, Titanium Binary Alloys, Trans. AIME, Vol. 188, 1950, p. 485.
6. D. J. McPherson and M. G. Fontana, Preparation and Properties of Titanium-Chromium Binary Alloys, Trans. ASM, Vol. 43, 1951, p. 1098.
7. M. K. McQuillan, A Provisional Constitutional Diagram of the Chromium-Titanium System, Journal, Institute of Metals, Vol. 79, 1951, p. 379.
8. P. Duwez and J. L. Taylor, A Partial Titanium-Chromium Phase Diagram and the Crystal Structure of $TiCr_2$, Trans. ASM, Vol. 44, 1952, p. 495.
9. F. B. Cuff, N. J. Grant and C. F. Floe, Titanium-Chromium Phase Diagram, Trans. AIME, Vol. 194, 1952, p. 848.
10. H. W. Wormer, The Constitution of Titanium-Rich Alloys of Iron and Titanium, Journal, Institute of Metals, Vol. 79, 1951, p. 173.
11. W. J. Fretague, C. S. Barker and E. A. Peretti, The Titanium-Iron Phase Diagram, Air Force Technical Report 6597, Parts 1 and 2, November, 1951 and March, 1952, respectively.
12. A. D. McQuillan, The Application of Hydrogen Equilibrium-Pressure Measurements to the Investigation of Titanium Alloy Systems, Journal, Institute of Metals, Vol. 79, 1951, p. 73.
13. B. W. Levinger, High Temperature Modification of $TiCr_2$, Journal of Metals, Vol. 5, February, 1953, p. 196.
14. M. Hansen and H. D. Kessler, Titanium Alloy Development, SAE Preprint No. 43, January 16, 1953.
15. W. M. Parris, L. L. Hirsch, and P. D. Frost, Low Temperature Aging in Titanium Alloys, Journal of Metals, Vol. 5, February, 1953, p. 178.

Contrails

16. E. S. Bumps, H. D. Kessler, and M. Hansen, Titanium-Aluminum System, Trans. AIME, Vol. 194, 1952, p. 609.
17. E. S. Bumps, H. D. Kessler, and M. Hansen, The Titanium-Oxygen System, Trans. ASM, Vol. 45, 1953, p. 1008.
18. R. I. Jaffee, H. R. Ogden, and D. J. Maykuth, Alloys of Titanium with Carbon, Oxygen, and Nitrogen, Trans. AIME, Vol. 188, 1950, p. 1261.
19. I. Cadoff and J. P. Nielsen, Titanium-Carbon Phase Diagram, Journal of Metals, Vol. 5, February, 1953, p. 248.
20. F. Laves and H. J. Wallbaum, The Crystal Chemistry of Titanium Alloys, Naturwiss, Vol. 27, 1939, p. 674.
21. P. Duwez and J. L. Taylor, The Structure of Intermediate Phases in Alloys of Titanium with Iron, Cobalt and Nickel, Trans. AIME, Vol. 188, 1950, p. 1173.
22. N. Karlsson, An X-ray Study of the Phases in the Copper-Titanium System, Journal, Institute of Metals, Vol. 79, 1951, p. 391.
23. A. Joukainen, N. J. Grant, and C. F. Floe, Titanium-Copper Binary Phase Diagram, Trans. AIME, Vol. 194, 1952, p. 766.
24. D. J. Maykuth, H. R. Ogden, and R. I. Jaffee, Titanium-Manganese System, Journal of Metals, Vol. 5, 1953, p. 225.
25. N. Karlsson, Metallic Oxides with the Structure of High Speed Steel Carbide, Nature, Vol. 168, September 29, 1951, p. 558.
26. C. C. Wang, N. J. Grant, and C. F. Floe, Titanium-Rich Titanium-Chromium-Oxygen Ternary System, Wright Air Development Center Technical Report No. 52-255, November, 1952.
27. H. Margolin, E. Ence, and J. P. Nielsen, Titanium-Nickel Phase Diagram, Journal of Metals, Vol. 5, 1953, p. 243.

Contrails